
Electronic Thesis and Dissertation Repository

10-15-2019 11:00 AM

Lysosomes Mediate Rab27b-Dependent Secretion of Beta-Amyloid

Shany Lahan, *The University of Western Ontario*

Supervisor: Pasternak, Stephen H., *The University of Western Ontario*

A thesis submitted in partial fulfillment of the requirements for the Master of Science degree in Neuroscience

© Shany Lahan 2019

Follow this and additional works at: <https://ir.lib.uwo.ca/etd>



Part of the [Molecular and Cellular Neuroscience Commons](#)

Recommended Citation

Lahan, Shany, "Lysosomes Mediate Rab27b-Dependent Secretion of Beta-Amyloid" (2019). *Electronic Thesis and Dissertation Repository*. 6603.

<https://ir.lib.uwo.ca/etd/6603>

This Dissertation/Thesis is brought to you for free and open access by Scholarship@Western. It has been accepted for inclusion in Electronic Thesis and Dissertation Repository by an authorized administrator of Scholarship@Western. For more information, please contact wlsadmin@uwo.ca.

Abstract

Extracellular deposition of beta-Amyloid (A β) is an early event in Alzheimer's disease development. However, it is not known how A β is secreted. Lysosomes readily undergo calcium-dependent exocytosis, a process that relies on small GTPase Rab27b. In addition, lysosomal enzymes have been found within extracellular amyloid plaques. We hypothesized that lysosomes mediate Rab27b-dependent exocytosis of A β . Neuro-2a cells were transfected with wild-type or mutant Rab27b constructs and/or a lysosomal marker. Cells were incubated with A β monomers and imaged using a confocal microscope before and after stimulation of calcium-dependent exocytosis. We observed a significant decrease in lysosome and A β co-localization post-treatment in comparison to pre-treatment in control samples. We also observed a significant increase in lysosome and A β co-localization post-treatment in Rab27b dominant-negative mutants in comparison to control. These results demonstrate that lysosomes can mediate Rab27b-dependent exocytosis of A β , thus elucidating a mechanism by which A β could be secreted in Alzheimer's disease.

Keywords

Alzheimer's disease (AD), beta-Amyloid (A β), A β ₄₂, A β ₄₀, small GTPase Rab27b, lysosomes, calcium-dependent (regulated) exocytosis, secretion

Summary for Lay Audience

Alzheimer's disease is the leading form of dementia, in which patients experience progressive cognitive decline. In Alzheimer's disease, a toxic protein named beta-Amyloid is produced within and subsequently released from cells, forming deposits within the brain. It has been suggested that the production of beta-Amyloid triggers a cascade of events that results in the development of Alzheimer's disease. However, it is not known how beta-Amyloid is released from cells.

Previous research has implicated the involvement of lysosomes in Alzheimer's disease progression. Lysosomes are classically viewed as waste disposal compartments within the cell. Recent studies have shown that lysosomes are also capable of discharging their contents to the outside of the cell. This process has been suggested to be dependent on protein Rab27b, which brings lysosomes closer to the membrane of a cell. When lysosomes are near the cell's membrane, an increase in calcium within the cell enables lysosomes to release their contents. In this study, it was hypothesized that beta-Amyloid is discharged from lysosomes with the assistance of protein Rab27b.

To investigate this hypothesis, cells were manipulated to express inactive, active, or overactive protein Rab27b and/or a lysosome indicator. Cells were also loaded with beta-Amyloid. In this manner, lysosomes and beta-Amyloid present within cells that were or were not manipulated to express inactive, active, or overactive Rab27b were able to be observed under a microscope. Cells were then stimulated to discharge the contents of their lysosomes by increasing the amount of calcium within these cells. Cells were again observed under a microscope. Microscope images taken before and after stimulation of discharge were compared to determine differences in beta-Amyloid release. It was observed that lysosomes can release beta-Amyloid from cells with the assistance of protein Rab27b.

By the year 2050, it is predicted that more than 130 million new cases of Alzheimer's disease will arise worldwide. Understanding how beta-Amyloid is released from cells would facilitate the development of targeted treatments for Alzheimer's disease, which are essential to preventing future disease progression.

Abbreviations

A β	Beta-Amyloid
ACh	Acetylcholine
AChE	Acetylcholinesterase
AD	Alzheimer's Disease
ADAM	A Disintegrin And Metalloprotease
AP	Adaptor Protein
APH-1	Anterior Pharynx-Defective 1
APP	Amyloid Precursor Protein
BACE1	Beta-Site APP-Cleaving Enzyme 1
BMP/LBPA	Bis(Monoacylglycero)Phosphate/Lysobisphosphatidic Acid
ChAT	Choline Acetyl Transferase
CICR	Calcium-Induced Calcium Release
CGN	<i>Cis</i> -Golgi Network
CTF	C-Terminal Fragment
DMSO	Dimethyl Sulfoxide
DPBS	Dulbecco's Phosphate-Buffered Saline
EBFP	Enhanced Blue Fluorescent Protein
ER	Endoplasmic Reticulum
ESCRT	Endosomal Sorting Complexes Required for Transport
FAD	Familial Alzheimer's Disease
GAP	GTPase-Activating Protein
GD	Gaucher's Disease
GDF	GDI Displacement Factor
GDI	GDP Dissociation Inhibitor
GDP	Guanosine Diphosphate
GEF	Guanine (GDP/GTP) Exchange Factor
GFP	Green Fluorescent Protein
GS	Griscelli Syndrome
GTP	Guanosine Triphosphate

HBSS	Hank's Balanced Salt Solution
HFIP	1,1,1,3,3,3-Hexafluoro-2-Propanol
Hrs	Hepatocyte Growth Factor-Regulated Tyrosine Kinase Substrate
ILV	Intraluminal Vesicle
IP ₃ R	Inositol 1,4,5-Triphosphate Receptor
LAMP1	Lysosomal-Associated Membrane Protein 1
LRO	Lysosome-Related Organelle
LSD	Lysosomal Storage Disease
MAP	Microtubule-Associated Protein
M6P	Mannose-6-Phosphate
mChFP	Monomeric Cherry Fluorescent Protein
MEM	Minimum Essential Medium
Munc	Mammalian Uncoordinated
MVB	Multivesicular Body
N2A	Neuro-2a
NMDA	<i>N</i> -methyl-D-aspartate
NMHC-IIA	Non-Muscle Myosin Heavy Chain IIA
PEN-2	Presenilin Enhancer 2
PFA	Paraformaldehyde
PHF	Paired Helical Filament
PS	Presenilin
RyR	Ryanodine Receptor
siRNA	Small Interfering Ribonucleic Acid
SNAP	Soluble <i>N</i> -Ethylmaleimide-Sensitive Factor Attachment Protein
SNARE	Soluble <i>N</i> -Ethylmaleimide-Sensitive Factor Attachment Receptor
TGN	<i>Trans</i> -Golgi Network
TIR-FM	Total Internal Reflection Fluorescence Microscopy
TM	Transmembrane
UCE	Uncovering Enzyme
VAMP	Vesicle-Associated Membrane Protein
WT	Wild-Type

Acknowledgements

I would like to offer my sincerest gratitude to my supervisor, Dr. Stephen Pasternak, for your continued mentorship and guidance throughout my graduate career. Despite your incredibly busy schedule, you continuously made yourself available to provide me with valuable advice and suggestions regarding my research.

I would also like to thank my advisors, Dr. Bryan Heit, Dr. Jane Rylett, and Dr. Shawn Whitehead, for keeping me on track and focused as I delved into experiments. I greatly appreciated our discussions.

I would like to thank our laboratory manager, Claudia Seah, for teaching me essential protocols and techniques that I consistently used when completing experiments. Thank you as well to my laboratory members, Adrianna Tsang and Jordan Krupa, for your help and patience every step of the way. I could not have completed my research without the support of the Pasternak Laboratory.

Last but certainly not least, thank you to my family and friends. Your endless encouragement pushed me onward and allowed me to maintain my partial sanity. I would like to dedicate this thesis to you.

Table of Contents

Abstract	i
Keywords	i
Summary for Lay Audience	ii
Abbreviations	iii
Acknowledgements	v
Table of Contents	vi
List of Tables	ix
List of Figures	x
List of Appendices	xii
Chapter 1	1
1 Introduction	1
1.1 Lysosomes	2
1.1.1 Overview	2
1.1.2 Secretory Lysosomes and Lysosome-Related Organelles	3
1.1.3 Sorting of Normal Material to the Lysosome	5
1.1.4 Lysosomal Storage Diseases	7
1.2 Exocytosis	9
1.2.1 Calcium-Dependent Exocytosis in the Context of Neuronal Lysosomes	9
1.3 Small GTPase Rab27b	13
1.3.1 Small GTPases: An Overview	13
1.3.2 Small GTPase Rab27b	14
1.4 Alzheimer's Disease	17
1.4.1 Dementia	17
1.4.2 Overview of Alzheimer's Disease	17

1.4.3	Pathogenesis of Alzheimer’s Disease	19
1.5	Rationale	24
1.5.1	Overview	24
1.5.2	Hypothesis.....	25
1.5.3	Objectives	26
1.5.4	Predictions.....	26
Chapter 2	27
2	Materials and Methods	27
2.1	Cell Culture.....	27
2.2	DNA Constructs.....	27
2.3	A β ₄₀ and A β ₄₂ Preparation	28
2.4	Ionomycin Treatment.....	29
2.5	Confocal Microscopy	29
2.6	Widefield Microscopy	29
2.7	Co-Localization Analyses.....	30
2.8	Statistical Analyses	31
Chapter 3	33
3	Results	33
3.1	Exogenous A β Accumulates Within Lysosomes.....	33
3.1.1	Intracellular A β Localization	33
3.1.2	Between-Group Comparison	36
3.2	A β Secretion is Mediated by Lysosomes.....	37
3.2.1	Within-Group Comparison	37
3.2.2	Between-Group Comparison	38
3.3	Subcellular Distribution of Rab27b	39

3.3.1	No Differences in Rab27b and Lysosome Co-Localization	40
3.3.2	Differences in Rab27b and A β Co-Localization.....	43
3.4	Rab27b Mutants Alter Lysosomal-Mediated Secretion of Exogenous A β	46
3.4.1	A β ₄₂ : Pre-Treatment Between-Group Comparison.....	47
3.4.2	A β ₄₂ : Within-Group Comparison.....	48
3.4.3	A β ₄₂ : Post-Treatment Between-Group Comparison	54
3.4.4	A β ₄₀ : Pre-Treatment Between-Group Comparison.....	55
3.4.5	A β ₄₀ : Within-Group Comparison.....	56
3.4.6	A β ₄₀ : Post-Treatment Between-Group Comparison	62
3.5	Differences in A β Secretion in Rab27b Samples.....	63
Chapter 4	65
4	Discussion	65
4.1	A β Secretion is Mediated by Lysosomes.....	66
4.1.1	Intracellular and Extracellular A β Observations.....	66
4.2	Subcellular Distribution of Rab27b	67
4.3	Rab27b Mutants Alter Lysosomal-Mediated Secretion of Exogenous A β	69
4.4	Relation to <i>In Vivo</i> Calcium-Dependent Exocytosis	72
4.5	Conclusion	73
4.5.1	Significance.....	73
4.5.2	Limitations	74
4.5.3	Future Directions	76
References	77
Appendices	97
Curriculum Vitae	98

List of Tables

Table 1 – Raw mean co-localization of Rab27b-EBFP and LAMP1-mChFP	39
Table 2 – Raw mean co-localization of Rab27b-EBFP and A β	40
Table 3 – Raw mean co-localization of LAMP1-mChFP and A β	46

List of Figures

Figure 1 – Lysosomal-mediated calcium-dependent exocytosis	12
Figure 2 – Small GTPase Rab27b switches between inactive and active forms	16
Figure 3 – Processing of APP	23
Figure 4 – A β secretion following intracellular trafficking and processing of APP	25
Figure 5 – Co-localization of LAMP1-mChFP and A β_{42}	34
Figure 6 – Co-localization of LAMP1-mChFP and A β_{40}	35
Figure 7 – Pre-treatment co-localization of LAMP1-mChFP and A β	36
Figure 8 – Mean co-localization of LAMP1-mChFP and A β	38
Figure 9 – Co-localization of LAMP1-mChFP and Rab27b-EBFP	41
Figure 10 – Mean co-localization of LAMP1-mChFP and Rab27b-EBFP	42
Figure 11 – Co-localization of Rab27b-EBFP and A β in Rab27b samples.....	44
Figure 12 – Mean co-localization of Rab27b-EBFP and A β in Rab27b samples	45
Figure 13 – Pre-treatment co-localization of LAMP1 and A β_{42} in Rab27b samples	47
Figure 14 – Co-localization of LAMP1-mChFP and A β_{42} in T23N samples.....	49
Figure 15 – Co-localization of LAMP1-mChFP and A β_{42} in N133I samples.....	50
Figure 16 – Co-localization of LAMP1-mChFP and A β_{42} in WT samples.....	51
Figure 17 – Co-localization of LAMP1-mChFP and A β_{42} in Q78L samples.....	52
Figure 18 – Mean co-localization of LAMP1-mChFP and A β_{42} in Rab27b samples	53
Figure 19 – Post-treatment co-localization of LAMP1 and A β_{42} in Rab27b samples	54

Figure 20 – Pre-treatment co-localization of LAMP1 and A β ₄₀ in Rab27b samples.....	55
Figure 21 – Co-localization of LAMP1-mChFP and A β ₄₀ in T23N samples.....	57
Figure 22 – Co-localization of LAMP1-mChFP and A β ₄₀ in N133I samples.....	58
Figure 23 – Co-localization of LAMP1-mChFP and A β ₄₀ in WT samples.....	59
Figure 24 – Co-localization of LAMP1-mChFP and A β ₄₀ in Q78L samples.....	60
Figure 25 – Mean co-localization of LAMP1-mChFP and A β ₄₀ in Rab27b samples	61
Figure 26 – Post-treatment co-localization of LAMP1 and A β ₄₀ in Rab27b samples.....	62
Figure 27 – Mean co-localization of LAMP1-mChFP and A β in Rab27b samples	64

List of Appendices

Appendix 1 – Imaris Software 7 Co-Localization Module.....	97
--	----

Chapter 1

1 Introduction

Extracellular beta-Amyloid ($A\beta$) deposition is an early event in the development of Alzheimer's disease (AD) [1]; however, it is not known how $A\beta$ is secreted. This study was therefore conducted to elucidate the means of $A\beta$ secretion in the context of AD. Previous research has suggested that lysosomes may be vital to calcium-dependent exocytosis of $A\beta$ [2]–[5]. Calcium-dependent exocytosis involves the coordinated activity of many different proteins, such as small GTPase Rab27b [6]–[9].

The related topics of lysosomes, exocytosis, small GTPase Rab27b, and AD were reviewed in-depth in Chapter 1 to provide the reader with a foundation for this study. To determine whether lysosomes mediate calcium-dependent exocytosis of $A\beta$ and further, to determine whether this exocytotic process is dependent on Rab27b, we conducted a group of experiments described in detail in Chapters 2 and 3. These experiments included transfecting Neuro-2a (N2A) cells with fluorescent Rab27b mutant or wild-type (WT) constructs and/or a fluorescent lysosomal marker, incubating the cells with dye-labeled $A\beta$ monomers, imaging the cells under confocal microscopy before and after stimulation of calcium-dependent exocytosis with ionomycin treatment, and conducting co-localization analyses of the images obtained. Results of this study were presented in Chapter 3. Briefly, a significant decrease in lysosome and $A\beta$ co-localization post-treatment in comparison to pre-treatment in control samples was observed, indicative of lysosomal-mediated secretion of $A\beta$. A significant reduction of lysosomal-mediated secretion of $A\beta$ in Rab27b dominant-negative mutants in comparison to control samples was also observed. These results were discussed in Chapter 4, in the context of the literature reviews provided in Chapter 1. Overall, the results of this study demonstrate that $A\beta$ secretion is mediated by lysosomes in a Rab27b-dependent manner, thus elucidating a mechanism by which $A\beta$ could be secreted in AD.

1.1 Lysosomes

1.1.1 Overview

Lysosomes are membrane-bound, acidic organelles that are found in eukaryotic cells in varying amounts. Each conventional lysosome contains over 50 different types of acid hydrolases, or enzymes that function optimally in acidic environments [10]. The restricted pH optimum of acid hydrolases allows conventional lysosomes to degrade a vast array of material that is trafficked to them, while also offering protection for the rest of the cell. Specifically, if the lysosomal membrane were to become compromised and acid hydrolases were to be released to the cytosol, material in the cytosol would not be degraded. This is due to activity of acid hydrolases within the acidic environment of the lysosome (pH of 4.5 to 5) and inactivity of acid hydrolases within the neutral environment of the cytosol (pH of approximately 7.2) [10], [11]. To maintain the lysosomal lumen at a low pH, the lysosome must actively transport protons (H^+ ions) from the cytosol to the lysosomal lumen via a proton pump known as vacuolar ATPase [12]. In order to offset a large positive electrochemical gradient, transport of H^+ ions from the lysosomal lumen to the cytosol and transport of chloride ions (Cl^-) from the cytosol to the lysosomal lumen occurs simultaneously, primarily via Cl^- / H^+ antiporter CIC-7 [13], [14].

Material that can be degraded by lysosomal acid hydrolases includes intracellular and extracellular proteins, lipids, carbohydrates, and nucleic acids that are aberrant or otherwise damaged [10], [11]. Lysosomal-mediated turnover of intracellular material, such as damaged organelles, primarily occurs through a process termed macroautophagy [15]. Macroautophagy is dependent on the formation of a vesicle, a continuous lipid bilayer(s) that encloses either extracellular fluid or cytoplasm and may contain soluble and/or membrane-bound material [16]. The specialized double membrane-bound intracellular vesicle formed during macroautophagy is called an autophagosome. An autophagosome can eventually fuse with a lysosome to form an autolysosome, which exposes intraluminal material to lysosomal acid hydrolases that catalyze their digestion [15].

Extracellular material destined for degradation by the lysosome must first be internalized by the cell in a process termed endocytosis [10], [11]. Two main types of endocytic mechanisms that direct extracellular material to the lysosome for degradation are phagocytosis and pinocytosis [17], [18]. Phagocytosis refers to the engulfment of extracellular material by the plasma membrane and subsequent budding of this membrane to form a phagosome. Similar to the mechanism of macroautophagy, a phagosome is an intracellular vesicle that fuses with a lysosome to form a phagolysosome, ultimately enabling digestion of phagocytosed material via exposure to lysosomal acid hydrolases. Material that is endocytosed in this manner can include large extracellular pathogens (equal to or greater than 0.5 μm) and dead cell debris [19]. Pinocytosis refers to invagination of the cell's membrane to form a non-specific fluid and material-filled intracellular vesicle. This vesicle can then fuse with a lysosome for degradation of its contents [17].

1.1.2 Secretory Lysosomes and Lysosome-Related Organelles

Apart from the ability to degrade material via resident acid hydrolases, a subset of lysosomes present within most cell types additionally possess the ability to store and release material to the extracellular space in a process termed calcium-dependent exocytosis (calcium-dependent exocytosis is described in detail in Section 1.2.1). These lysosomes are referred to as secretory lysosomes [20], [21]. Despite the additional ability of secretory lysosomes to undergo exocytosis, there are no differences in morphology of secretory lysosomes when compared to conventional lysosomes [20]. In functionality, secretory lysosomes are related to secretory vesicles, early endosomes, and late endosomes/multivesicular bodies (MVBs) [20], [21].

Secretory lysosomes that are specific to the cell type they are found in are termed lysosome-related organelles (LROs). LROs are specialized compartments that share many properties with secretory lysosomes, including the ability to undergo calcium-dependent exocytosis. However, as these compartments are cell-specific, they release cell-specific proteins to the extracellular space [20], [22]. Examples of LROs include lytic granules of cytotoxic T cells, which secrete cytolytic proteins (immune cell effectors), and melanosomes of melanocytes, which secrete melanin (a pigment) [20]–[22]. Lytic granules and melanosomes are discussed in greater detail in Section 1.1.4.

Many studies use Total Internal Reflection Fluorescence Microscopy (TIR-FM) to observe lysosomes undergoing calcium-dependent exocytosis *in vitro* [5], [7], [23]. In TIR-FM, a laser is reflected off the surface of a confocal plate or coverslip at a critical reflection angle, such that only a small amount of energy (termed an evanescent wave) can penetrate a cell. This process excites fluorophores present within 70-250 nm of the cell's surface. As such, background signal that may be captured under epifluorescence microscopy is omitted in TIR-FM. Moreover, time-lapse videos can be captured within milliseconds between frames under TIR-FM. TIR-FM is therefore a technique that enables researchers to observe processes occurring adjacent to a live cell's plasma membrane in detail and in real-time [24]. However, as only a small amount of energy can penetrate a cell under TIR-FM, a major limitation of this microscopy technique is the need for relatively high laser powers for efficient excitation of fluorophores. The use of high laser powers can in turn result in rapid photobleaching of these fluorophores. Confocal microscopy and live-cell widefield microscopy can be used as alternative techniques to TIR-FM when observing indirect or direct lysosomal-mediated secretion, respectively. With confocal and widefield microscopy, images can be taken at resolutions (confocal) and speeds (widefield) comparable to TIR-FM [25].

Numerous luminal and membrane lysosomal markers have been developed to observe lysosomal-mediated secretion under microscopy. Many lysosomal markers used in live-cell imaging make use of the organelle's acidic lumen [5], [23], [26]. For example, our laboratory has previously utilized construct mApple-LAMP1-pHluorin (Addgene plasmid #54918). mApple fluorescent protein labels the cytosolic end of the transmembrane (TM) glycoprotein Lysosomal-Associated Membrane Protein 1 (LAMP1) red, and ecliptic pHluorin labels the luminal end of LAMP1 green. Ecliptic pHluorin is a pH-sensitive Green Fluorescent Protein (GFP) that increases in fluorescence intensity when it is exposed to a less acidic environment (higher pH) [27]. As lysosomes are acidic organelles and the extracellular environment more basic in comparison, gradual increases in fluorescence intensity of ecliptic pHluorin-labeled lysosomes previously enabled our laboratory to visualize lysosomal-mediated secretion of A β in real-time using live-cell microscopy techniques such as TIR-FM and widefield.

1.1.3 Sorting of Normal Material to the Lysosome

Lysosomal sorting of normal material, such as resident membrane-bound glycoproteins and resident soluble acid hydrolases, can occur through indirect and direct pathways [21], [28].

The indirect sorting pathway entails trafficking of a newly-synthesized membrane-bound protein from the *trans*-Golgi network (TGN) to the plasma membrane via constitutive exocytosis (described in Section 1.2), internalization of the membrane-bound protein from the plasma membrane via receptor-mediated (clathrin-mediated) endocytosis, and intracellular trafficking of this protein to the lysosome via the endocytic pathway. Many resident TM glycoproteins, including LAMPs, are sorted to the lysosome in this manner [28], [29]. Clathrin-mediated endocytosis refers to invagination of the cell's membrane and associated proteins to form endocytic vesicles lined by an outer clathrin protein coat. Cell surface TM proteins that are destined for transport to the lysosome contain tyrosine- (YXXØ) or dileucine- ([DE]XXXL[LI]) based motifs on their cytoplasmic domains [30]. During clathrin-mediated endocytosis, these motifs enable clathrin adaptor protein (AP) complex AP-2 to bind and subsequently recruit clathrin proteins for the construction of a lattice that aids in the assembly of a clathrin-coated vesicle upon invagination of the plasma membrane [18], [31]. Following the endocytic pathway, clathrin-coated vesicles then fuse with an early endosome for transfer of cargo. Early endosomes are membrane-bound organelles that function as sorting centers for internalized material [32]. The maturation of an early endosome into a late endosome/MVB is necessary for material that is destined for transport to the lysosome. This maturation process involves acidification of the lumen, from a pH of approximately 6.5 to a pH of approximately 5.5. Maturation also involves the generation of intraluminal vesicles (ILVs) [33].

The generation of ILVs within the early endosome is dependent on endosomal sorting complexes required for transport (ESCRT). ESCRT promotes inward budding and scission of the limiting membrane of the early endosome to form these ILVs. ESCRT is comprised of cytosolic protein complexes ESCRT-0, ESCRT-I, ESCRT-II, and ESCRT-III that are each capable of recognizing different components of the early endosome and/or its associated cargo [34], [35]. For example, early endosomes that carry material destined for transport to the lysosome contain discontinuous and bi-layered flat clathrin coats that lack

APs and are thus morphologically distinct from the clathrin coats of endocytic vesicles [36]. Recruitment of ESCRT to an early endosome carrying such material is dependent on the recognition of its flat clathrin coat via ESCRT-0 protein, hepatocyte growth factor-regulated tyrosine kinase substrate (Hrs). This interaction is mediated through a clathrin box motif present within the C-terminal domain of Hrs [32].

Upon maturation, the late endosome/MVB can fuse with a lysosome for transfer of its ILVs or associated cargo [33]. ILV membranes contain bis (monoacylglycero) phosphate / lysobisphosphatidic acid (BMP/LBPA), a negatively-charged phospholipid that can enable back-fusion of the ILV membrane with the limiting membrane of the late endosome/MVB, for release of membrane-bound cargo to the late endosome/MVB membrane [37]. BMP/LBPA is also capable of recruiting positively-charged lipid hydrolases for breakdown of the ILV membrane, for release of soluble cargo to the late endosome/MVB lumen [33].

The direct sorting pathway to the lysosome involves trafficking of a soluble or membrane-bound protein from the TGN to a late endosome/MVB. This late endosome/MVB can then fuse with the lysosome for transport of its cargo [28], [29]. The majority of newly-synthesized lysosomal acid hydrolases are sorted in this manner. These acid hydrolases must first be post-translationally modified with a unique marker that signals the proteins for direct sorting to the lysosome. Modification involves the addition of mannose-6-phosphate (M6P) groups to oligosaccharides of acid hydrolases within the lumen of the *cis*-Golgi network (CGN) [38]. This post-translational modification is catalyzed by the enzymes *N*-acetylglucosamine-1-phosphotransferase (GlcNAc-1-phosphotransferase) and GlcNAc-1-phosphodiester α -*N*-acetylglucosaminidase (also known as “uncovering enzyme” or UCE) [29]. Once modified, M6P-tagged proteins are transported to the lumen of the TGN, where they recognize and attach to the ligand-binding sites of TM M6P receptors [39]. On the cytosolic side of the TGN, these same receptors bind the clathrin AP complex AP-1. AP-1 then recruits clathrin proteins to form clathrin-coated vesicles that bud from the TGN for transport to late endosomes/MVBs [30], [31]. The specific binding of M6P-tagged proteins to M6P receptors occurs within the TGN at a pH of approximately 6.5. Release of M6P-tagged proteins from M6P receptors occurs during fusion of clathrin-coated vesicles and late endosomes/MVBs, upon exposure to a more acidic MVB luminal

pH of approximately 5.5 [11]. Fusion of late endosomes/MVBs with lysosomes enables sorting of soluble acid hydrolases to the lysosome [29].

1.1.4 Lysosomal Storage Diseases

When a lysosome is unable to digest a certain kind of material, this material can accumulate within the lysosome and produce symptoms that are characteristic of one of 50 lysosomal storage diseases (LSDs) in humans. In common LSDs, a gene encoding a lysosomal enzyme is mutated such that the enzyme is deficient in activity or amount, or cannot be produced altogether [40]. For example, the most common type of LSD is Gaucher's disease (GD) [41]. GD can be caused by autosomal recessive mutations in the *GBA* gene, in turn resulting in reduced expression of the lysosomal acid hydrolase β -glucocerebrosidase. This enzyme hydrolyzes a glycosidic bond within the cell membrane lipid glucocerebroside [41], [42]. When cells undergo cell death, macrophages and other phagocytic cells can phagocytose these dead cell components (including glucocerebroside of the plasma membrane) and subsequently traffic them to lysosomes for degradation [17], [19]. Deficiency of β -glucocerebrosidase therefore results in accumulation of glucocerebroside, primarily within lysosomes of macrophages throughout the body [43], [44]. This results in symptoms ranging from anemia to hepatosplenomegaly (enlargement of the liver and spleen) in non-neuronopathic forms of GD (Type 1). In neuronopathic forms of GD (Type 2 and Type 3), cognitive impairment and seizures are also observed [45].

LSDs can also occur when multiple lysosomal enzymes cannot be incorporated into lysosomes, such that non-specific material accumulates within lysosomes. Inclusion-cell disease (also known as I-cell disease or Mucopolidosis II) is caused by an autosomal recessive mutation in the *GNPTA* gene. This mutation reduces GlcNAc-1-phosphotransferase expression, which results in a decreased amount of newly-synthesized acid hydrolases that are post-translationally modified with M6P groups [46]. As these acid hydrolases do not contain a signal sequence, they cannot be sorted to the lysosome and are instead secreted to the extracellular space via constitutive exocytosis [47]. Due to mis-sorting of multiple types of acid hydrolases, certain material in the lysosome cannot be degraded. This results in non-specific inclusions within the lysosomal lumen. Symptoms of I-cell disease include severe developmental and growth delays [46].

In addition, certain types of LSDs can arise when genes encoding proteins that are involved in vesicle trafficking or vesicle docking are mutated, such that the vesicle cannot undergo normal exocytosis. For example, Griscelli syndrome (GS) is an autosomal recessive disorder that affects the secretion of melanosomes or their contents [48]–[50]. The melanosome is a type of LRO found within melanocytes and is required for transfer of melanin to keratinocytes of the skin. The transfer of variable types and amounts of melanin results in differences in skin colour [51]. Although there have been various theories regarding the mechanism of melanin transfer, all involve secretion of the melanosome or its contents [52]. In melanocytes, transport of perinuclear melanosomes along microtubules and actin filaments, and docking of melanosomes to the plasma membrane [53], is dependent on a complex comprised of three proteins: myosin Va, Rab27a, and melanophilin (also known as Slac2-a) [48]–[50]. GS is clinically divided into three different types of syndromes depending on the protein that is affected, with all three types of GSs resulting in hypopigmentation of the hair and skin due to reduction in secretion and subsequent melanin transfer [22]. However, proteins such as Rab27a are normally expressed within several different cell types, including cytotoxic T cells. Lack of *RAB27A* expression within cytotoxic T cells of GS Type 2 patients thus results in additional immunodeficiency, due to a decrease in exocytosis of lytic granules and consequent reductions in extracellular cytolytic proteins, such as granzymes and perforins [50].

1.2 Exocytosis

Exocytosis can be defined as the release of intraluminal material to the plasma membrane or extracellular space. All eukaryotic cells can undergo constitutive exocytosis (also known as non-regulated, non-calcium-dependent, or default exocytosis), wherein material is secreted without an initial signal or stimulus. Constitutive exocytosis occurs when proteins that have been newly-synthesized in the endoplasmic reticulum (ER) are not post-translationally modified in the TGN to contain a translocation sequence that would otherwise direct their transport to another subcellular location. These proteins are packaged into secretory vesicles within the TGN for direct transport to the plasma membrane. Calcium-dependent exocytosis (also known as regulated exocytosis) can only occur in a portion of eukaryotic cells and is contingent on an initial signal or stimulus for secretion of material. Types of vesicles that can undergo calcium-dependent exocytosis as described below include some secretory vesicles, late endosomes/MVBs, secretory lysosomes, and LROs [20], [21].

1.2.1 Calcium-Dependent Exocytosis in the Context of Neuronal Lysosomes

Calcium-dependent exocytosis in neurons transpires in four or five steps: 1) vesicle trafficking, 2) vesicle tethering, 3) vesicle docking, 4) vesicle priming, and 5) vesicle fusion [20], [21]. Vesicle trafficking involves the anterograde transport of vesicles containing newly-synthesized proteins (from the TGN toward the plasma membrane), along microtubules, with the aid of motor protein kinesin-1 [54], [55]. Once the vesicle is adjacent to the plasma membrane, it detaches from kinesin-1 and travels the rest of the distance toward the plasma membrane through a region of filamentous actin, primarily with the aid of motor protein myosin homologue non-muscle myosin heavy chain IIA (NMHC-IIA) [56]. Rather than immediately undergoing exocytosis, vesicles generated in the TGN can instead be stored distal to the plasma membrane in “recycling” or “reserve” pools. Upon initiation of calcium-dependent exocytosis, these vesicles can undergo anterograde vesicle trafficking (from areas distal, to areas proximal to the plasma membrane). Recycling pools of vesicles refer to vesicles that can be trafficked to the membrane under physiological stimulatory conditions. Reserve pools of vesicles refer to vesicles that can only be trafficked to the membrane when the cell is exposed to excessive stimulation. Readily

releasable pools of vesicles are stored proximal to the plasma membrane after generation in the TGN [5], [57]. These vesicles have therefore undergone trafficking prior to initiation of calcium-dependent exocytosis. Regardless of whether a vesicle must first be trafficked or is already proximal in location to the plasma membrane, the next step of calcium-dependent exocytosis involves tethering of this vesicle to the plasma membrane. Vesicle tethering occurs via formation of an octameric protein tethering complex named exocyst [58]. Mammalian subunits EXOC2 to EXOC6 and EXOC8 are localized to the vesicle membrane, and mammalian subunits EXOC1 and EXOC7 are localized to the plasma membrane [59]. The interaction between exocyst subunits localized to vesicle and plasma membranes results in formation of the aforementioned exocyst complex [58]. Vesicle docking at the plasma membrane requires further interaction of exocyst subunits with active Rab GTPases localized to the vesicle membrane [60]. Docking of lysosomes and LROs, for example, is dependent on an interaction between EXOC6 (SEC15 in *Saccharomyces cerevisiae*) and active Rab27 [61]. The interaction between active Rab GTPases and exocyst subunits recruits Rab effector proteins, such as the Rab27 effector Munc13-4 [7], [9]. Previous studies have suggested that the Rab27-Munc13-4 complex of lysosomes serves as a “nucleation point” or “coincidence detection unit” for self-assembly or chance interaction between soluble *N*-ethylmaleimide-sensitive factor attachment receptor (SNARE) proteins [7]. SNARE proteins are categorized according to whether they are localized to the vesicle membrane (v-SNAREs) or target (plasma) membrane (t-SNAREs) [62]. Vesicle priming is dependent on interactions between v- and t-SNAREs for the formation of a highly stable ternary SNARE complex. This ternary complex is comprised of v-SNARE Vesicle-Associated Membrane Protein (VAMP; also known as Synaptobrevin), t-SNARE Syntaxin, and t-SNARE soluble *N*-ethylmaleimide-sensitive factor attachment protein (SNAP) isoforms [63]. An essential step preceding ternary bundle formation involves the stabilization of Syntaxin isoforms in closed conformations by Munc18 regulatory proteins [64]. In relation to lysosome- and LRO-mediated exocytosis, Munc18-2 stabilizes Syntaxin-11 in its closed conformation [65]. Dissociation of Munc18-2 enables Syntaxin-11 to convert to its open conformation, which may allow Syntaxin-11 to interact with VAMP isoforms (such as VAMP-2) and SNAP isoforms (such as SNAP-23) via SNARE motifs to form a ternary bundle [66], [67]. It has previously been suggested

that regulation by Munc18 is an essential intermediate step required for proper timing of ternary complex formation [64]. Another regulatory protein named Complexin (also known as Synaphin) can stabilize the bundle upon its formation to prime the vesicle for fusion with the plasma membrane [68]. Vesicle fusion with the plasma membrane is dependent on an influx of calcium ions (Ca^{2+}) from voltage-gated calcium channels that are present near the primed vesicle [69]. This influx of Ca^{2+} also enables Ca^{2+} to bind to ER ryanodine receptors (RyRs) and inositol 1,4,5-trisphosphate receptors (IP_3Rs) to allow calcium-induced calcium release (CICR) from ER stores [70]–[72]. An increase in intracellular Ca^{2+} concentration is required for Ca^{2+} to bind to C2 domains of a Synaptotagmin calcium sensor, such as Synaptotagmin-VII of lysosomes [66], [73], and for subsequent detachment of Complexin from the ternary bundle [68] (Figure 1). Once Complexin has disassociated, the hydrophobic lipid bilayers of the vesicle membrane and the plasma membrane can fuse via kiss-and-run (partial) or complete fusion. In kiss-and-run fusion, vesicles transiently fuse with the plasma membrane such that soluble cargo is released to the extracellular space, and the vesicle membrane remains separate from the plasma membrane. This method of fusion allows vesicles to be recycled to the TGN. In complete fusion, vesicles permanently fuse with the plasma membrane such that soluble cargo is released to the extracellular space and membrane-bound cargo is secreted into the plasma membrane. This method of fusion involves the diffusion of the vesicle membrane into the plasma membrane, where it then becomes a permanent part of the plasma membrane [74], [75]. The mechanism that regulates kiss-and-run versus complete vesicle fusion is presently unclear.

Calcium-dependent exocytosis can be stimulated *in vitro* by ionomycin. Ionomycin is a biological carrier ionophore produced by the bacterium *Streptomyces conglobatus*. It functions to transport extracellular Ca^{2+} to the inside of a cell and is therefore considered a calcium ionophore. As a lipid molecule, it is hydrophobic and can bind to the plasma membrane of a cell. Ionomycin can then bind Ca^{2+} to shield its positive charge from the hydrophobic membrane, thus allowing the ion to pass across the membrane [76].

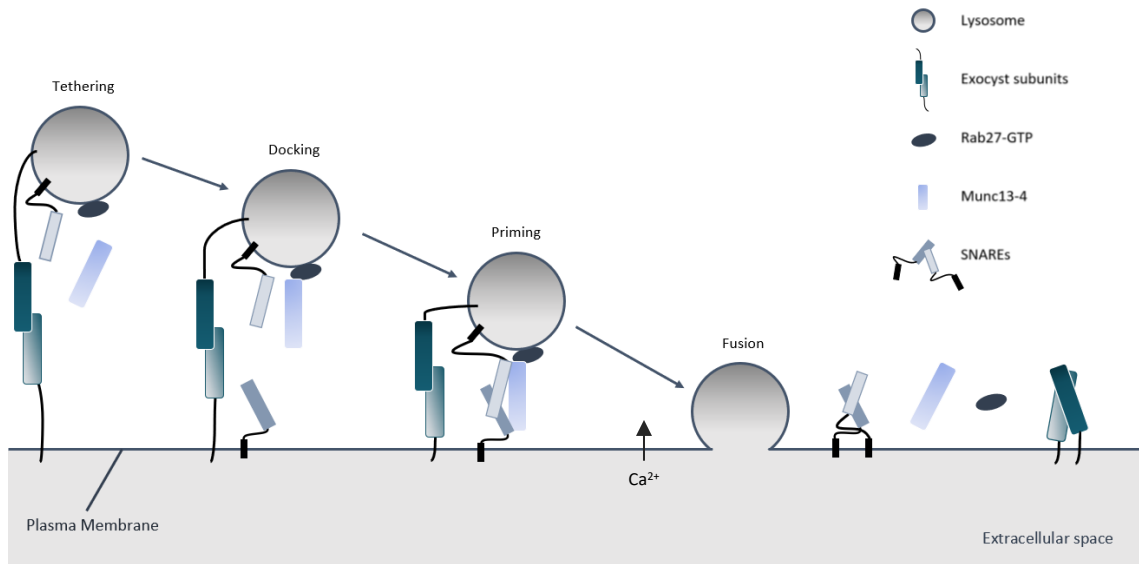


Figure 1 – Lysosomal-mediated calcium-dependent exocytosis

Lysosomal-mediated calcium-dependent exocytosis entails a series of steps. The first step is tethering, which involves the formation of an octameric protein tethering complex termed exocyst. Exocyst subunits recruit and interact with active small GTPase proteins, such as Rab27. Interaction with Rab27 in particular recruits effector protein Munc13-4, which docks the lysosome at the plasma membrane. The Rab27-Munc13-4 complex serves as a nucleation point for self-assembly of SNARE proteins into a ternary complex, comprised of VAMP, Syntaxin, and SNAP protein isoforms. The formation of this ternary complex primes the lysosome at the plasma membrane. Upon an influx of calcium ions via voltage-gated calcium channels, intracellular calcium concentration increases and Synaptotagmin-VII protein enables fusion of the lysosome with the plasma membrane.

1.3 Small GTPase Rab27b

1.3.1 Small GTPases: An Overview

Small GTPases are guanosine nucleotide-bound proteins that are important for a wide variety of intracellular signalling processes. There are over 150 different types of small GTPases that have been discovered to date; among the first to be discovered were members of the Ras family of small GTPases. Prior to establishing their role in normal subcellular signal transduction, Ras GTPases were considered oncoproteins due to the detection of oncogenic mutations in genes encoding these Ras GTPases. Today, all small GTPases are considered part of the Ras superfamily of small GTPases. The Ras GTPase superfamily consists of at least five different families: 1) Ras, 2) Rho, 3) Rab, 4) Arf, and 5) Ran [78]. Small GTPases that belong to each of these families share common genetic sequences and physical structures. These families can be further divided into subfamilies based on their hypervariable C-terminal domains, which have been shown to play a role in subcellular localization of the small GTPase and may alter the effector protein(s) that is targeted [79], [80].

Small GTPases exist in active forms bound to guanosine triphosphate (GTP) and inactive forms bound to guanosine diphosphate (GDP). When a small GTPase is bound to GDP, a guanine exchange factor (GEF) can augment the intrinsic conversion from an inactive GDP-bound form, to an active GTP-bound form. Specifically, a GEF can modify the nucleotide-binding site of the small GTPase such that the affinity for GDP is reduced and GDP is released to the cytoplasm [81]. As the cytoplasmic concentration of GTP is ten times greater than that of GDP, the dissociation of GDP enables GTP to bind in its place [82]. A small GTPase bound to GTP can then interact with an effector protein, and enable downstream cell signaling processes to occur. To terminate cell signaling, GTP bound to the small GTPase must undergo hydrolysis. Although small GTPases possess the ability to catalyze their own GTP hydrolysis at a slow rate, this intrinsic process can be enhanced by a GTPase-activating protein (GAP) (Figure 2). GTP hydrolysis will result in an inactive GDP-bound small GTPase upon release of the γ (third) phosphate of GTP to the cytoplasm [81].

This study focuses on the Rab family of small GTPases, which can be divided into 10 subfamilies: Rab1, Rab3, Rab4, Rab5, Rab6, Rab8, Rab11, Rab22, Rab27, and Rab40 [83]. Post-translational modifications of all Rab GTPases include prenylation, or the addition of hydrophobic groups to certain residues. These hydrophobic groups act as lipid anchors to attach Rab GTPases to the cytosolic face of specific compartment membranes [84]. For example, the post-translational addition of two geranylgeranyl groups to one or two cysteine residues at the C-terminal domain of Rab27 enables active Rab27 to attach to the membranes of lysosomes and LROs during exocytosis [85].

The attachment of prenylated Rab GTPases to compartment membranes is regulated by GDP dissociation inhibitors (GDIs) and GDI displacement factors (GDFs) [86], [87]. At a cell's steady state, prenylated and inactive (GDP-bound) Rab is sequestered in the cytosol by Rab-GDI. For sequestration to occur, Rab-GDI must first shield the hydrophobic groups of Rab from the aqueous cytosolic environment [88]. Rab-GDI can then inhibit the activation of Rab by stabilizing Rab in its inactive conformation [88], [89]. During stimulation of the cell, Rab-GDI can deliver the inactive and prenylated Rab to its specific subcellular location, where it can interact with a GDF [90]. Here, GDF can release the Rab GTPase from sequestration by Rab-GDI. GDP is then free to dissociate from the Rab GTPase, and Rab can re-activate upon binding GTP [86]. GDF has also been shown to be responsible for the initial recruitment of the Rab-GDI-Rab GTPase complex to its specific subcellular location [89].

1.3.2 Small GTPase Rab27b

The Rab27 subfamily in particular is essential for lysosome and LRO trafficking and docking during exocytosis. Isoforms Rab27a and Rab27b have been observed to act separately, cooperatively, redundantly, or sequentially, depending on the cell type and secretory pathway in question [9]. For example, secretion of the melanosome or its contents is dependent on the sequential action of isoform Rab27a. According to this sequential model, Rab27a initially targets and recruits effector protein melanophilin (Slac2-a) for trafficking of the melanosome to the plasma membrane. Rab27a can then target and recruit effector protein Slp2-a (also known as exophilin-4) for docking of the melanosome at the plasma membrane [53]. Conversely, Rab27b has been shown in previous studies to

separately target and recruit effector protein Munc13-4 for calcium-dependent exocytosis. Specifically, effector protein Munc13-4 can catalyze the conformational change of Syntaxin-11, from a closed complex with Munc18-2 into the ternary SNARE bundle [7]. Munc13-4 can also promote the proper Syntaxin-11/VAMP-2 configuration during ternary bundle assembly [67]. In cooperation with Munc18-2, Munc13-4 may be able to ensure the proper Syntaxin-11/SNAP-23 arrangement within this ternary bundle [67], [91]. The Munc13-4 binding domain has been previously mapped to the N-terminal domain of Rab27b, between its C2A domain and MUN domain (amino acids 240 to 543) [92].

In this study, Rab27b T23N, N133I, and Q78L mutants were utilized. Rab27b T23N and N133I are dominant-negative mutants of Rab27b, conferring Rab27b proteins that are defective in binding GTP. Rab27b T23N and N133I are therefore always inactive and as such, cannot interact with effector Munc13-4 to enable calcium-dependent exocytosis to occur. Conversely, Rab27b Q78L is a constitutively-active mutant, conferring a Rab27b protein that is defective in GTP hydrolysis. Rab27b Q78L is therefore always active and as such, continuously interacts with Munc13-4 to enable calcium-dependent exocytosis to occur [93].

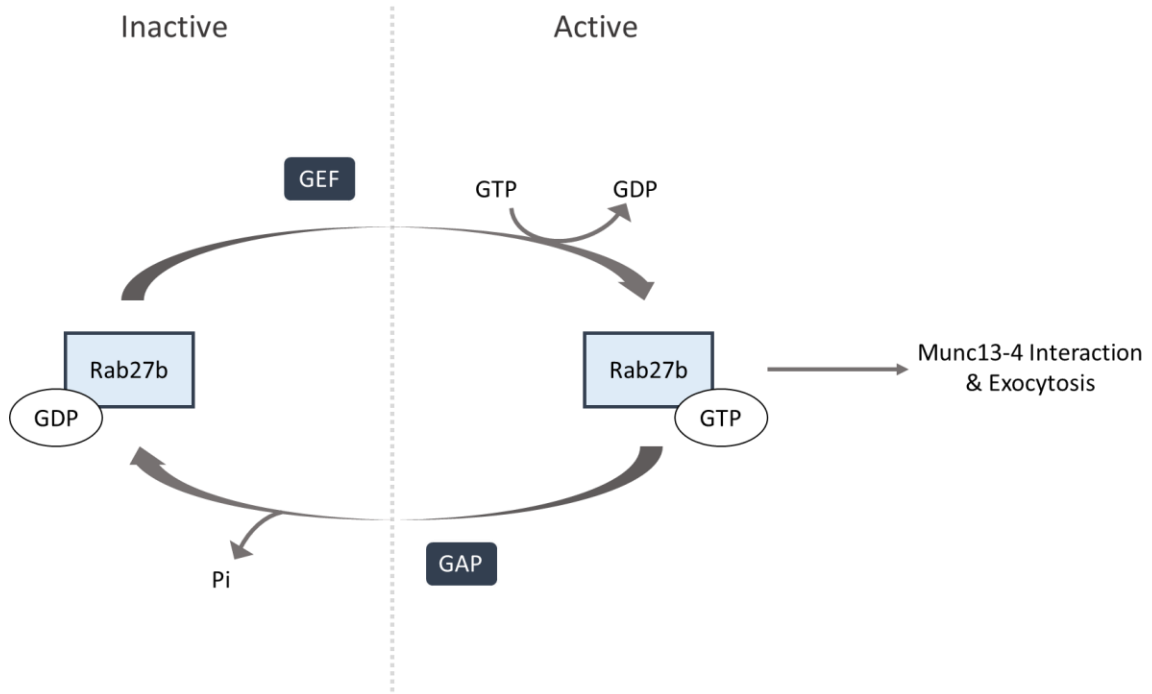


Figure 2 – Small GTPase Rab27b switches between inactive and active forms

Guanine exchange factors (GEFs) catalyze the conversion from inactive Rab27b (bound to GDP) to active Rab27b (bound to GTP) by reducing the affinity of the Rab27b-binding site for GDP. Active Rab27b can subsequently interact with Munc13-4 to enable calcium-dependent exocytosis to occur. GTPase-activating proteins (GAPs) catalyze the conversion from active Rab27b to inactive Rab27b by promoting GTP hydrolysis. Adapted from [94].

1.4 Alzheimer's Disease

1.4.1 Dementia

Dementia is a syndrome that can be medically defined as cognitive dysfunction that is severe enough to interfere with occupational and/or social functioning. These cognitive dysfunctions include varying degrees of impairment in memory, reasoning, planning, language, and/or visuospatial function [95]. Dementia begins when cells in certain regions of the brain lose their synapses and consequently lose the ability to communicate with one another [96], [97]. For example, loss of synapses within the hippocampus can impact one's spatial memory [98], [99]. Abuse of alcohol [100], traumatic brain injuries [101], and neurodegenerative diseases [102] can all lead to some form of dementia. In cases such as alcohol abuse, removing the initial cause of the dementia may prevent further cell damage, but will not result in improvement of cognitive symptoms [100]. Despite the existence of medications that may temporarily ease cognitive and coinciding psychological symptoms, dementia experienced as an effect of a neurodegenerative disease is not only irreversible, it is also progressive in its severity [102].

1.4.2 Overview of Alzheimer's Disease

Alzheimer's disease (AD) is a neurodegenerative disease that accounts for approximately 70% of dementia cases worldwide [103]. As such, AD is the most prevalent form of dementia. The greatest risk factor for development of AD is increasing age [104]; after the age of 65, the risk for developing AD doubles every five years [103].

AD was first described by Dr. Alois Alzheimer in a 51-year-old woman named Auguste Deter. Auguste was an asylum patient who displayed various symptoms of dementia, including short-term memory loss and language impairment [105], [106]. After her death in 1906, Dr. Alzheimer was able to examine histological sections of Auguste's brain using Bielschowsky's silver stain [105]. In addition to extensive cortical atrophy, he observed intracellular fibril bundles and extracellular aggregates within her brain [106]. Respectively, these deposits have since been established as intracellular neurofibrillary tangles comprised of hyperphosphorylated protein tau and extracellular plaques comprised of aggregated protein beta-Amyloid ($A\beta$) [107]. In addition to modern psychological and

neurological testing, the only method of conclusively diagnosing an individual with AD requires post-mortem examination of the brain using methods similar to those used by Dr. Alzheimer over 100 years ago, for observation of both A β and tau deposits [108], [109].

Since the findings of Dr. Alzheimer, intracellular neurofibrillary tangles have been characterized to be present in association cortices and limbic areas (such as the hippocampus) of affected individuals [110], while extracellular amyloid plaques have been characterized to be present diffusely, throughout the cerebral cortex [111]. The topographical pattern of neurofibrillary tangle burden in particular has been observed to be closely coupled to the atrophy of associated brain regions. From mild (early) to severe (late) AD stages, neurofibrillary tangle burden and associated atrophy can first be detected in entorhinal and perirhinal cortices, then in the hippocampus, then in association cortices, and ultimately in the primary neocortex [109], [112].

Presently, there is no curative treatment for AD [113]. As mentioned in Section 1.4.1, medications that exist for neurodegenerative diseases today are only able to ameliorate certain psychological and cognitive symptoms, while regions of the brain continue to atrophy [114], [115]. Neurotransmitter acetylcholine (ACh) has previously been the focus of many drug trials, due to the established role of ACh in the encoding of new episodic memories [116]. In addition, many studies related to AD have observed deficits in the cholinergic system. These observations include lack of cholinergic neurotransmission to the cerebral cortex due to degeneration of cholinergic neurons in the nucleus basalis of Meynert [117], and declines in synthesis of ACh mediated by choline acetyltransferase (ChAT) due to reductions in the expression of this enzyme [118]. Thus, medications to inhibit the function of enzyme acetylcholinesterase (AChE) were developed to prevent the AChE-mediated breakdown of ACh into acetate and choline, and in turn increase amount of ACh available within neuronal synaptic clefts [119]. While alleviating symptoms of dementia, these medications did not target the underlying cause of AD and as such, studies related to this neurodegenerative disease continue to be conducted worldwide to this day [113].

1.4.3 Pathogenesis of Alzheimer's Disease

The most widely accepted theories regarding the pathophysiology of AD center around proteins tau and A β . Many researchers believe that the development of AD ensues with the hyperphosphorylation of tau (the tau hypothesis) [120]. However, strong evidence supports the theory that AD begins with the generation of soluble A β monomers from Amyloid Precursor Protein (APP; the amyloid cascade hypothesis) [121].

APP is a Type I (single-pass) TM protein that is present in all cells. After it is produced within the ER and processed within the TGN, APP can be trafficked to the plasma membrane via constitutive exocytosis. Also present as a TM protein at the plasma membrane is enzyme α -secretase, a type of ADAM (a disintegrin and metalloprotease domain) protein [122]. Co-localization of APP and α -secretase on the plasma membrane of a cell results in progression of the non-amyloidogenic pathway: constitutive α -secretase-mediated cleavage of APP at its Lys16-Leu17 bond and subsequent formation of sAPP α [122], [123]. sAPP α is a soluble fragment of APP that is released to the extracellular space and has been shown in many studies to elicit neuroprotective benefits, such as defence against excitotoxic insults [124], [125]. APP cleavage can also be mediated via the amyloidogenic pathway, which conversely results in formation of toxic peptide A β . In accordance with the amyloidogenic pathway, APP can be internalized via clathrin-mediated endocytosis or pinocytosis prior to cleavage by α -secretase at the plasma membrane [126], [127]. Following the endocytic pathway, internalized APP can be sorted to early endosomes, late endosomes/MVBs, and lysosomes [126]–[128]. Similarly present as a TM protein anchored to the membranes of late endosomes/MVBs and lysosomes is the enzyme β -secretase. β -secretase, also known as β -site APP-cleaving enzyme 1 (BACE1), is an aspartyl protease [129]. It contains one active site with two aspartic acid residues that are each present at a characteristic motif; therefore, β -secretase has previously been suggested to function as a dimer (with each monomer providing one aspartic acid residue) [130]. Although β -secretase can also be found at the early endosome and plasma membrane, it functions optimally at an acidic pH of approximately 4.5. Therefore, the activity of β -secretase is most likely restricted to acidic late endosomes/MVBs and lysosomes [131]. As the active site of β -secretase is targeted toward the lumens of the organelles that it is

localized to, β -secretase-mediated cleavage of APP results in formation and release of soluble fragment sAPP β into the lumens of late endosomes/MVBs and lysosomes. This process leaves behind a TM C-terminal fragment (CTF) known as β -CTF, or C99 [129]. Cleavage of C99 and subsequent formation of A β is now dependent on a TM complex referred to as γ -secretase (Figure 3). The γ -secretase complex is comprised of at least four subunits, including presenilin (PS) 1 or 2, nicastrin, anterior pharynx-defective 1 (APH-1), and presenilin enhancer 2 (PEN-2) [132]. PS has previously been observed to contain the critical catalytic subunit of γ -secretase. Catalysis is specifically dependent on two conserved aspartates in the sixth and seventh TM domains of each PS homologue. Akin to β -secretase, γ -secretase thus functions as an aspartyl protease [133]. Unlike β -secretase, however, γ -secretase presents with a “spatial paradox”: although γ -secretase has been localized to the ER and Golgi apparatus, the production of A β has been observed at the plasma membrane, late endosomes/MVBs, and lysosomes [134]. Furthermore, there is presently little consensus regarding the pH optimum of γ -secretase activity. Enzymatic activity has been observed at a neutral pH of approximately 7.0 [135], at a broad range of pH 6.0-8.4 [136], and even at an acidic pH of approximately 4.5 [134]. Despite this spatial paradox, most researchers believe that the majority of A β production is dependent on internalization of APP from the plasma membrane. In particular, inhibiting clathrin-mediated internalization of APP by altering endocytic signal sequences or blocking scission of vesicles can reduce A β production by 70% [127], [137]. Inhibiting pinocytosis similarly decreases A β production by more than 30% [126]. In addition, strong evidence suggests that this A β production occurs specifically within lysosomes. For example, knockdown of PS1 results in accumulation of C99 at the lysosomal membrane [138]. Acidic pH has also been shown to promote the formation and aggregation of A β [3], [139], with exogenous A β observed to accumulate specifically within the lysosomal lumen [140]. Ultimately, it is likely that γ -secretase-mediated cleavage of C99 and subsequent production of A β occurs at the plasma membrane, late endosomes/MVBs, and lysosomes to varying degrees.

Cleavage by γ -secretase is imprecise and can occur at multiple sites of C99. This results in the production of soluble A β peptide monomers that vary in length, from 39 to 43 amino acids. The most common variants of A β that are generated in a given cell are A β ₄₀ and A β ₄₂, with A β ₄₀ comprising approximately 80-90% of all A β produced and A β ₄₂ comprising

approximately 5-10% of all A β produced [1]. Regardless of length, all A β monomers possess the intrinsic ability to aggregate. This ability is attributable to hydrophobic residues present at the C-terminal domain of the peptide. Although it is less abundant, A β_{42} contains two additional hydrophobic amino acids at its C-terminal domain, which enhance the propensity of A β_{42} to aggregate in comparison to A β_{40} . A β_{42} is therefore the most prevalent A β variant found in amyloid plaques [141], [142]. Aggregation of A β can also result in the formation of oligomers and fibrils. Of these species, oligomers in particular have been implicated in neurotoxicity and associated cell death [143]. Due to its hydrophobicity, A β has also been shown to associate with the lipid bilayer and associated lipid rafts of the plasma membrane [144], [145]. Lipid rafts are ordered microdomains of membranes that contain cholesterol and sphingolipids [145], and have been shown in previous studies to facilitate the formation of A β oligomers at the plasma membrane [146]. Association of A β oligomers with lipid rafts can induce neurotoxicity indirectly through hyperphosphorylation of protein tau [146]–[148].

Tau is a microtubule-associated protein (MAP) necessary for the assembly and stabilization of microtubules within cells. Microtubules are rigid components of the cytoskeleton that are required to maintain a cell's shape and structure [149]. After it is expressed, tau is able to undergo many post-translational modifications that alter its interaction with microtubules, including phosphorylation [150], [151]. Phosphorylation of tau is dynamically regulated by the enzymatic activity of kinases, which catalyze the addition of a phosphate group, and phosphatases, which catalyze the removal of a phosphate group [151]. Phosphorylation of tau has been shown in previous studies to negatively regulate its association with microtubules. Tau hyperphosphorylation would therefore result in a drastic decrease in the ability of tau to bind to microtubules, and its intrinsic ability to aggregate with itself and other MAPs would increase in propensity [152], [153]. This would ultimately decrease the stability of the cell and result in cell death [154]. This would also result in the formation of the primary component of neurofibrillary tangles: paired helical filaments (PHFs) [153]. Tau hyperphosphorylation can occur through upregulation of kinases, downregulation of phosphatases, and altered post-translational modifications of kinases (such as decreased O-GlcNAcylation) that increase kinase activity [152], [155]. As mentioned above, hyperphosphorylation of tau can also occur upon binding of A β to lipid

rafts [146]. Binding of $A\beta$ to lipid rafts forms pores in the plasma membrane [147], which can enable large amounts of extracellular Ca^{2+} to enter the cell. An excessive influx of Ca^{2+} can result in the persistent activation of tau kinases and succeeding tau hyperphosphorylation [148]. Activation of *N*-methyl-D-aspartate (NMDA) receptors by $A\beta$, potentially through interactions with lipid rafts [146], [156], can similarly induce influx of Ca^{2+} and subsequent activation of tau kinases [157].

Additional support for the amyloid cascade hypothesis emerged after the discovery of early-onset forms of AD termed Familial AD (FAD). FAD can surface as a direct result of underlying autosomal dominant mutations in *PSEN1*, *PSEN2*, or *APP* genes [158]. Approximately 1% to 5% of all AD cases are attributed to mutations in these genes [159], [160], which respectively encode proteins PS1, PS2, and APP. While mutations in *PSEN1* or *PSEN2* increase the propensity of γ -secretase to produce $A\beta_{42}$ in particular, mutations in *APP* increase the amount of overall $A\beta$ produced [158]. As the *APP* gene is found on chromosome 21, individuals with Trisomy 21 (Down syndrome) are similarly likely to develop AD due to overexpression of APP and increased production of $A\beta$ [161], [162].

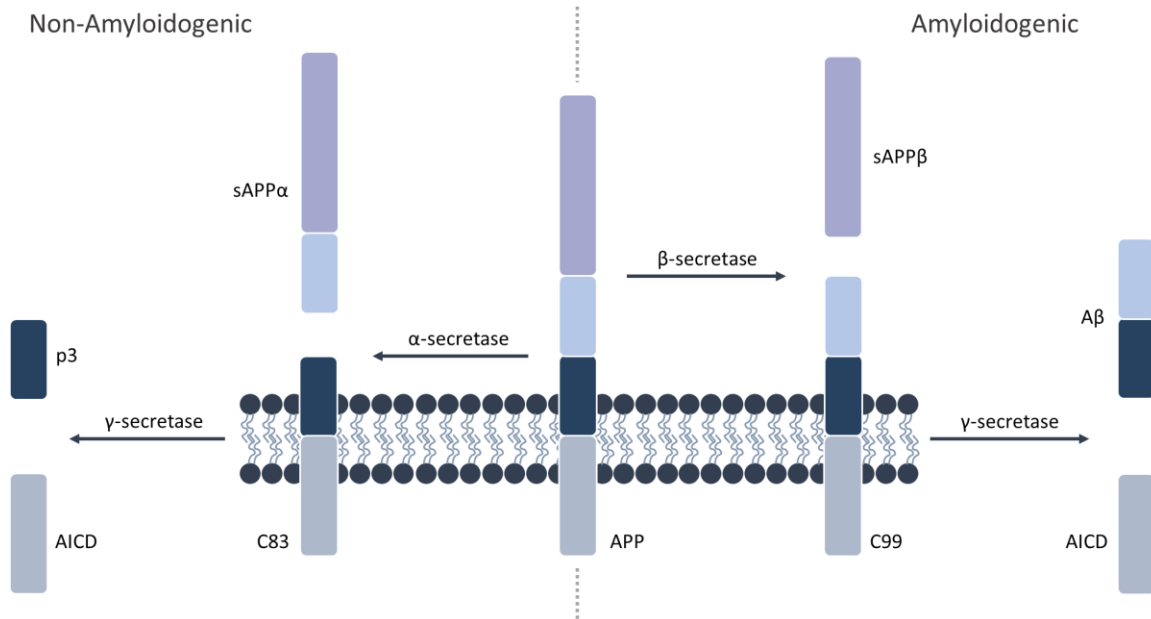


Figure 3 – Processing of APP

Following the amyloidogenic pathway, cleavage of APP by β -secretase leads to the production of soluble fragment sAPP β and membrane-bound C99. Consecutive cleavage by γ -secretase generates A β and APP intracellular domain (AICD). Following the non-amyloidogenic pathway, α -secretase-mediated cleavage of APP produces soluble fragment sAPP α and membrane-bound C83. Consecutive cleavage by γ -secretase generates p3 peptide and AICD. Cleavage of APP by α -secretase thus precludes the generation of A β . Adapted from [163].

1.5 Rationale

1.5.1 Overview

AD can be characterized in post-mortem brain samples by the presence of both extracellular A β plaques and intracellular neurofibrillary tau tangles [108], [109]. While many researchers agree that A β plays a critical early role in the progression of AD, it is not clear how this protein can be found within extracellular amyloid plaques.

A β is generated by β - and γ -secretase-mediated cleavage of TM protein APP [163]. APP can be internalized from the plasma membrane and subsequently trafficked to lysosomes directly [126], [128], or indirectly via the endocytic pathway [127]. Co-localization of APP, active β -secretase, and active γ -secretase at late endosomes/MVBs and lysosomes results in the production of soluble A β monomers within these compartments [134]. A β generated in late endosomes/MVBs can also be trafficked to lysosomes via fusion of lysosomes with late endosomes/MVBs [33].

Studies have shown that A β can not only be generated within and trafficked amongst late endosomes/MVBs and lysosomes, it can also aggregate and be resistant to degradation within these compartments. For example, A β_{42} can aggregate within cultured neuronal cells at a higher rate and to a greater extent at an acidic pH in comparison to a more basic pH [3]. Apart from the ability to break down materials, lysosomes have recently been shown to have the ability to undergo calcium-dependent exocytosis. This was observed by one group upon an increase in fluorescence of lysosomal markers in the presence of extracellular Ca²⁺, but no change in fluorescence of the same lysosomal markers in the presence of calcium chelator ethylene glycol bis(2-aminoethyl)tetraacetic acid (EGTA) [164]. Furthermore, A β_{42} has been observed to specifically accumulate within lysosomes and late endosomes/MVBs when exocytosis was inhibited using tetanus toxin [165]. Interestingly, studies of human AD brains and AD mouse model brains have provided evidence that lysosomal aspartyl protease cathepsin D, which is normally found within the lumens of lysosomes, can also be found in extracellular amyloid plaques [4], [166]. Taken together, results from previous studies provide a great deal of evidence for the existence of lysosomes that are able to release A β to the extracellular space.

Although there is no known protein that is specific to lysosomal-mediated exocytosis, previous studies have shown that small GTPase Rab27b is one of the most important proteins for this process. This is due to the activity of Rab27b effector protein Munc13-4. Munc13-4 is able to interact with SNARE proteins, such as t-SNAREs Syntaxin-11 [167] and SNAP-23 [91], to enable efficient lysosomal membrane to plasma membrane priming during the process of calcium-dependent exocytosis [7], [9].

1.5.2 Hypothesis

It is hypothesized that secretion of A β is mediated by lysosomes in a Rab27b-dependent manner (Figure 4).

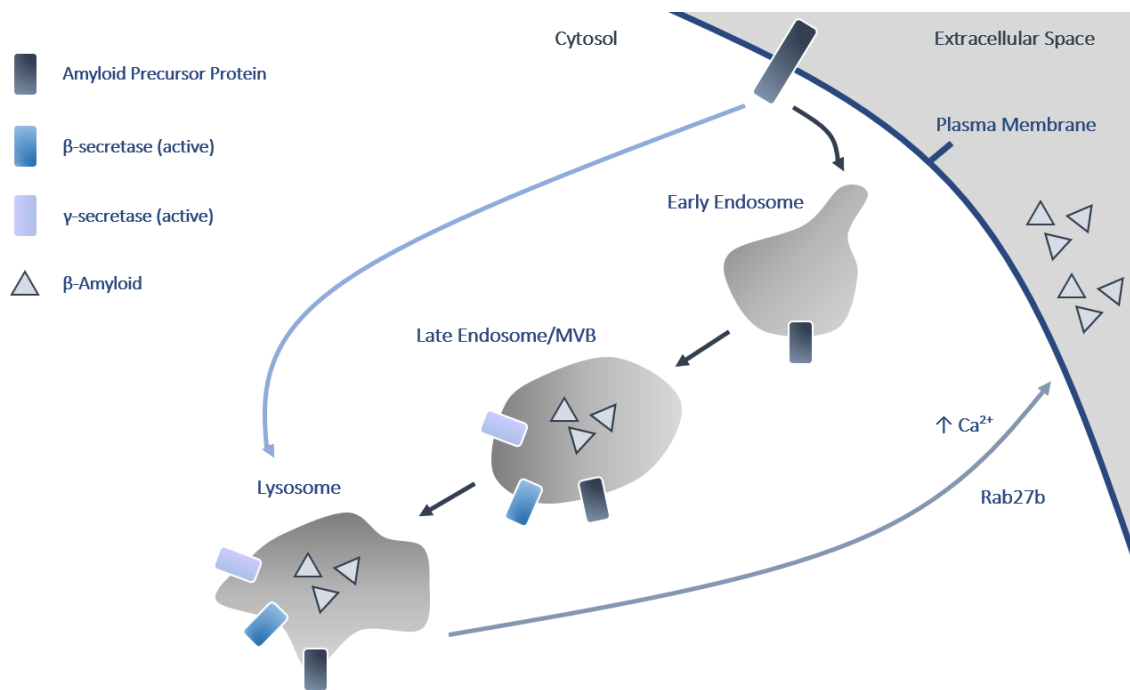


Figure 4 – A β secretion following intracellular trafficking and processing of APP

Amyloid Precursor Protein (APP) can be internalized from the plasma membrane and subsequently trafficked to lysosomes directly, or indirectly via the endocytic pathway. Co-localization of APP, active β -secretase, and active γ -secretase at late endosomes/MVBs and lysosomes results in the production of soluble A β monomers within these compartments. A β generated in late endosomes/MVBs can also be trafficked to lysosomes via fusion of lysosomes with late endosomes/MVBs. Lysosomes can then mediate calcium- and Rab27b-dependent exocytosis of A β .

1.5.3 Objectives

The objectives of this study included:

- 1) To demonstrate storage of A β ₄₂ and A β ₄₀ within lysosomes.
- 2) To demonstrate lysosomal-mediated secretion of A β ₄₂ and A β ₄₀.
- 3) To establish the effects of Rab27b mutants on Rab27b distribution.
- 4) To establish the effects of Rab27b mutants on secretion of A β ₄₂ and A β ₄₀.

1.5.4 Predictions

The predictions of this study were as follows:

- 1) Loading of Neuro-2a (N2A) cells with exogenous A β ₄₀ and A β ₄₂ will result in storage of exogenous A β ₄₂ and A β ₄₀ in lysosomes.
- 2) Initiation of calcium-dependent exocytosis with calcium ionophore ionomycin will result in secretion of lysosome-stored exogenous A β ₄₂ and A β ₄₀.
- 3) There will be an increase in co-localization of Rab27b and lysosomes post-treatment with ionomycin in comparison to pre-treatment in Rab27b wild-type (WT) samples loaded with A β ₄₂ or A β ₄₀.
- 4) There will be no significant differences in co-localization of Rab27b and lysosomes post-treatment in comparison to pre-treatment in Rab27b mutant (T23N, N133I, and Q78L) samples loaded with A β ₄₂ or A β ₄₀.
- 5) There will be a decrease in co-localization of Rab27b and A β ₄₂ or A β ₄₀ post-treatment in comparison to pre-treatment in Rab27b WT samples.
- 6) There will be no significant differences in co-localization of Rab27b and A β ₄₂ or A β ₄₀ post-treatment in comparison to pre-treatment in Rab27b mutant samples.
- 7) Rab27b T23N and N133I samples will secrete significantly less A β ₄₂ and A β ₄₀ in comparison to Rab27b WT, Q78L and control samples, when stimulated with ionomycin.
- 8) Rab27b Q78L samples will secrete significantly more A β ₄₂ and A β ₄₀ in comparison to Rab27b T23N, N133I, WT and control samples.
- 9) There will be no significant differences in secretion of A β ₄₂ in comparison to secretion of A β ₄₀, in control and Rab27b samples.

Chapter 2

2 Materials and Methods

2.1 Cell Culture

Neuro-2a (N2A; ATCC) cells were cultured in Minimum Essential Medium (MEM; Gibco) supplemented with 10% v/v Fetal Bovine Serum (FBS; Gibco) and maintained in 5% CO₂ at 37°C. On day one, 2×10^5 cells were seeded onto 35 mm uncoated glass-bottom (14 mm, No. 1.5 coverslip) confocal dishes (MatTek) in MEM supplemented with 10% FBS. 24 hours later (day two), samples were transiently transfected using Lipofectamine 2000 (Invitrogen), according to manufacturer's instructions. 4.5 hours later, samples were incubated with A β (AnaSpec) overnight in serum-free MEM. 18 hours later (day three), cells were either subjected to ionomycin treatment or imaged under confocal or widefield microscopy. Cells were sub-cultured using 0.25% Trypsin-EDTA (1X; Gibco) every three or four days.

2.2 DNA Constructs

Samples to be imaged under confocal microscopy were transiently transfected with 0.3 μ g LAMP1 tagged to monomeric Cherry Fluorescent Protein (mChFP; control samples) *or* 0.3 μ g LAMP1-mChFP and 0.8 μ g Rab27b T23N, N133I, wild-type (WT), or Q78L tagged to Enhanced Blue Fluorescent Protein (EBFP; Rab27b samples) using Lipofectamine 2000, according to manufacturer's instructions. In this manner, we were able to visualize lysosomes in control samples *or* lysosomes and Rab27b T23N, N133I, WT, or Q78L in Rab27b samples.

DNA construct LAMP1-mChFP was previously cloned in our laboratory. DNA constructs Rab27b-EBFP T23N, N133I, WT, and Q78L were newly generated via subcloning. Specifically, Rab27b-GFP T23N, N133I, WT, and Q78L genes of interest were PCR-amplified using high-fidelity KOD Hot Start DNA polymerase, according to manufacturer's instructions (Sigma-Aldrich). Custom primers used for this reaction included forward primer 5' – ATACAGATCTATGACCGATGGAGACTATGATT – 3' (containing a *Bgl*III restriction site) and reverse primer 5' –

ATACAAGCTTCTAGCAGATACATTTCTTCTCTGG – 3' (containing a *HindIII* restriction site) (Invitrogen). Enzymes *BglIII* and *HindIII* were used for restriction site digestion (Thermo Fisher Scientific), and digested products were respectively extracted and purified using QIAquick Gel Extraction and PCR Purification kits (Qiagen), according to manufacturer's instructions. PCR products were ligated into an EBFP-C1 vector (Addgene plasmid #54738) at a 3:1 ratio using T4 DNA ligase (New England Biolabs), and the recombinant DNA plasmids were sequenced. These recombinant DNA plasmids were then transformed using DH5 α competent *Escherichia coli* cells (Thermo Fisher Scientific). Construct Rab27b-GFP WT was provided by Dr. Reinhard Jahn (Max Planck Institute, Munich, Germany). Rab27b-GFP T23N, N133I, and Q78L constructs were provided by Dr. Miguel Seabra (Imperial College London, London, England).

Samples to be imaged under widefield microscopy were transiently transfected with 0.8 μ g mApple-LAMP1-pHluorin (Addgene plasmid #54918) using Lipofectamine 2000, according to manufacturer's instructions. This allowed us to visualize lysosomal-mediated secretion in real-time.

2.3 A β ₄₀ and A β ₄₂ Preparation

1 mg of human HiLyte Fluor 647-labeled A β ₄₀ or A β ₄₂ (AnaSpec) was resuspended to 1 mM using 1,1,1,3,3,3-hexafluoro-2-propanol (HFIP; Sigma-Aldrich). HFIP was evaporated using medium-speed vacuum centrifugation at room temperature for one hour, yielding A β ₄₀ or A β ₄₂ peptide films. To generate non-aggregates (peptide monomers), peptide films were resuspended to 1 mM using dimethyl sulfoxide (DMSO; Sigma-Aldrich) and exposed to bath sonication at room temperature for 15 minutes. Non-aggregates were diluted to 100 μ M with ice-cold Dulbecco's phosphate-buffered saline (DPBS; Sigma-Aldrich) and vortexed immediately for 30 seconds. Aliquots of non-aggregates were stored at -80°C until use.

2.4 Ionomycin Treatment

1 μ M ionomycin (Sigma-Aldrich) was added to live N2A cells 18 hours after incubation with A β (day three), either bench-side (prior to confocal microscopy) or at the microscope (during widefield microscopy). Bench-side samples were immediately fixed using 4% paraformaldehyde (PFA; Alfa Aesar) after two minutes of treatment with ionomycin. Widefield microscopy samples were discarded after treatment with ionomycin (after time-lapse videos were recorded).

2.5 Confocal Microscopy

Cells were imaged under confocal microscopy using a Leica TCS SP8 inverted microscope (Leica Camera AG, Wetzlar, Germany) operated by Leica LAS X Software, before (live-cell microscopy) and after (fixed-cell microscopy) treatment with ionomycin. All pre- and post-treatment images, including Z-stack images, were acquired using an HC PL APO CS2 63x / 1.40 oil objective. A 50 mW DMDO diode laser was used to excite wavelengths of 405 nm (HyD detector; EBFP fluorophore). A 20 mW AOTF diode laser was used to excite wavelengths of 552 nm (PMT detector; mChFP fluorophore). A 30 mW AOTF diode laser was used to excite wavelengths of 638 nm (HyD detector; HiLyte Fluor 647 fluorophore). 30-frame Z-stack images were acquired at section intervals of 0.1 μ m.

2.6 Widefield Microscopy

Live cells were imaged under widefield microscopy using a Leica DMI6000B inverted microscope (Leica Camera AG, Wetzlar, Germany) operated by Leica LAS X Software. Time-lapse videos were acquired using an HC PL APO 100x / 1.40 oil objective and a Hamamatsu Photometrics Delta EvOLVE EM-CCD camera. An EL6000 metal-halide lamp was used to excite wavelengths of 535 nm (FITC filter cube; ecliptic pHluorin fluorophore), 605 nm (CY3 filter cube; mApple fluorophore), and 705 nm (CY5 filter cube; HiLyte Fluor 647 fluorophore). Samples were placed on a heated and CO₂-perfused stage. 1 μ M ionomycin was added to each sample five seconds after start of time-lapse. Time-lapse videos were recorded for a length of five minutes, and images were acquired at an interval of 0.341 seconds between frames.

2.7 Co-Localization Analyses

Before undergoing co-localization analyses, images of cells taken using the Leica TCS SP8 confocal microscope were first chosen for co-localization analyses. Criteria for choosing a pre-treatment cell required the cell to appear: 1) well-transfected with LAMP1-mChFP (in control samples) *or* LAMP1-mChFP and Rab27b-EBFP WT, Q78L, T23N, or N133I (in Rab27b samples), and 2) well-loaded with HiLyte Fluor 647-labeled A β ₄₀ or A β ₄₂. Criteria for choosing a post-treatment cell required the cell to: 1) appear well-transfected with LAMP1-mChFP (in control samples) *or* LAMP1-mChFP and Rab27b-EBFP WT, Q78L, T23N, or N133I (in Rab27b samples), and 2) contain HiLyte Fluor 647-labeled A β ₄₀ or A β ₄₂ within the field of vision of the cell (intracellular and/or extracellular).

Imaris Software 7 (Bitplane) was used to conduct all co-localization analyses (Appendix 1). This included co-localization of: 1) HiLyte Fluor 647-labeled A β ₄₀ or A β ₄₂ and LAMP1-mChFP (control and Rab27b samples), 2) Rab27b-EBFP (T23N, N133I, WT, or Q78L) and LAMP1-mChFP (Rab27b samples), and 3) Rab27b-EBFP (T23N, N133I, WT, or Q78L) and HiLyte Fluor 647-labeled A β ₄₀ or A β ₄₂ (Rab27b samples). Co-localization can be defined as the occurrence of two fluorochromes in one location. Imaris measures co-localization using a method founded by Costes and Lockett (NIH, NCI/SAIC). This method considers the degree of overlap of two channels by measuring fluorescence intensity of voxels. As such, Imaris automatically corrects for differences in high- and low-intensity voxels (Coloc intensity option: Source channels), rather than simply measuring number of overlapping voxels. Imaris furthermore enables the user to manually set a threshold for percent of data that will be used for signal analysis. To allow for datasets to be compared amongst one another, the threshold set for each channel (green channel: LAMP1-mChFP; red channel: A β ₄₂ and A β ₄₀; blue channel: Rab27b-EBFP T23N, N133I, WT and Q78L) remained constant throughout all analyses that were conducted.

A co-localization channel was built using the specified settings, producing a variety of statistical values. The statistical values used for the purposes of this study were: “percentage of channel A material above threshold A that is co-localized” and “percentage of channel B material above threshold B that is co-localized”. Use of the former or latter value was dependent on the two channels in question. For example, “percentage of channel

A material above threshold A that is co-localized” was used for co-localization analysis of the red channel ($A\beta$) and green channel (LAMP1-mChFP) when the red channel was introduced to the module as channel A. Imaris consequently analyzed, “percentage of $A\beta$ above threshold A that is co-localized with LAMP1-mChFP” instead of “percentage of LAMP1-mChFP above threshold B that is co-localized with $A\beta$ ”. This statistical value was considered the raw data for all subsequent analyses.

2.8 Statistical Analyses

Before statistical analyses were completed, all post-treatment raw data was placed under an exclusion criterion. This exclusion criterion was specific to each corresponding pre- and post-treatment dataset and was regarded as the mean of the pre-treatment raw data. This mean was considered the threshold for exocytosis and as such, any corresponding post-treatment raw data value that was at or above the threshold was excluded from the subsequent statistical analyses, as the cell did not undergo exocytosis. For example, if the mean co-localization percentage of LAMP1-mChFP and $A\beta_{42}$ in control samples was 40% pre-treatment (raw), any co-localization value at or above 40% within the corresponding post-treatment dataset (raw) would be excluded from statistical analyses.

In order to be able to compare between datasets, post-treatment raw data was normalized to corresponding pre-treatment raw data. GraphPad Prism 8 was used to normalize raw data as follows: 1) Each pre-treatment value within a dataset was normalized to 100% by setting 0% as 0 and setting 100% as the mean of the pre-treatment raw data, 2) Each post-treatment value was normalized to its corresponding pre-treatment data by setting 0% as 0 and setting 100% as $Y = \text{mean of the pre-treatment raw data}$. When comparing between pre-treatment datasets, pre-treatment raw data was not normalized.

All subsequent statistical analyses were again performed using GraphPad Prism 8. All groups were tested with a Shapiro-Wilk normality test. An unpaired t-test with Welch’s correction was conducted when determining whether there was a statistically significant difference between pre- and post-treatment normalized data, within a dataset. Welch’s correction was necessary to correct for unequal variances within a dataset. A Brown-Forsythe and Welch’s one-way Analysis of Variance (ANOVA) followed by a post hoc

Dunnett's T3 multiple comparison test was conducted when determining whether there was a statistically significant difference between pre- or post-treatment normalized data, between datasets. Brown-Forsythe and Welch's corrections were necessary to correct for unequal variances between datasets.

All data herein is expressed as mean \pm standard error of the mean (SEM). $p < 0.05$ was considered a minimum critical value for statistical significance throughout this study.

Chapter 3

3 Results

3.1 Exogenous A β Accumulates Within Lysosomes

To demonstrate storage of A β within lysosomes, live N2A cells that were transfected with LAMP1-mChFP and loaded with exogenous A β were imaged under confocal microscopy. Acquired images were used to calculate percent co-localization of LAMP1-mChFP and HiLyte Fluor 647-labeled A β_{42} or A β_{40} using Imaris Software 7. In Imaris, a signal intensity threshold of the top 2% of the data was chosen for the green channel (LAMP1-mChFP), because lysosome burden within mammalian cells ranges from 1% to 15% [168]. Thresholding the top 2% of voxels omitted signals that might have arisen from low amounts of newly-synthesized LAMP1 found in the ER, Golgi apparatus, and/or late endosomes/MVBs [20], [21]. Conversely, A β signal was very bright and appeared to display a restricted pattern of localization (to lysosomes or to the plasma membrane). However, as A β cell burden can vary widely depending on the amount of A β that is internalized by the cell and the amount of A β that is secreted, the signal threshold for A β needed to be determined empirically across many images. To capture the majority of A β that was internalized or secreted, a signal intensity threshold range of the top 0.5% to 2% of the data was chosen for the red channel (A β_{42} and A β_{40}).

3.1.1 Intracellular A β Localization

51.86% \pm 0.93% of HiLyte Fluor 647-labeled A β_{42} co-localized with LAMP1-mChFP within N2A cells, prior to treatment with ionomycin (N=3, n=141) (Figure 5 and Figure 7). Similarly, 34.44% \pm 2.58% of HiLyte Fluor 647-labeled A β_{40} co-localized with LAMP1-mChFP within N2A cells, prior to treatment with ionomycin (N=5, n=106) (Figure 6 and Figure 7). Therefore, A β can accumulate within lysosomes.

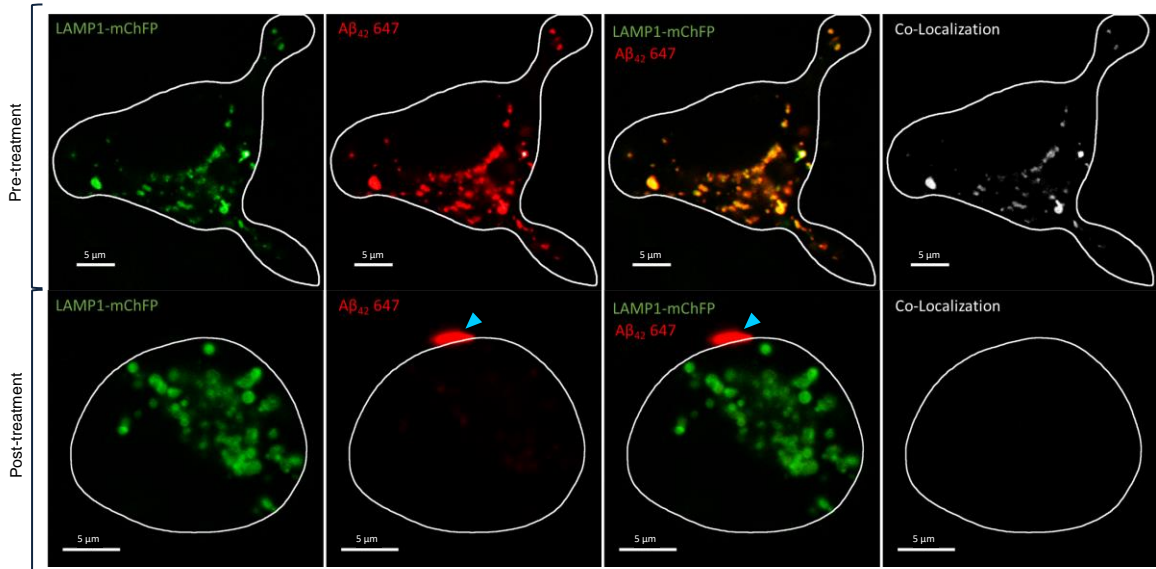


Figure 5 – Co-localization of LAMP1-mChFP and A β ₄₂

LAMP1-mChFP and HiLyte Fluor 647-labeled A β ₄₂ co-localized in N2A cells pre-treatment with ionomycin. Conversely, LAMP1-mChFP and HiLyte Fluor 647-labeled A β ₄₂ did not co-localize in N2A cells post-treatment with ionomycin. White outlines represent the plasma membranes of N2A cells. Blue arrowheads highlight extracellular accumulations of HiLyte Fluor 647-labeled A β ₄₂ proximal to the plasma membrane (post-treatment). Scale bars represent 5 μ m.

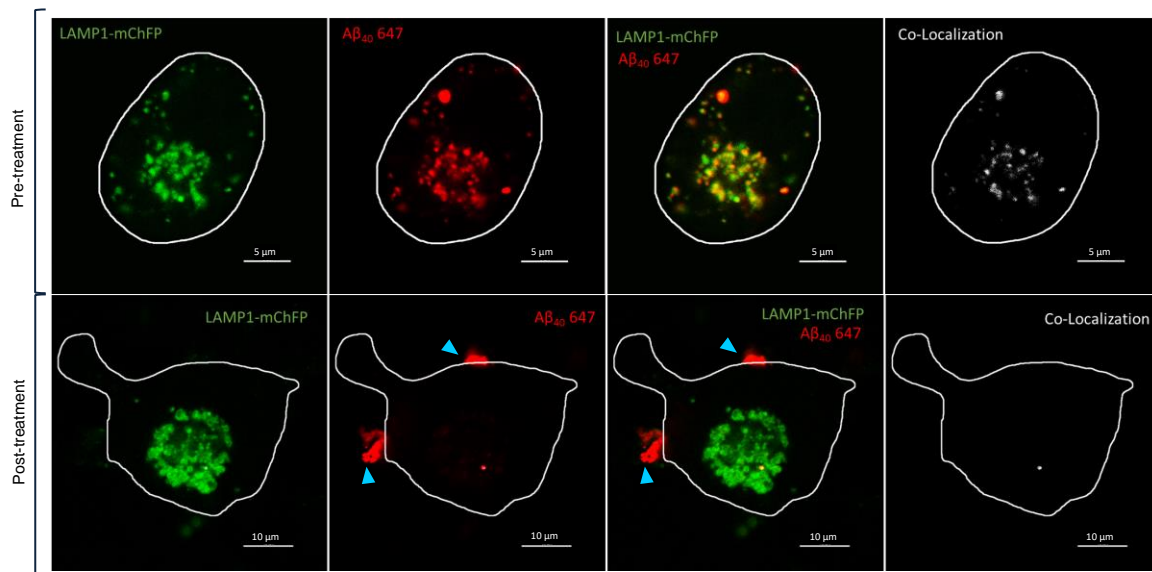


Figure 6 – Co-localization of LAMP1-mChFP and A β ₄₀

LAMP1-mChFP and HiLyte Fluor 647-labeled A β ₄₀ co-localized within N2A cells pre-treatment with ionomycin. Conversely, LAMP1-mChFP and HiLyte Fluor 647-labeled A β ₄₀ did not co-localize within N2A cells post-treatment with ionomycin. White outlines represent the plasma membranes of N2A cells. Blue arrowheads highlight extracellular accumulations of HiLyte Fluor 647-labeled A β ₄₀ proximal to the plasma membrane (post-treatment). Pre-treatment scale bars represent 5 μ m. Post-treatment scale bars represent 10 μ m.

Pre-treatment: LAMP1-mChFP & AB Co-Localization

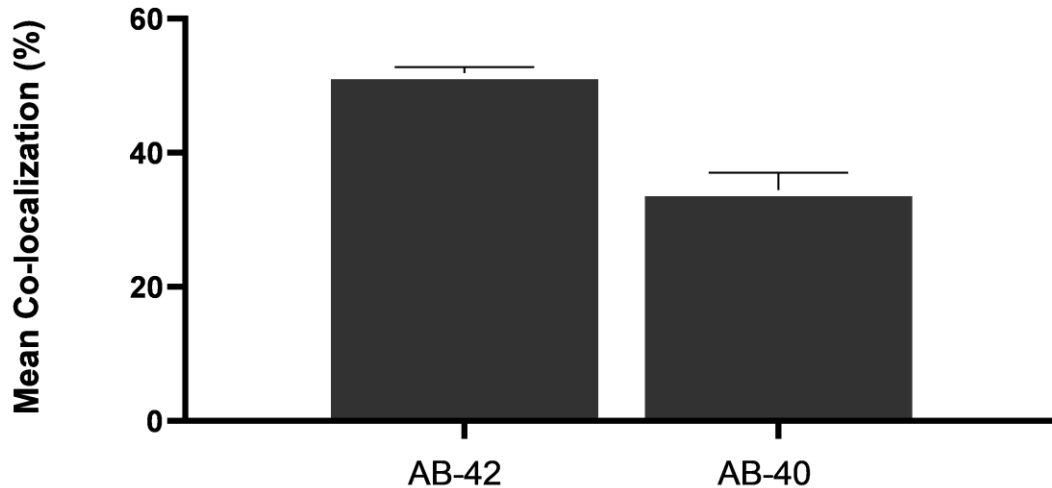


Figure 7 – Pre-treatment co-localization of LAMP1-mChFP and A β

There were no significant differences in LAMP1-mChFP and HiLyte Fluor 647-labeled A β co-localization between A β_{42} and A β_{40} samples, as determined by Brown-Forsythe and Welch ANOVA tests followed by post hoc Dunnett's T3 multiple comparisons tests. All results are presented as raw mean \pm SEM.

3.1.2 Between-Group Comparison

To determine whether there was a difference in A β loading between A β_{42} and A β_{40} samples, pre-treatment percent co-localization of LAMP1-mChFP and HiLyte Fluor 647-labeled A β_{42} (51.86% \pm 0.93%), and pre-treatment percent co-localization of LAMP1-mChFP and HiLyte Fluor 647-labeled A β_{40} (34.44% \pm 2.58%) were compared. Raw pre-treatment data was subjected to Brown-Forsythe and Welch ANOVA tests followed by post hoc Dunnett's T3 multiple comparisons tests. There were no significant differences pre-treatment with ionomycin when comparing between A β_{42} (N=3, n=141) and A β_{40} (N=5, n=106) groups. Therefore, there was no significant difference in A β loading between samples (Figure 7).

3.2 A β Secretion is Mediated by Lysosomes

To quantitatively demonstrate lysosomal-mediated secretion of A β , N2A cells that were transfected with LAMP1-mChFP and loaded with exogenous A β were treated with ionomycin, fixed, and imaged under confocal microscopy. Images acquired pre- and post-treatment with ionomycin were used to calculate percent co-localization of LAMP1-mChFP and HiLyte Fluor 647-labeled A β_{42} or A β_{40} using Imaris Software 7. A signal intensity threshold of the top 2% of the data was used for LAMP1-mChFP, and a signal intensity threshold range of the top 0.5% to 2% of the data was used for A β . The raw mean co-localization percentages of LAMP1-mChFP and HiLyte Fluor 647-labeled A β were as follows: 51.86% \pm 0.93% in pre-treatment A β_{42} samples, 34.44% \pm 2.58% in pre-treatment A β_{40} samples (Figure 7), 6.28% \pm 1.30% in post-treatment A β_{42} samples, and 8.41% \pm 1.91% in post-treatment A β_{40} samples (data not shown). To qualitatively observe lysosomal-mediated secretion of A β , N2A cells that were transfected with mApple-LAMP1-pHluorin and loaded with exogenous A β were treated with ionomycin during live-cell widefield microscopy (data not shown).

3.2.1 Within-Group Comparison

To determine whether A β_{42} and A β_{40} peptides undergo lysosomal-mediated secretion, pre-treatment percent co-localization of LAMP1-mChFP and HiLyte Fluor 647-labeled A β_{42} or A β_{40} was compared to post-treatment percent co-localization of LAMP1-mChFP and HiLyte Fluor 647-labeled A β_{42} or A β_{40} . Normalized data was subjected to unpaired t-tests with Welch's correction. LAMP1-mChFP and HiLyte Fluor 647-labeled A β_{42} co-localization significantly decreased post-treatment (N=3, n=48) with ionomycin in comparison to pre-treatment (N=3, n=141) ($p < 0.0001$) (Figure 5). This was an 87.89% \pm 3.09% decrease in co-localization (Figure 8). Similarly, LAMP1-mChFP and HiLyte Fluor 647-labeled A β_{40} co-localization significantly decreased post-treatment (N=3, n=37) with ionomycin in comparison to pre-treatment (N=5, n=106) ($p < 0.0001$) (Figure 6). This was a 75.58% \pm 9.32% decrease in co-localization (Figure 8). Therefore, A β_{42} and A β_{40} peptides underwent significant lysosomal-mediated secretion. Interestingly, secreted A β_{42} and A β_{40} peptides were observed to accumulate proximal to the plasma membranes of N2A cells (Figure 5 and Figure 6).

3.2.2 Between-Group Comparison

To determine whether there was a difference in lysosomal-mediated secretion of A β ₄₂ and A β ₄₀, post-treatment percent co-localization of LAMP1-mChFP and HiLyte Fluor 647-labeled A β ₄₂ was compared to post-treatment percent co-localization of LAMP1-mChFP and HiLyte Fluor 647-labeled A β ₄₀. Normalized post-treatment data was subjected to Brown-Forsythe and Welch ANOVA tests followed by post hoc Dunnett's T3 multiple comparisons tests. There were no significant differences post-treatment with ionomycin when comparing between A β ₄₂ (N=3, n=48) and A β ₄₀ (N=3, n=37) groups (Figure 8). Therefore, there was no difference in lysosomal-mediated secretion of A β ₄₂ and A β ₄₀.

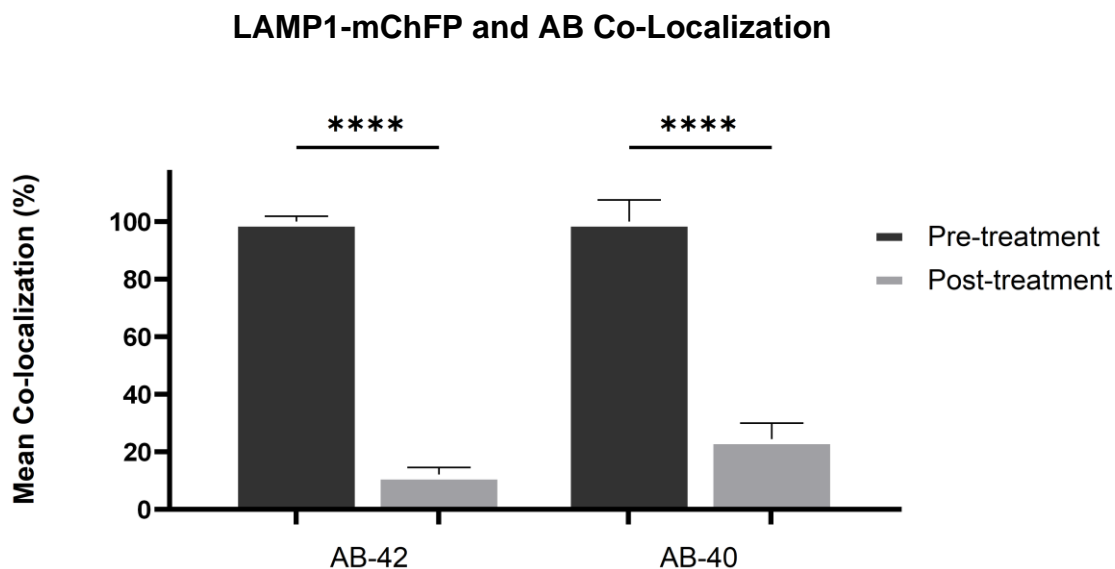


Figure 8 – Mean co-localization of LAMP1-mChFP and A β

LAMP1-mChFP and HiLyte Fluor 647-labeled A β ₄₂ co-localization significantly decreased post-treatment (N=3, n=48) with ionomycin in comparison to pre-treatment (N=3, n=141) ($p < 0.0001$). Similarly, LAMP1-mChFP and HiLyte Fluor 647-labeled A β ₄₀ co-localization significantly decreased post-treatment (N=3, n=37) with ionomycin in comparison to pre-treatment (N=5, n=106) ($p < 0.0001$). There were no significant differences pre- or post-treatment with ionomycin when comparing between A β ₄₂ and A β ₄₀ groups. Dark bars indicate pre-treatment with ionomycin, and light bars indicate post-treatment with ionomycin. All results are presented as normalized mean \pm SEM. Asterisks indicate statistically significant changes post-treatment with ionomycin in comparison to pre-treatment, as determined by unpaired t-tests with Welch's correction. **** $p < 0.0001$

3.3 Subcellular Distribution of Rab27b

To establish the effects of Rab27b mutants on Rab27b distribution, N2A cells that were transfected with LAMP1-mChFP and Rab27b-EBFP WT, Q78L, T23N, or N133I and loaded with exogenous A β were imaged under confocal microscopy before and after treatment with ionomycin. Images acquired pre- and post-treatment with ionomycin were used to calculate percent co-localization of Rab27b-EBFP and LAMP1-mChFP or Rab27b-EBFP and A β using Imaris Software 7. A signal intensity threshold of the top 2% of the data was chosen for LAMP1-mChFP, and a signal intensity threshold range of the top 0.5% to 2% of the data was chosen for A β . Although there has been no research to date regarding Rab27b cell burden, the majority of inactive Rab27b (WT) should be present diffusely in the cytoplasm, and the majority of active Rab27b (WT) should be localized to lysosomal membranes or the plasma membrane [169]. A signal intensity threshold range of the top 2% to 5% of the data for the blue channel (Rab27b-EBFP T23N, N133I, WT, and Q78L) was therefore required to capture the broad distribution of Rab27b. This threshold range was established empirically across many images. The raw mean co-localization percentages of Rab27b-EBFP and LAMP1-mChFP in Rab27b samples are listed in Table 1. The raw mean co-localization percentages of Rab27b-EBFP and A β in Rab27b samples are listed in Table 2.

Table 1 – Raw mean co-localization of Rab27b-EBFP and LAMP1-mChFP

A β	Rab27b	Pre-treatment Co-localization (%)	Post-treatment Co-localization (%)
A β ₄₂	T23N	6.61 \pm 0.58	5.40 \pm 0.50
	N133I	6.95 \pm 0.48	7.52 \pm 1.02
	WT	9.53 \pm 0.74	9.17 \pm 0.18
	Q78L	10.88 \pm 0.97	11.15 \pm 1.52
A β ₄₀	T23N	6.51 \pm 0.97	4.31 \pm 0.28
	N133I	6.68 \pm 0.86	5.25 \pm 0.40
	WT	10.68 \pm 1.31	10.03 \pm 1.12
	Q78L	12.57 \pm 0.49	14.24 \pm 1.60

Table 2 – Raw mean co-localization of Rab27b-EBFP and A β

A β	Rab27b	Pre-treatment Co-localization (%)	Post-treatment Co-localization (%)
A β ₄₂	T23N	10.82 \pm 0.45	10.59 \pm 3.66
	N133I	13.55 \pm 1.50	9.92 \pm 2.07
	WT	16.48 \pm 1.05	10.72 \pm 2.72
	Q78L	17.71 \pm 3.28	8.60 \pm 1.91
A β ₄₀	T23N	10.80 \pm 3.49	5.72 \pm 1.35
	N133I	9.69 \pm 0.77	6.42 \pm 0.93
	WT	18.57 \pm 2.87	9.11 \pm 2.53
	Q78L	18.26 \pm 1.56	12.65 \pm 3.09

3.3.1 No Differences in Rab27b and Lysosome Co-Localization

To determine whether there was a difference in co-localization of Rab27b and lysosomes in A β ₄₂ and A β ₄₀ groups, raw pre- and normalized post-treatment datasets were subjected to unpaired t-tests with Welch's correction, in addition to Brown-Forsythe and Welch ANOVA tests followed by post hoc Dunnett's T3 multiple comparisons tests. There were no significant differences in pre- and/or post-treatment co-localization of Rab27b-EBFP and LAMP1-mChFP in A β ₄₂ and A β ₄₀ groups amongst all Rab27b samples (Rab27b T23N, N133I, WT, and Q78L) (Figure 9 and Figure 10).

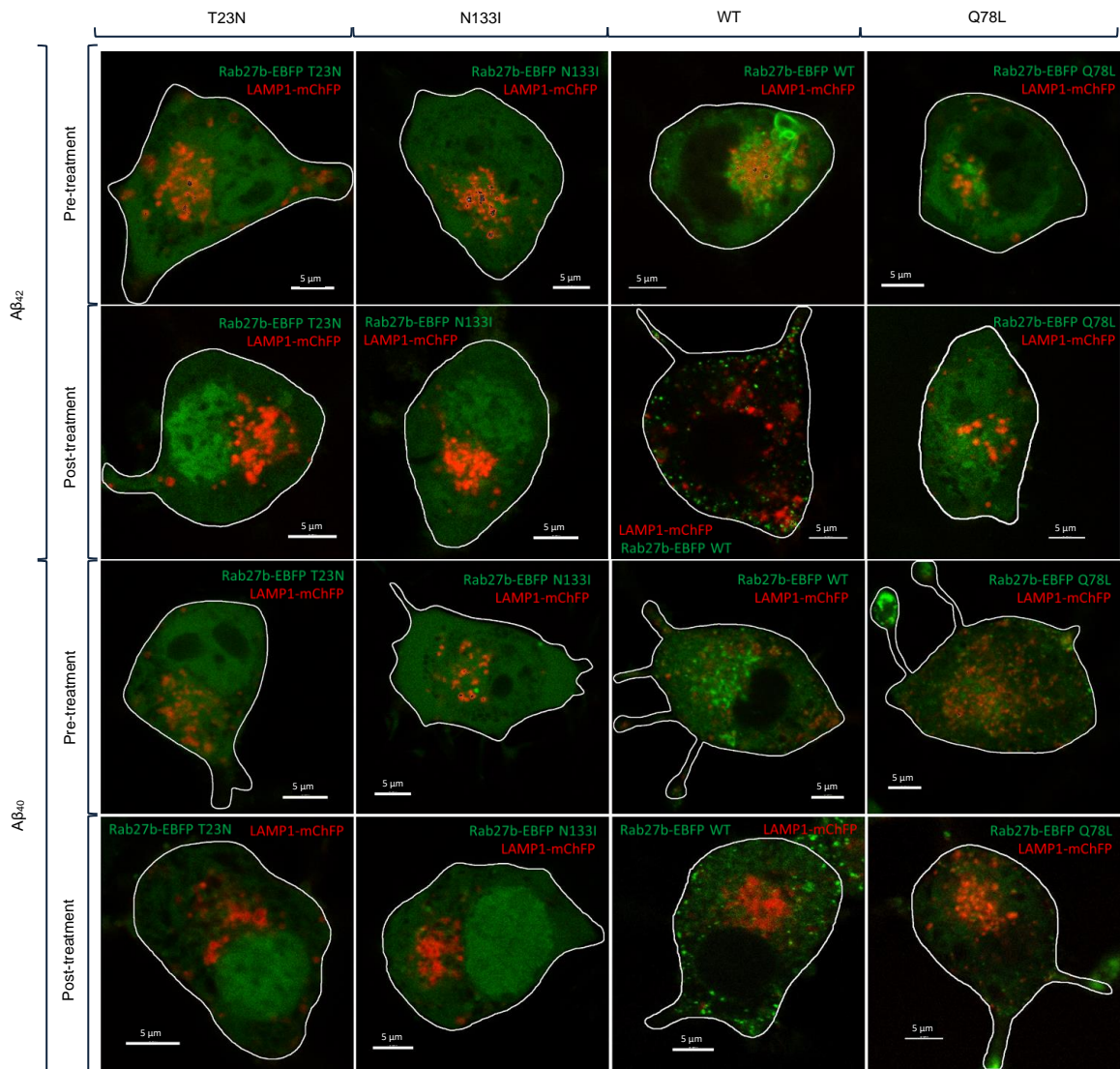


Figure 9 – Co-localization of LAMP1-mChFP and Rab27b-EBFP

Co-localization of LAMP1-mChFP and Rab27b-EBFP in HiLyte Fluor 647-labeled Aβ₄₂ and Aβ₄₀ samples pre- and post-treatment with ionomycin. White outlines represent the plasma membranes of N2A cells. Scale bars represent 5 μm.

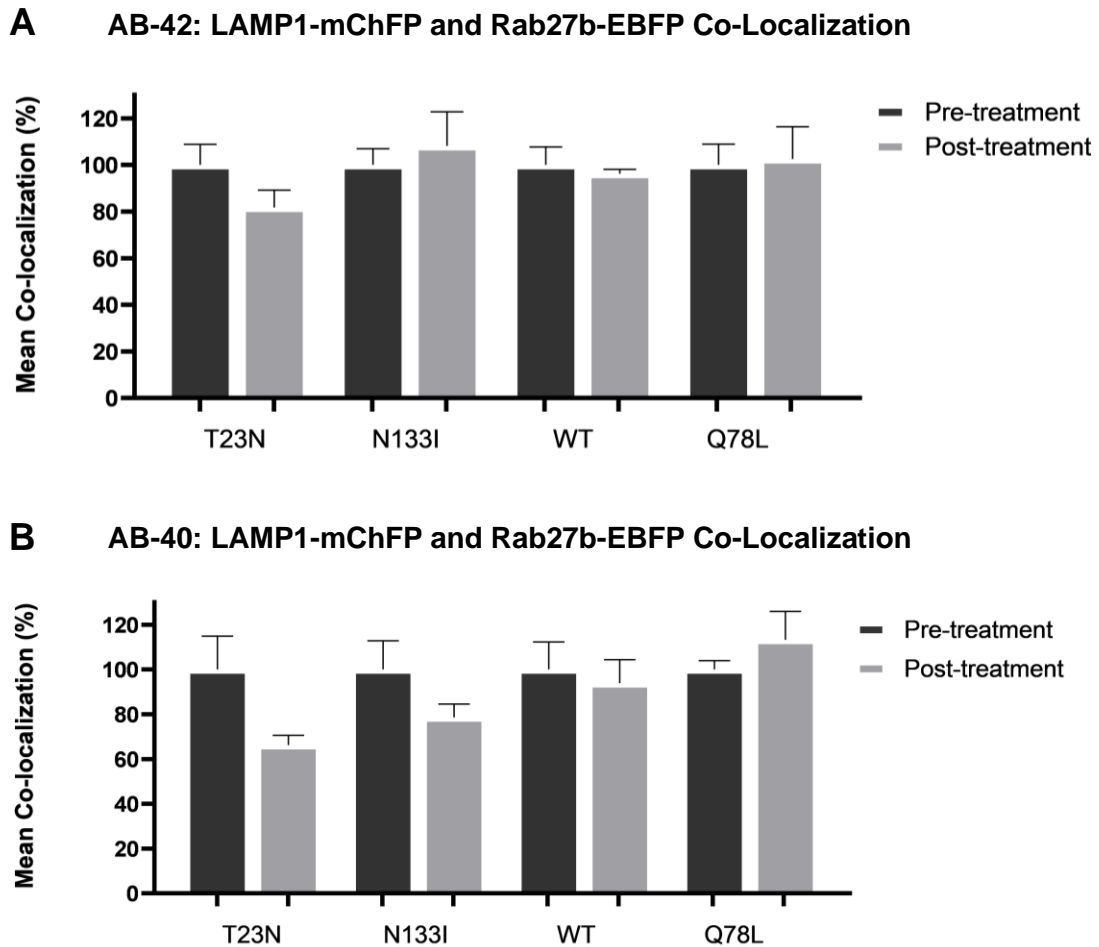


Figure 10 – Mean co-localization of LAMP1-mChFP and Rab27b-EBFP

There were no significant differences in pre- and/or post-treatment co-localization of LAMP1-mChFP and Rab27b-EBFP in (A) $A\beta_{42}$ and (B) $A\beta_{40}$ groups amongst all Rab27b samples, as determined by unpaired t-tests with Welch's correction, in addition to Brown-Forsythe and Welch ANOVA tests followed by post hoc Dunnett's T3 multiple comparisons tests. Dark bars indicate pre-treatment with ionomycin, and light bars indicate post-treatment with ionomycin. All results are presented as normalized mean \pm SEM.

3.3.2 Differences in Rab27b and A β Co-Localization

To determine whether there was a difference in co-localization of Rab27b and A β amongst Rab27b samples (Rab27b T23N, N133I, WT, and Q78L), raw pre- and normalized post-treatment datasets were subjected to unpaired t-tests with Welch's correction, in addition to Brown-Forsythe and Welch ANOVA tests followed by post hoc Dunnett's T3 multiple comparisons tests. Rab27b-EBFP Q78L and HiLyte Fluor 647-labeled A β_{42} co-localization significantly decreased post-treatment (N=5, n=28) with ionomycin in comparison to pre-treatment (N=7, n=36) ($p < 0.05$). This was a $51.46\% \pm 21.45\%$ decrease in co-localization (Figure 11 and Figure 12A). Rab27b-EBFP N133I and HiLyte Fluor 647-labeled A β_{40} co-localization significantly decreased post-treatment (N=5, n=35) with ionomycin in comparison to pre-treatment (N=5, n=40) ($p < 0.05$). This was a $33.77\% \pm 12.48\%$ decrease in co-localization. Rab27b-EBFP WT and HiLyte Fluor 647-labeled A β_{40} co-localization significantly decreased post-treatment (N=6, n=42) with ionomycin in comparison to pre-treatment (N=7, n=28) ($p < 0.05$). This was a $50.92\% \pm 20.61\%$ decrease in co-localization (Figure 11 and Figure 12B). There were no significant differences in co-localization of Rab27b and A β_{42} or A β_{40} between Rab27b samples.

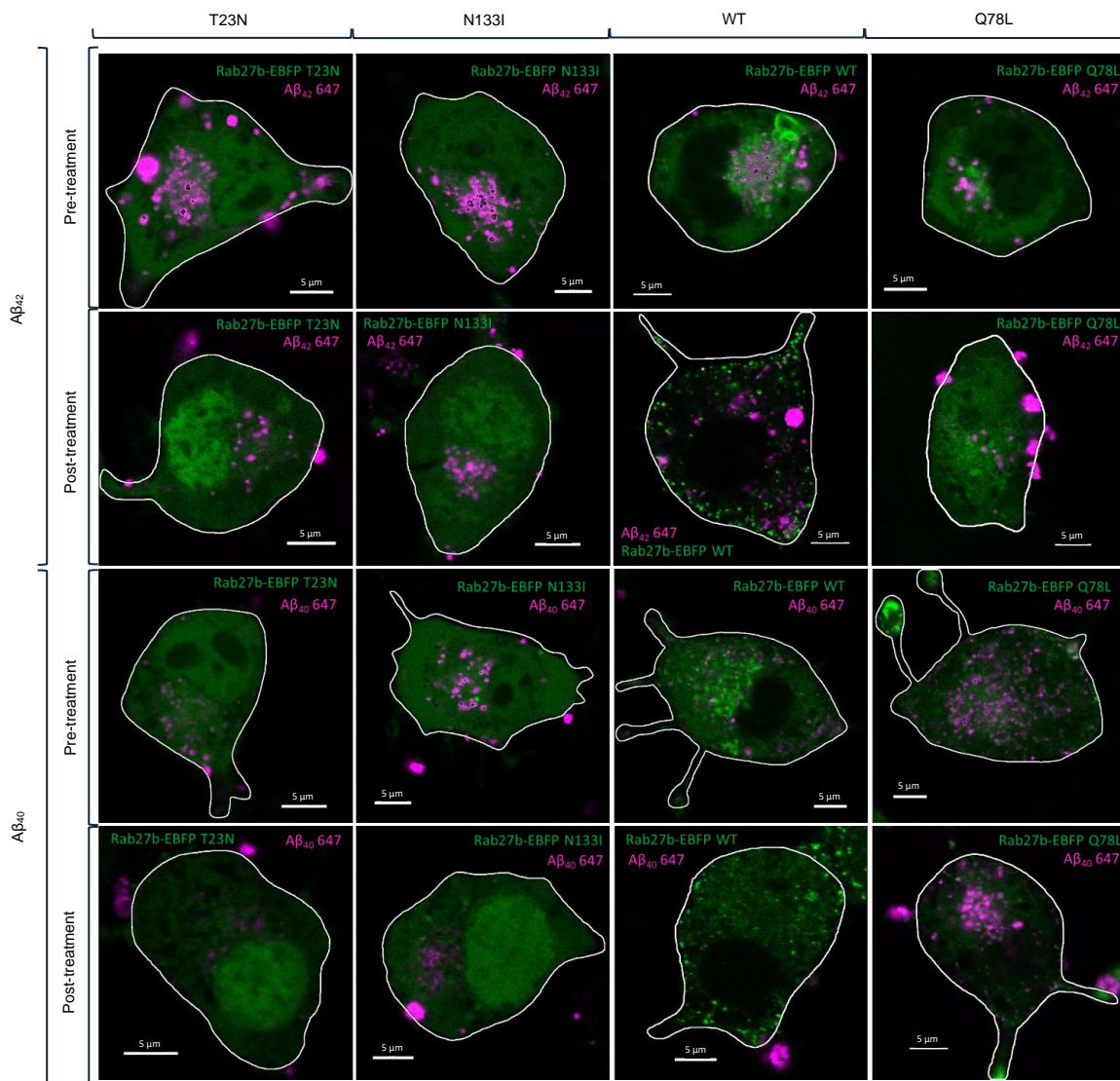


Figure 11 – Co-localization of Rab27b-EBFP and Aβ in Rab27b samples

Co-localization of Rab27b-EBFP and HiLyte Fluor 647-labeled Aβ₄₂ and Aβ₄₀ in N2A cells pre- and post-treatment with ionomycin. White outlines represent the plasma membranes of N2A cells. Scale bars represent 5 μm.

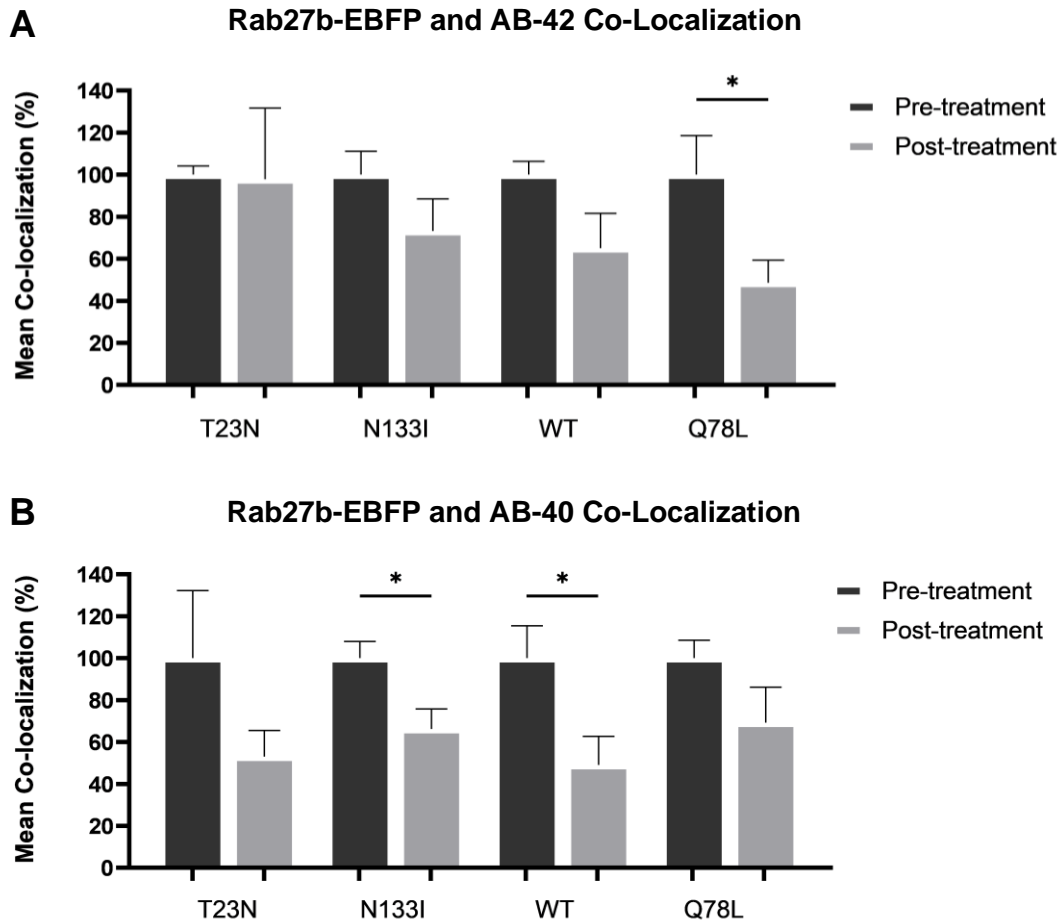


Figure 12 – Mean co-localization of Rab27b-EBFP and A β in Rab27b samples

(A) Rab27b-EBFP Q78L and HiLyte Fluor 647-labeled A β ₄₂ co-localization significantly decreased post-treatment (N=5, n=28) with ionomycin in comparison to pre-treatment (N=7, n=36) ($p < 0.05$). (B) Rab27b-EBFP N133I and HiLyte Fluor 647-labeled A β ₄₀ co-localization significantly decreased post-treatment (N=5, n=35) with ionomycin in comparison to pre-treatment (N=5, n=40) ($p < 0.05$). Rab27b-EBFP WT and HiLyte Fluor 647-labeled A β ₄₀ co-localization significantly decreased post-treatment (N=6, n=42) with ionomycin in comparison to pre-treatment (N=7, n=28) ($p < 0.05$).

There were no differences in co-localization of Rab27b-EBFP and A β ₄₂ or A β ₄₀ between Rab27b samples, as determined by Brown-Forsythe and Welch ANOVA tests followed by post hoc Dunnett's T3 multiple comparisons tests. Dark bars indicate pre-treatment with ionomycin, and light bars indicate post-treatment with ionomycin. All results are presented as normalized mean \pm SEM. Asterisks indicate statistically significant changes between pre- and post-treatment samples, as determined by unpaired t-tests with Welch's correction. * $p < 0.05$

3.4 Rab27b Mutants Alter Lysosomal-Mediated Secretion of Exogenous A β

To establish the effects of Rab27b mutants on secretion of A β , N2A cells that were transfected with LAMP1-mChFP and Rab27b-EBFP WT, Q78L, T23N, or N133I and loaded with exogenous A β were imaged under confocal microscopy before and after treatment with ionomycin. Images acquired pre- and post-treatment with ionomycin were used to calculate percent co-localization of LAMP1-mChFP and HiLyte Fluor 647-labeled A β_{42} or A β_{40} using Imaris Software 7. A signal intensity threshold of the top 2% of the data was used for LAMP1-mChFP, a signal intensity threshold range of the top 0.5% to 2% of the data was used for A β , and a signal intensity threshold range of the top 2% to 5% was used for Rab27b. The raw mean co-localization percentages of LAMP1-mChFP and A β in Rab27b samples are listed in Table 3.

Table 3 – Raw mean co-localization of LAMP1-mChFP and A β

A β	Rab27b	Pre-treatment Co-localization (%)	Post-treatment Co-localization (%)
A β_{42}	T23N	45.36 \pm 2.15	31.86 \pm 3.56
	N133I	47.09 \pm 3.68	34.01 \pm 2.40
	WT	44.49 \pm 1.87	26.56 \pm 7.90
	Q78L	37.41 \pm 4.95	14.92 \pm 4.91
A β_{40}	T23N	40.17 \pm 4.99	28.23 \pm 6.09
	N133I	35.00 \pm 5.13	25.30 \pm 2.82
	WT	32.48 \pm 3.42	13.21 \pm 4.59
	Q78L	37.99 \pm 3.47	22.28 \pm 6.15

3.4.1 A β ₄₂: Pre-Treatment Between-Group Comparison

To confirm that results observed were not due to differences in A β loading, pre-treatment percent co-localization of HiLyte Fluor 647-labeled A β ₄₂ and LAMP1-mChFP was compared between Rab27b and control samples. Raw pre-treatment data was subjected to Brown-Forsythe and Welch ANOVA tests followed by post hoc Dunnett's T3 multiple comparisons tests. There were no significant differences in HiLyte Fluor 647-labeled A β ₄₂ and LAMP1-mChFP co-localization between Rab27b and control samples pre-treatment with ionomycin (Figure 13). Therefore, there were no differences in A β ₄₂ loading between samples.

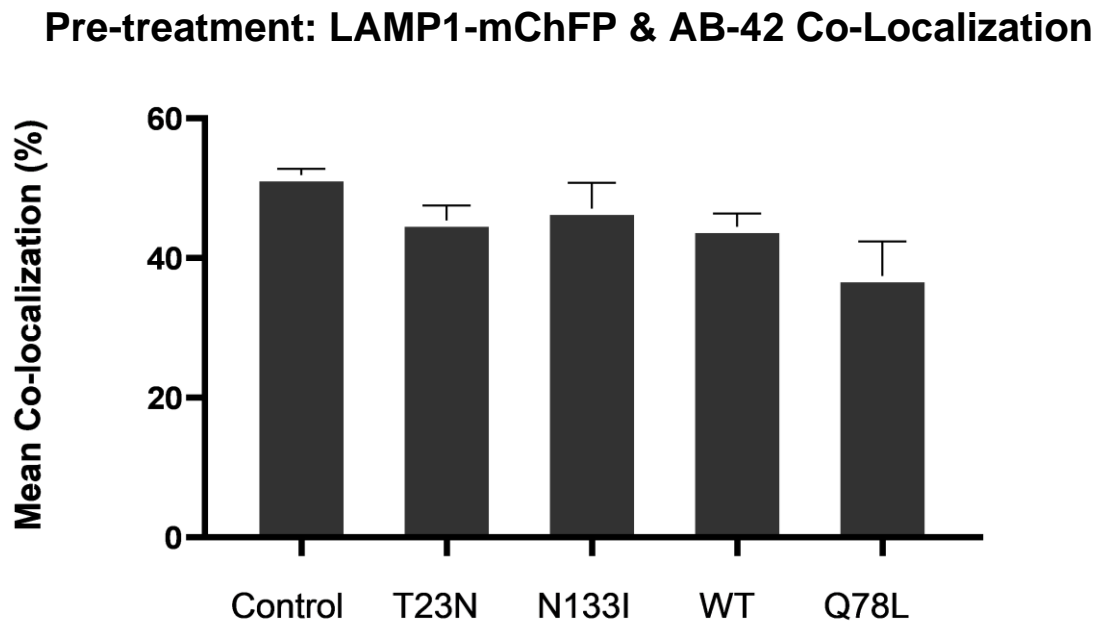


Figure 13 – Pre-treatment co-localization of LAMP1 and A β ₄₂ in Rab27b samples

There were no significant differences in LAMP1-mChFP and HiLyte Fluor 647-labeled A β ₄₂ co-localization between Rab27b and control samples pre-treatment with ionomycin, as determined by Brown-Forsythe and Welch ANOVA tests followed by post hoc Dunnett's T3 multiple comparisons tests. All results are presented as raw mean \pm SEM.

3.4.2 A β ₄₂: Within-Group Comparison

To determine whether there was a difference in pre- and post-treatment percent co-localization of LAMP1-mChFP and HiLyte Fluor 647-labeled A β ₄₂, normalized data was subjected to unpaired t-tests with Welch's correction. LAMP1-mChFP and HiLyte Fluor 647-labeled A β ₄₂ co-localization significantly decreased post-treatment (N=3, n=48) with ionomycin in comparison to pre-treatment (N=3, n=141) ($p < 0.0001$) in control samples (Figure 5 and Figure 18). LAMP1-mChFP and HiLyte Fluor 647-labeled A β ₄₂ co-localization significantly decreased post-treatment (N=6, n=39) with ionomycin in comparison to pre-treatment (N=6, n=39) ($p < 0.05$) in Rab27b T23N samples. This was a $29.76\% \pm 9.17\%$ decrease in co-localization (Figure 14 and Figure 18). LAMP1-mChFP and HiLyte Fluor 647-labeled A β ₄₂ co-localization significantly decreased post-treatment (N=5, n=28) with ionomycin in comparison to pre-treatment (N=7, n=36) ($p < 0.05$) in Rab27b N133I samples. This was a $27.79\% \pm 9.33\%$ decrease in co-localization (Figure 15 and Figure 18). There were no significant differences in LAMP1-mChFP and HiLyte Fluor 647-labeled A β ₄₂ co-localization post-treatment (N=5, n=28) with ionomycin in comparison to pre-treatment (N=7, n=32) in Rab27b WT samples (Figure 16 and Figure 18). LAMP1-mChFP and HiLyte Fluor 647-labeled A β ₄₂ co-localization significantly decreased post-treatment (N=5, n=28) with ionomycin in comparison to pre-treatment (N=7, n=36) ($p < 0.01$) in Rab27b Q78L samples. This was a $60.12\% \pm 18.63\%$ decrease in co-localization (Figure 17 and Figure 18). Overall, Rab27b mutants and control underwent significant lysosomal-mediated A β ₄₂ secretion.

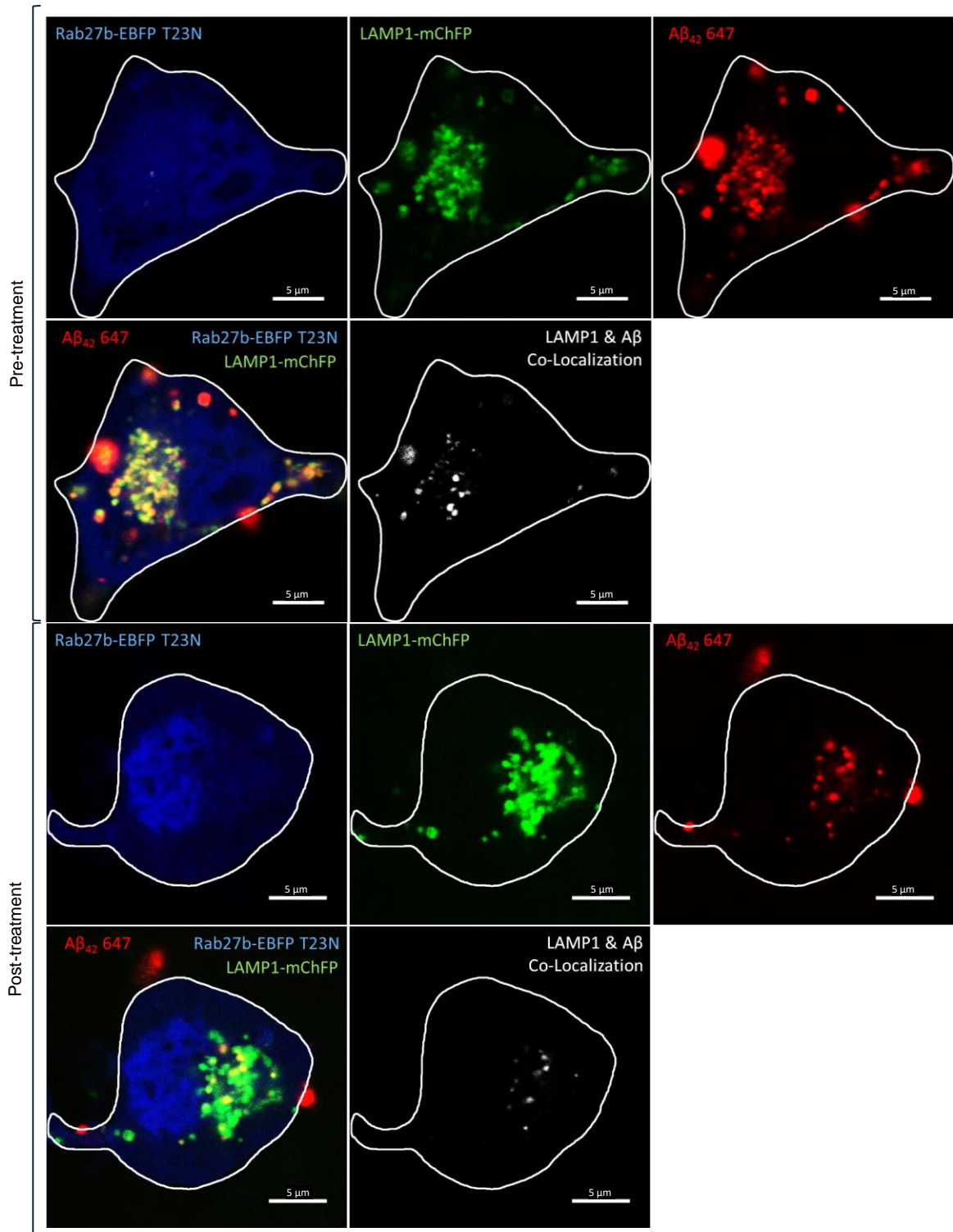


Figure 14 – Co-localization of LAMP1-mChFP and Aβ₄₂ in T23N samples

LAMP1-mChFP and Aβ₄₂ co-localization decreased post-treatment in comparison to pre-treatment in Rab27b T23N samples. White outlines represent the plasma membranes of N2A cells. Scale bars represent 5 μm.

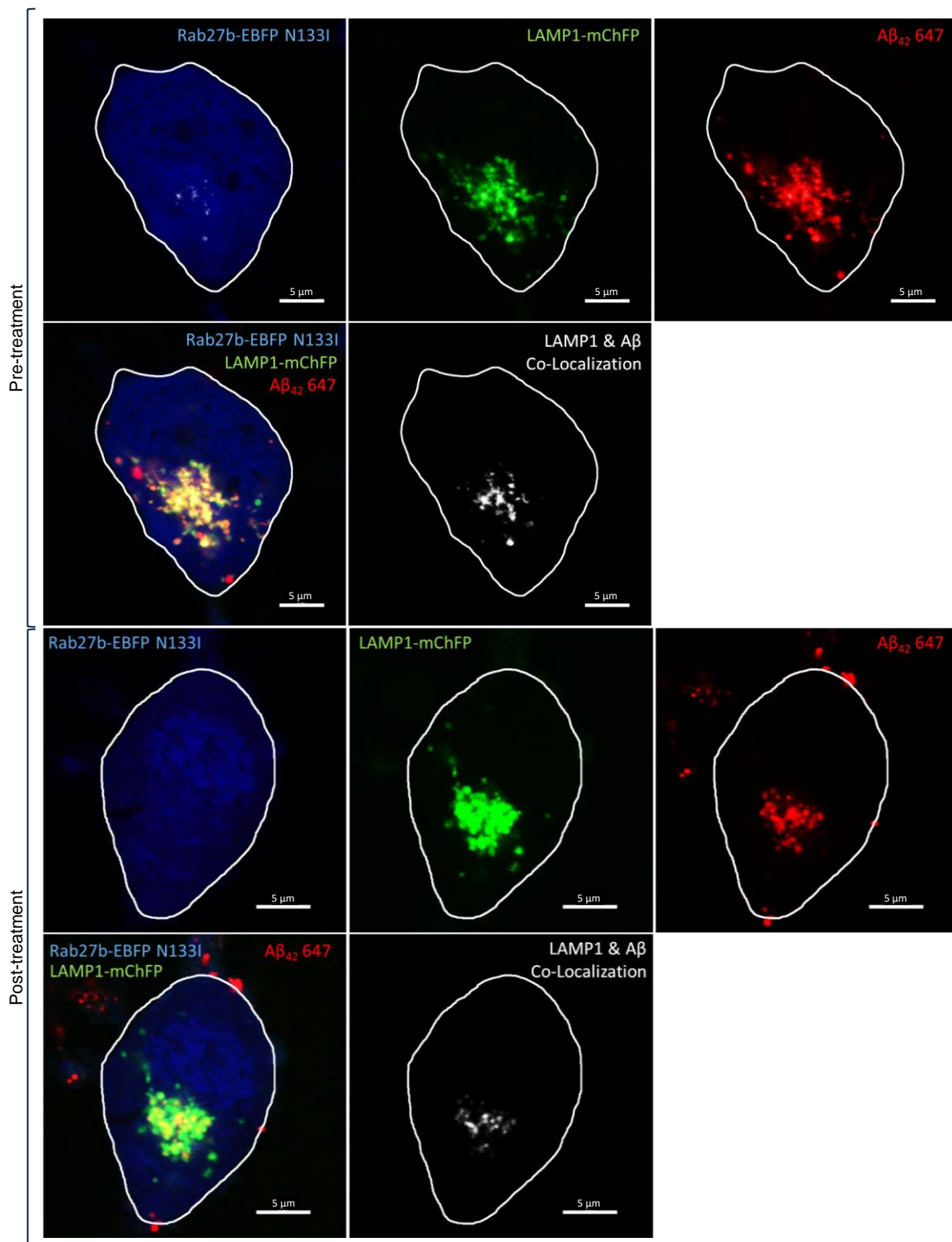


Figure 15 – Co-localization of LAMP1-mChFP and Aβ₄₂ in N133I samples

LAMP1-mChFP and Aβ₄₂ co-localization decreased post-treatment in comparison to pre-treatment in Rab27b N133I samples. White outlines represent the plasma membranes of N2A cells. Scale bars represent 5 μm.

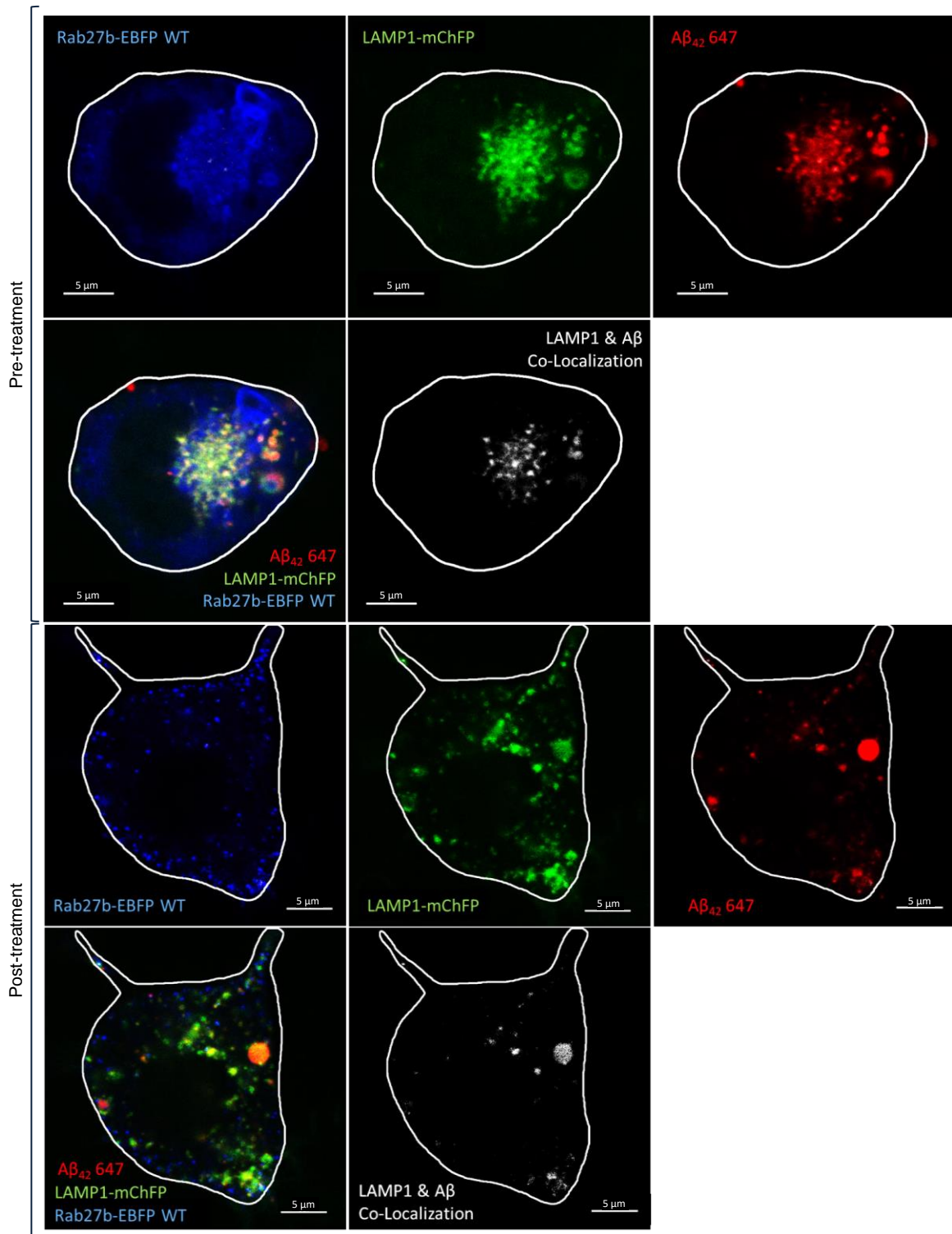


Figure 16 – Co-localization of LAMP1-mChFP and A β_{42} in WT samples

LAMP1-mChFP and A β_{42} co-localization did not decrease post-treatment in comparison to pre-treatment in Rab27b WT samples. White outlines represent the plasma membranes of N2A cells. Scale bars represent 5 μ m.

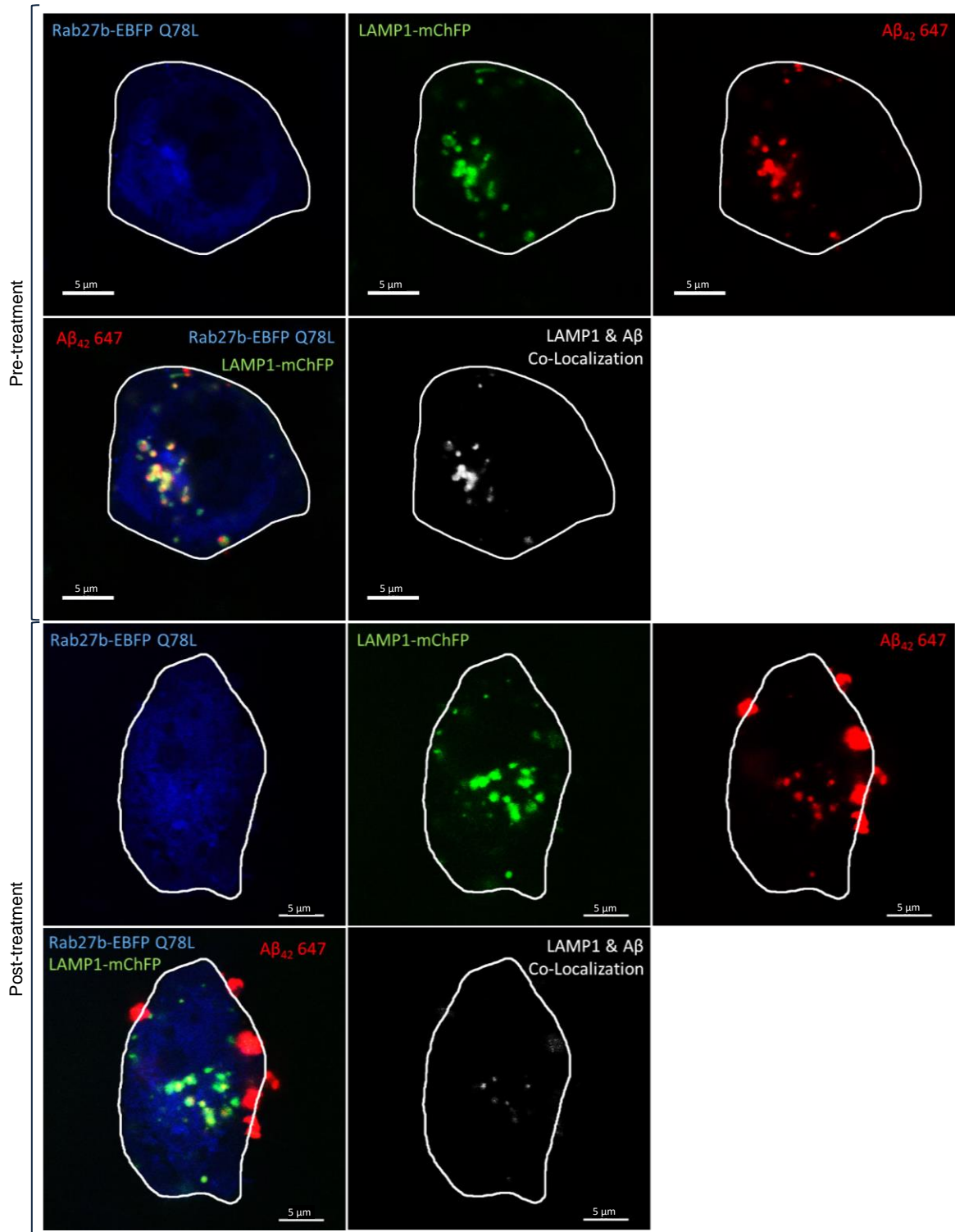


Figure 17 – Co-localization of LAMP1-mChFP and Aβ₄₂ in Q78L samples

LAMP1-mChFP and Aβ₄₂ co-localization decreased post-treatment in comparison to pre-treatment in Rab27b Q78L samples. White outlines represent the plasma membranes of N2A cells. Scale bars represent 5 μm.

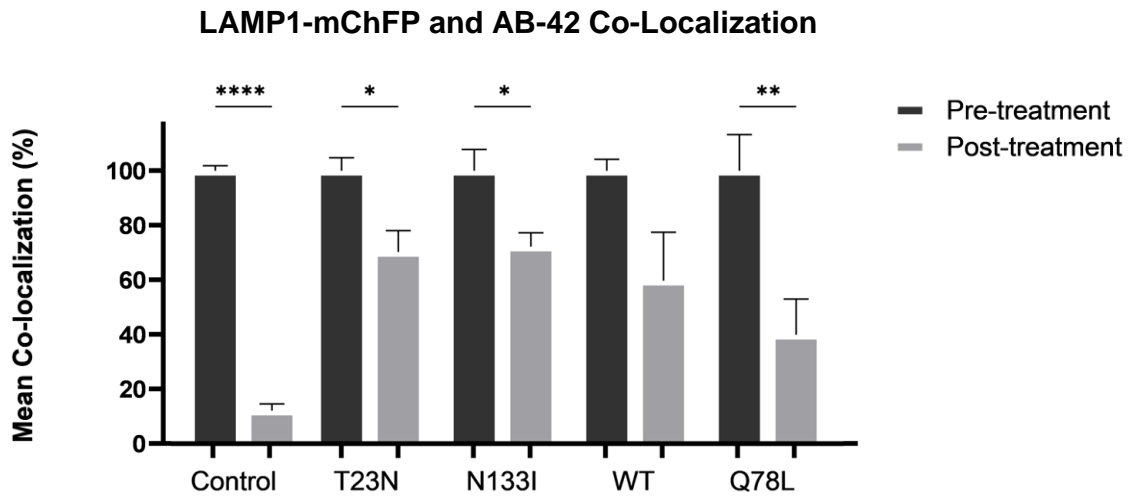


Figure 18 – Mean co-localization of LAMP1-mChFP and A β ₄₂ in Rab27b samples

LAMP1-mChFP and HiLyte Fluor 647-labeled A β ₄₂ co-localization significantly decreased post-treatment (N=3, n=48) with ionomycin in comparison to pre-treatment (N=3, n=141) ($p < 0.0001$) in control samples. LAMP1-mChFP and HiLyte Fluor 647-labeled A β ₄₂ co-localization significantly decreased post-treatment (N=6, n=39) with ionomycin in comparison to pre-treatment (N=6, n=39) ($p < 0.05$) in Rab27b T23N samples. LAMP1-mChFP and HiLyte Fluor 647-labeled A β ₄₂ co-localization significantly decreased post-treatment (N=5, n=28) with ionomycin in comparison to pre-treatment (N=7, n=36) ($p < 0.05$) in Rab27b N133I samples. LAMP1-mChFP and HiLyte Fluor 647-labeled A β ₄₂ co-localization significantly decreased post-treatment (N=5, n=28) with ionomycin in comparison to pre-treatment (N=7, n=36) ($p < 0.01$) in Rab27b Q78L samples. Dark bars indicate pre-treatment with ionomycin, and light bars indicate post-treatment with ionomycin. All results are presented as normalized mean \pm SEM. Asterisks indicate statistically significant changes post-treatment with ionomycin in comparison to pre-treatment, as determined by unpaired t-tests with Welch's correction. * $p < 0.05$, ** $p < 0.01$, **** $p < 0.0001$

3.4.3 A β ₄₂: Post-Treatment Between-Group Comparison

To determine whether there was a difference in lysosomal-mediated secretion of A β ₄₂ between Rab27b and control samples, post-treatment percent co-localization of LAMP1-mChFP and HiLyte Fluor 647-labeled A β ₄₂ was compared. Normalized post-treatment data was subjected to Brown-Forsythe and Welch ANOVA tests followed by post hoc Dunnett's T3 multiple comparisons tests. LAMP1-mChFP and HiLyte Fluor 647-labeled A β ₄₂ co-localization was significantly lower in control samples (N=3, n=48) post-treatment with ionomycin in comparison to Rab27b T23N (N=6, n=39) (p<0.01) and N133I samples (N=5, n=35) (p<0.001). This was a percent difference of 58.13% \pm 8.24% and 60.11% \pm 5.68%, respectively. There were no significant differences in LAMP1-mChFP and A β ₄₂ co-localization amongst WT and Q78L samples post-treatment with ionomycin (Figure 19). Therefore, Rab27b dominant-negative mutants significantly reduced lysosomal-mediated A β ₄₂ secretion when compared to control.

Post-treatment: LAMP1-mChFP & AB-42 Co-Localization

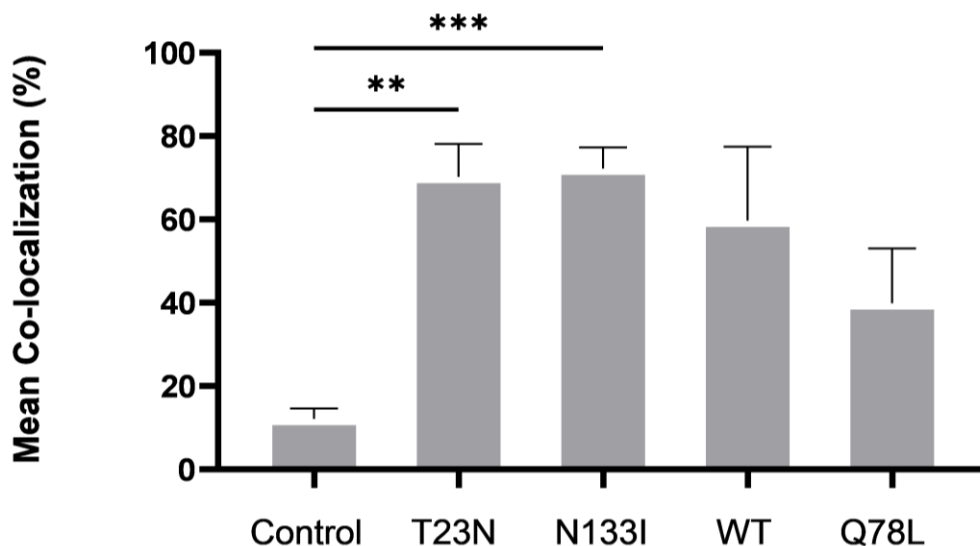


Figure 19 – Post-treatment co-localization of LAMP1 and A β ₄₂ in Rab27b samples

LAMP1-mChFP and HiLyte Fluor 647-labeled A β ₄₂ co-localization was significantly lower in control samples (N=3, n=48) post-treatment with ionomycin in comparison to Rab27b T23N (N=6, n=39) (p<0.01) and N133I samples (N=5, n=35) (p<0.001). All results are presented as normalized mean \pm SEM. Asterisks indicate statistically significant changes between post-treatment samples, as determined by Brown-Forsythe and Welch ANOVA tests followed by post hoc Dunnett's T3 multiple comparisons tests. **p<0.01, ***p<0.001

3.4.4 A β ₄₀: Pre-Treatment Between-Group Comparison

To confirm that results observed were not due to differences in A β loading, pre-treatment percent co-localization of HiLyte Fluor 647-labeled A β ₄₀ and LAMP1-mChFP was compared between Rab27b and control samples. Raw pre-treatment data was subjected to Brown-Forsythe and Welch ANOVA tests followed by post hoc Dunnett's T3 multiple comparisons tests. Similar to A β ₄₂, there were no significant differences in HiLyte Fluor 647-labeled A β ₄₀ and LAMP1-mChFP co-localization between Rab27b and control samples pre-treatment with ionomycin (Figure 20). Therefore, there were no differences in A β ₄₀ loading between samples.

Pre-treatment: LAMP1-mChFP & AB-40 Co-Localization

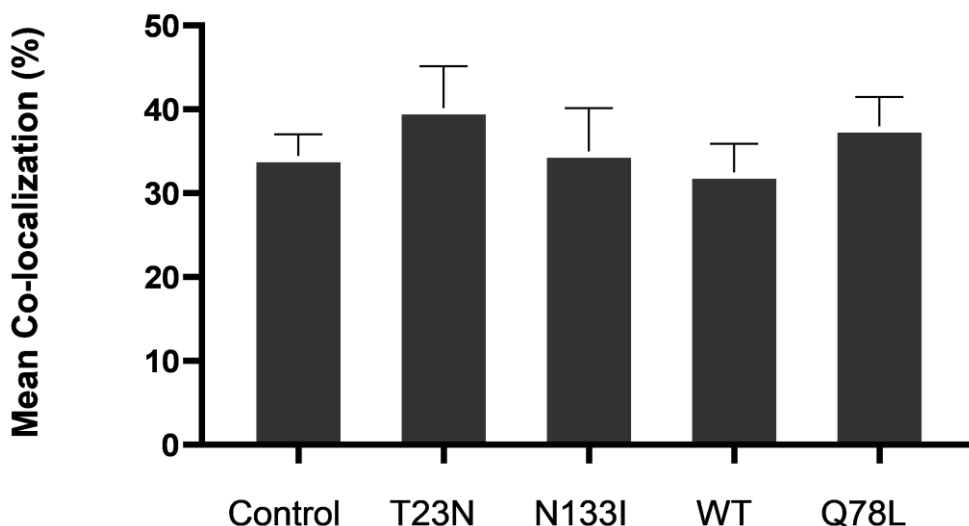


Figure 20 – Pre-treatment co-localization of LAMP1 and A β ₄₀ in Rab27b samples

There were no significant differences in LAMP1-mChFP and HiLyte Fluor 647-labeled A β ₄₀ co-localization between Rab27b and control samples pre-treatment with ionomycin, as determined by Brown-Forsythe and Welch ANOVA tests followed by post hoc Dunnett's T3 multiple comparisons tests. All results are presented as raw mean \pm SEM.

3.4.5 A β ₄₀: Within-Group Comparison

To determine whether there was a difference in pre- and post-treatment percent co-localization of LAMP1-mChFP and HiLyte Fluor 647-labeled A β ₄₀, normalized data was subjected to unpaired t-tests with Welch's correction. LAMP1-mChFP and HiLyte Fluor 647-labeled A β ₄₀ co-localization significantly decreased post-treatment (N=3, n=37) with ionomycin in comparison to pre-treatment (N=5, n=106) ($p < 0.0001$) in control samples (Figure 6 and Figure 25). There were no significant differences in LAMP1-mChFP and HiLyte Fluor 647-labeled A β ₄₀ co-localization post-treatment (N=7, n=44) with ionomycin in comparison to pre-treatment (N=4, n=19) in Rab27b T23N samples (Figure 21 and Figure 25). There were no significant differences in LAMP1-mChFP and HiLyte Fluor 647-labeled A β ₄₀ co-localization post-treatment (N=7, n=43) with ionomycin in comparison to pre-treatment (N=5, n=18) in Rab27b N133I samples (Figure 22 and Figure 25). LAMP1-mChFP and HiLyte Fluor 647-labeled A β ₄₀ co-localization significantly decreased post-treatment (N=6, n=42) with ionomycin in comparison to pre-treatment (N=7, n=28) ($p < 0.01$) in Rab27b WT samples. This was a $59.33\% \pm 17.62\%$ decrease in co-localization (Figure 23 and Figure 25). There were no significant differences in LAMP1-mChFP and A β ₄₀ co-localization post-treatment (N=6, n=35) in comparison to pre-treatment (N=6, n=24) in Rab27b Q78L samples (Figure 24 and Figure 25). Overall, Rab27b WT and control underwent significant lysosomal-mediated A β ₄₀ secretion.

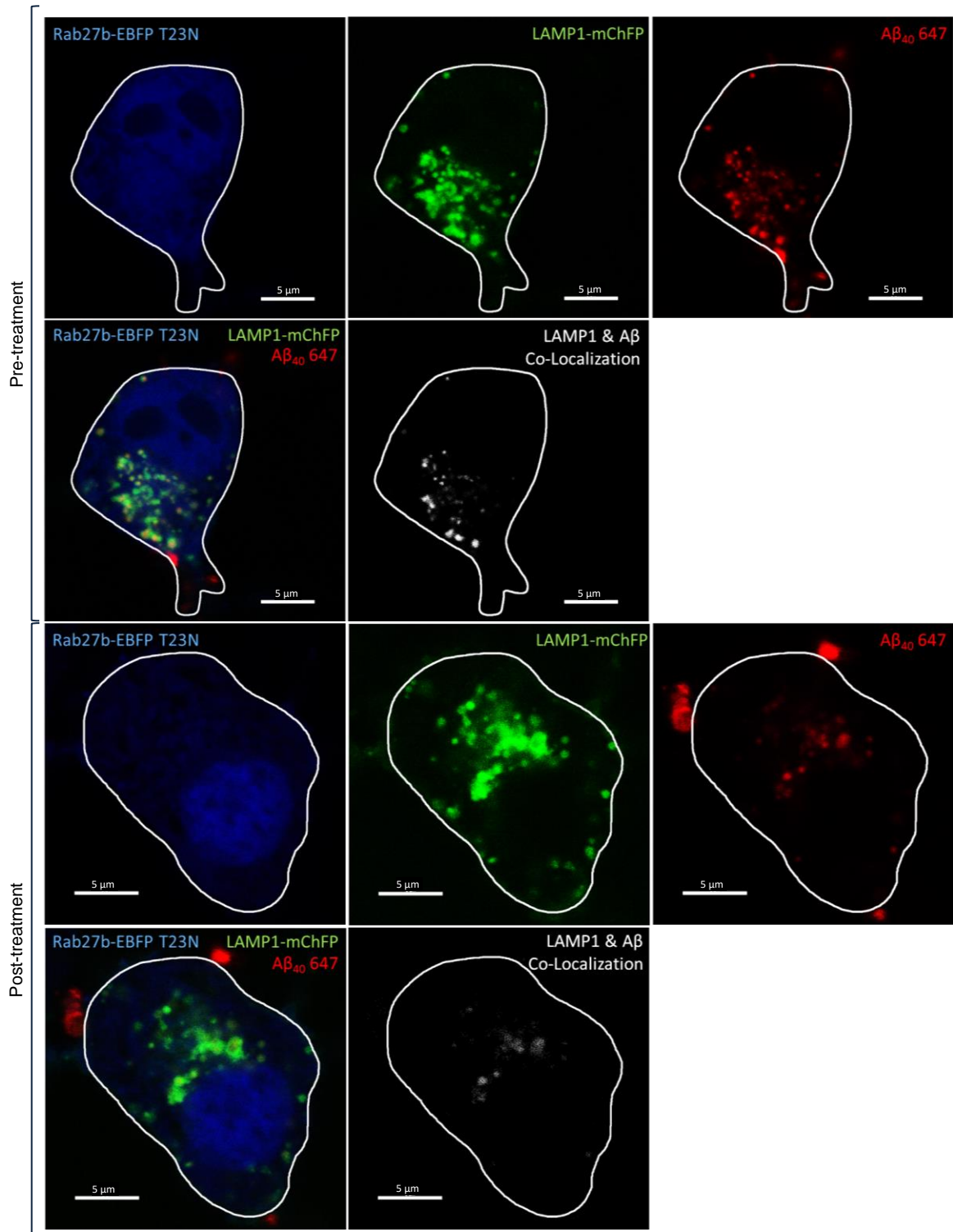


Figure 21 – Co-localization of LAMP1-mChFP and Aβ₄₀ in T23N samples

LAMP1-mChFP and Aβ₄₀ co-localization did not decrease post-treatment in comparison to pre-treatment in Rab27b T23N samples. White outlines represent the plasma membranes of N2A cells. Scale bars represent 5 μm.

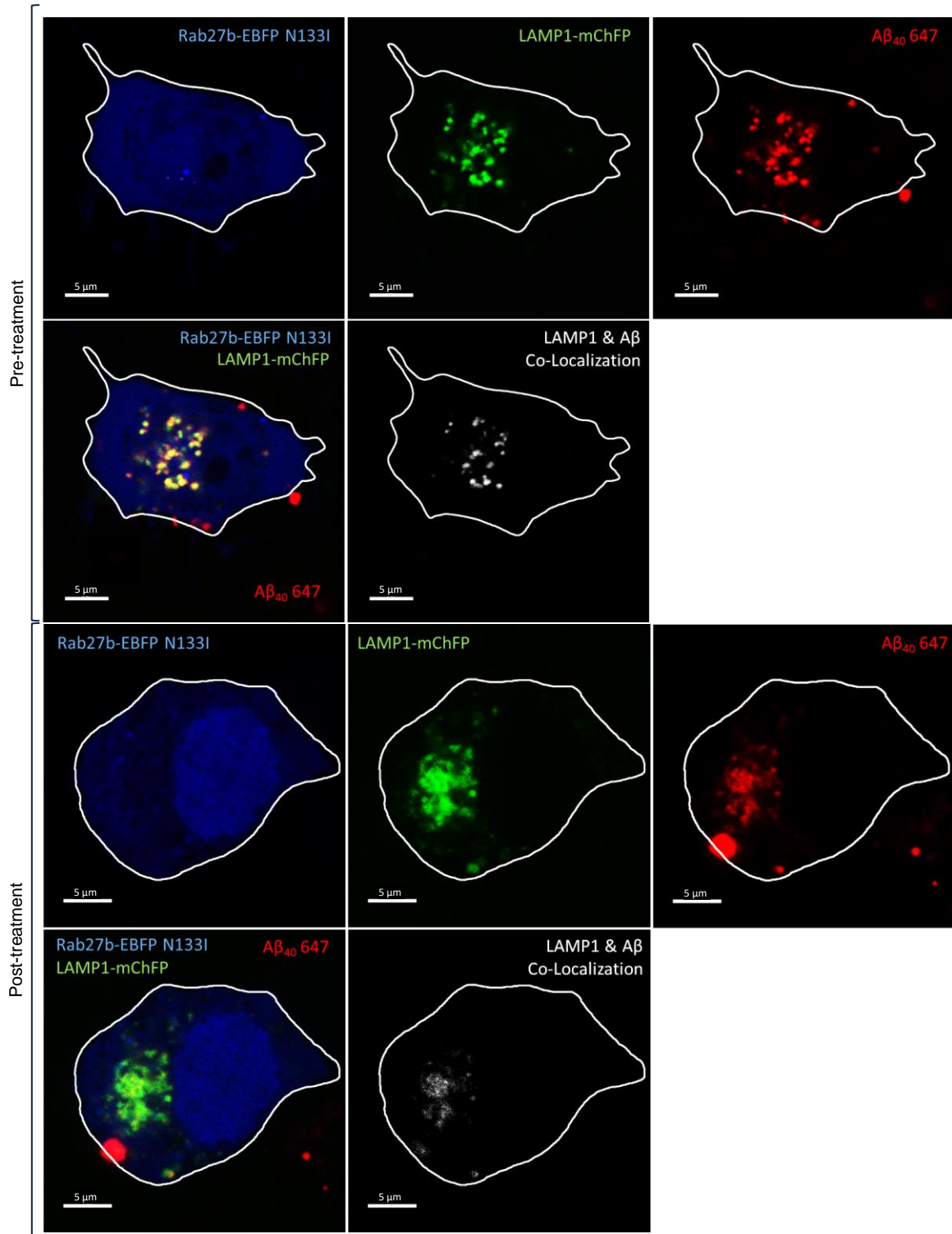


Figure 22 – Co-localization of LAMP1-mChFP and Aβ₄₀ in N133I samples

LAMP1-mChFP and Aβ₄₀ co-localization did not decrease post-treatment in comparison to pre-treatment in Rab27b N133I samples. White outlines represent the plasma membranes of N2A cells. Scale bars represent 5 μm.

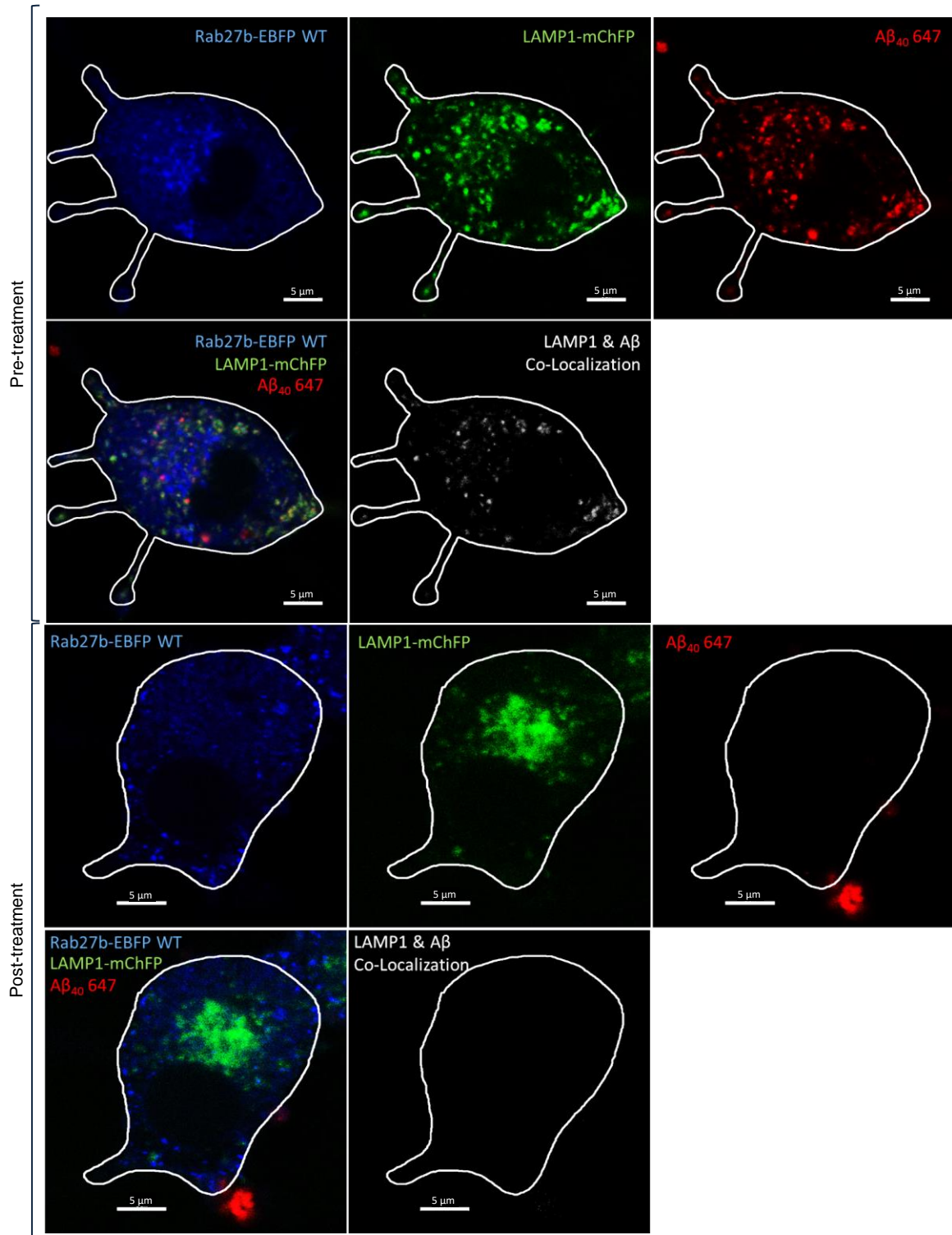


Figure 23 – Co-localization of LAMP1-mChFP and Aβ₄₀ in WT samples

LAMP1-mChFP and Aβ₄₀ co-localization decreased post-treatment in comparison to pre-treatment in Rab27b WT samples. White outlines represent the plasma membranes of N2A cells. Scale bars represent 5 μm.

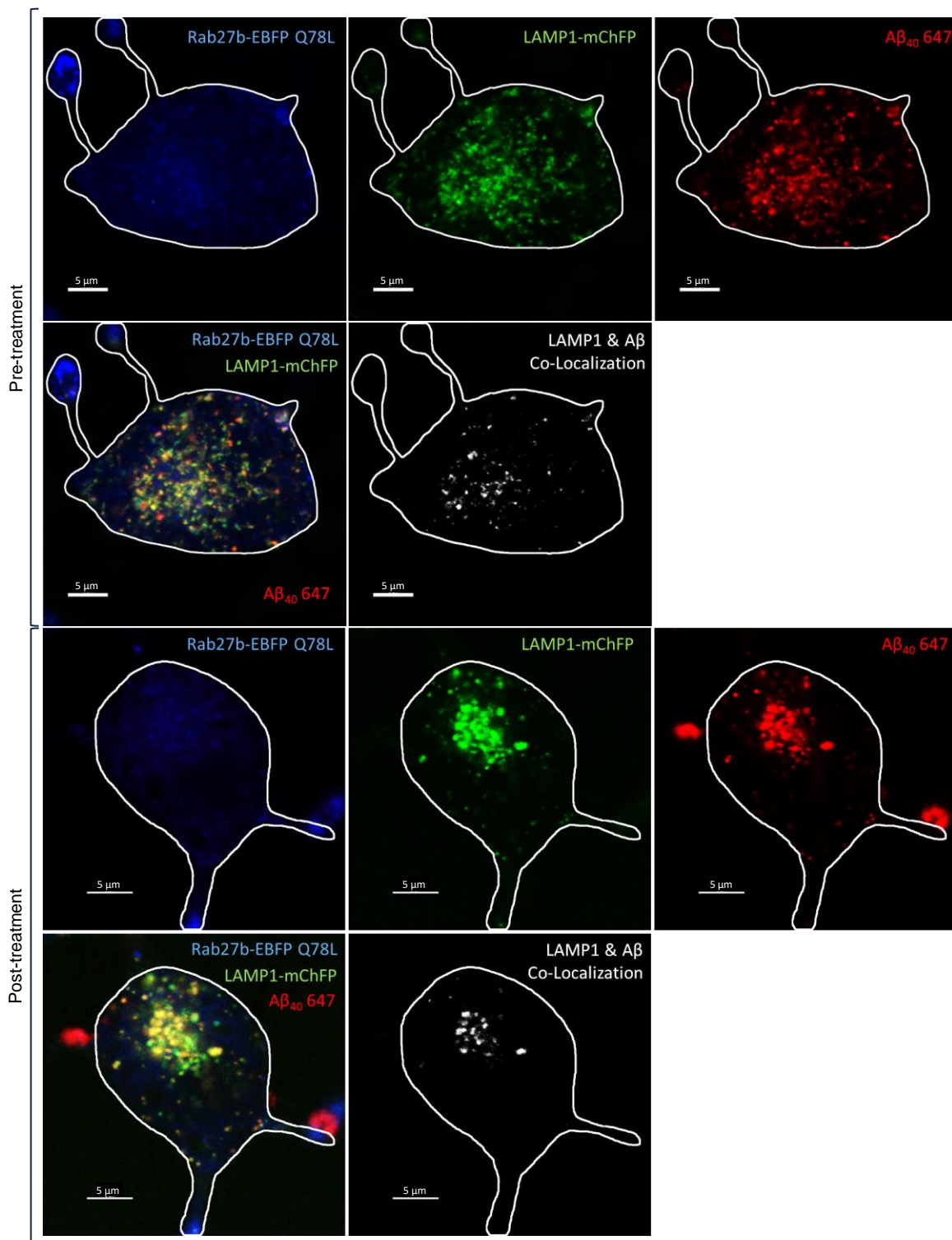


Figure 24 – Co-localization of LAMP1-mChFP and Aβ₄₀ in Q78L samples

LAMP1-mChFP and Aβ₄₀ co-localization did not decrease post-treatment in comparison to pre-treatment in Rab27b Q78L samples. White outlines represent the plasma membranes of N2A cells. Scale bars represent 5 μm.

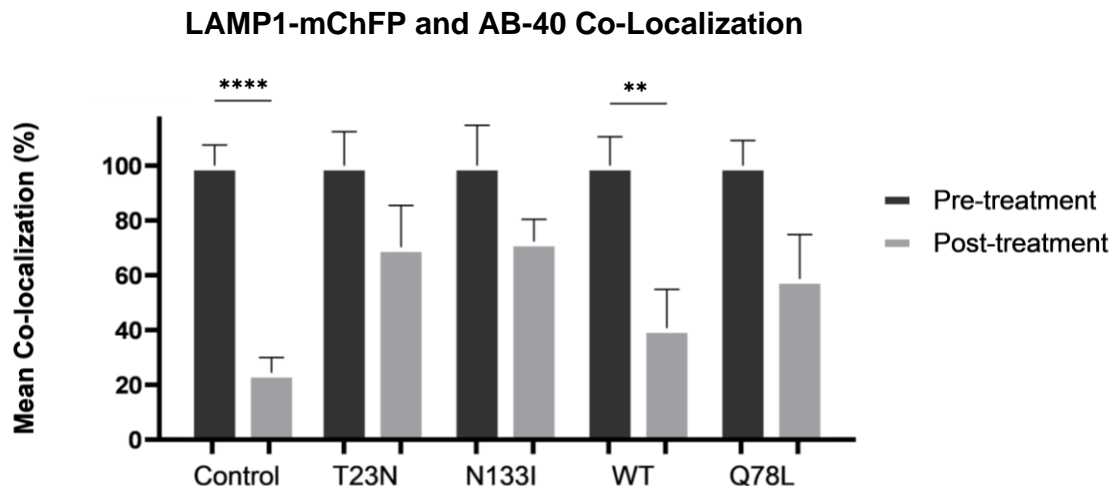


Figure 25 – Mean co-localization of LAMP1-mChFP and A β ₄₀ in Rab27b samples

LAMP1-mChFP and HiLyte Fluor 647-labeled A β ₄₀ co-localization significantly decreased post-treatment (N=3, n=37) with ionomycin in comparison to pre-treatment (N=5, n=106) ($p < 0.0001$) in control samples. LAMP1-mChFP and HiLyte Fluor 647-labeled A β ₄₀ co-localization significantly decreased post-treatment (N=6, n=42) with ionomycin in comparison to pre-treatment (N=7, n=28) ($p < 0.01$) in Rab27b WT samples. Dark bars indicate pre-treatment with ionomycin, and light bars indicate post-treatment with ionomycin. All results are presented as normalized mean \pm SEM. Asterisks indicate statistically significant changes post-treatment with ionomycin in comparison to pre-treatment, as determined by unpaired t-tests with Welch's correction. ** $p < 0.01$, **** $p < 0.0001$

3.4.6 A β ₄₀: Post-Treatment Between-Group Comparison

To determine whether there was a difference in lysosomal-mediated secretion of A β ₄₀ between Rab27b and control samples, post-treatment percent co-localization of LAMP1-mChFP and HiLyte Fluor 647-labeled A β ₄₀ was compared. Normalized post-treatment data was subjected to Brown-Forsythe and Welch ANOVA tests followed by post hoc Dunnett's T3 multiple comparisons tests. LAMP1-mChFP and HiLyte Fluor 647-labeled A β ₄₀ co-localization was significantly lower in control samples (N=3, n=37) post-treatment with ionomycin in comparison to Rab27b N133I samples (N=7, n=43) (p<0.01). This was a percent difference of 47.87% \pm 9.79% (Figure 26). Therefore, Rab27b N133I significantly reduced lysosomal-mediated A β ₄₀ secretion when compared to control.

Post-treatment: LAMP1-mChFP and AB-40 Co-Localization

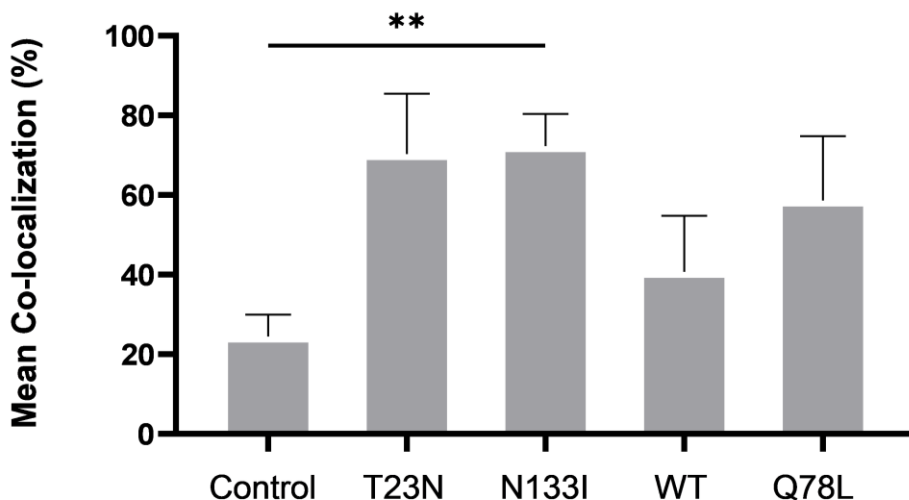


Figure 26 – Post-treatment co-localization of LAMP1 and A β ₄₀ in Rab27b samples

LAMP1-mChFP and HiLyte Fluor 647-labeled A β ₄₀ co-localization was significantly lower in control samples (N=3, n=37) post-treatment with ionomycin in comparison to Rab27b N133I samples (N=7, n=43) (p<0.01). All results are presented as normalized mean \pm SEM. Asterisks indicate statistically significant changes between post-treatment samples, as determined by Brown-Forsythe and Welch ANOVA tests followed by post hoc Dunnett's T3 multiple comparisons tests. **p<0.01

3.5 Differences in A β Secretion in Rab27b Samples

To determine whether there was a difference between A β_{42} and A β_{40} secretion in Rab27b samples, normalized pre- and post-treatment data were subjected to unpaired t-tests with Welch's correction, in addition to Brown-Forsythe and Welch ANOVA tests followed by post hoc Dunnett's T3 multiple comparisons tests. There were no significant differences post-treatment with ionomycin in comparison to pre-treatment when comparing between A β_{40} and A β_{42} groups, in Rab27b T23N, N133I, WT, and Q78L samples (Figure 27).

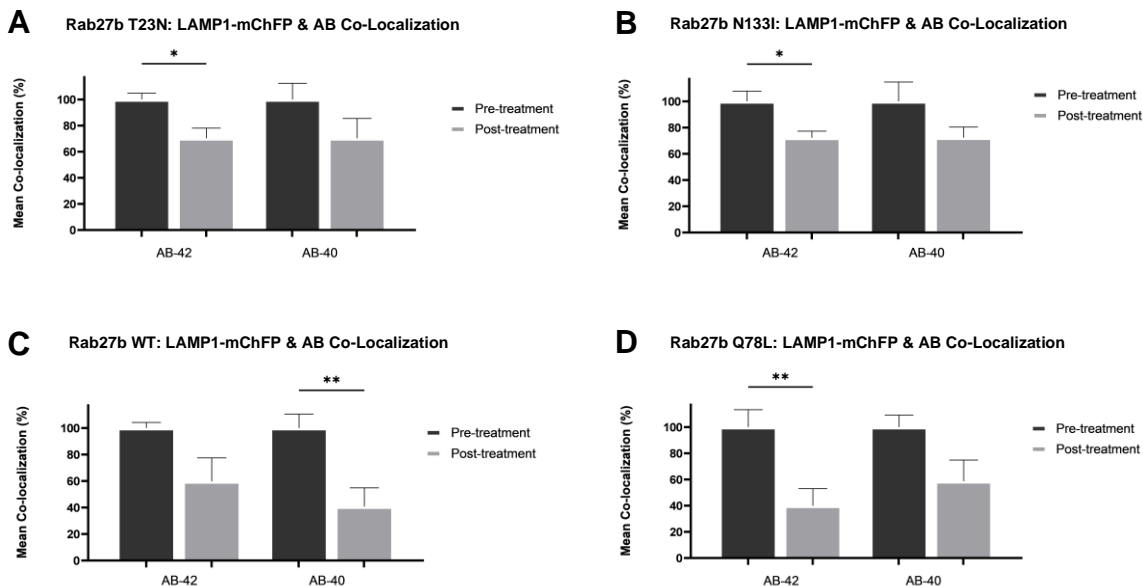


Figure 27 – Mean co-localization of LAMP1-mChFP and A β in Rab27b samples

(A) LAMP1-mChFP and HiLyte Fluor 647-labeled A β_{42} co-localization significantly decreased post-treatment (N=6, n=39) with ionomycin in comparison to pre-treatment (N=6, n=39) ($p < 0.05$) in Rab27b T23N samples. (B) LAMP1-mChFP and HiLyte Fluor 647-labeled A β_{42} co-localization significantly decreased post-treatment (N=5, n=35) with ionomycin in comparison to pre-treatment (N=5, n=40) ($p < 0.05$) in Rab27b N133I samples. (C) LAMP1-mChFP and HiLyte Fluor 647-labeled A β_{40} co-localization significantly decreased post-treatment (N=6, n=42) with ionomycin in comparison to pre-treatment (N=7, n=28) ($p < 0.01$) in Rab27b WT samples. (D) LAMP1-mChFP and HiLyte Fluor 647-labeled A β_{42} co-localization significantly decreased post-treatment (N=5, n=28) with ionomycin in comparison to pre-treatment (N=7, n=36) ($p < 0.01$) in Rab27b Q78L samples. There were no significant differences in co-localization of LAMP1-mChFP and HiLyte Fluor 647-labeled A β in Rab27b T23N, N133I, WT, and Q78L samples when comparing between A β_{42} and A β_{40} groups. Dark bars indicate pre-treatment with ionomycin, and light bars indicate post-treatment with ionomycin. All results are presented as normalized mean \pm SEM. Asterisks indicate statistically significant changes between pre- and post-treatment samples, as determined by unpaired t-tests with Welch's correction. * $p < 0.05$, ** $p < 0.01$

Chapter 4

4 Discussion

This study was conducted to establish the means of A β secretion in the context of Alzheimer's disease (AD). In accordance with results observed in numerous studies [2]–[4], [137], [142], [165], it was hypothesized that secretion of A β would be mediated by lysosomes in a Rab27b-dependent manner (Figure 4). We aimed to: 1) demonstrate storage of A β_{42} and A β_{40} within lysosomes, 2) demonstrate lysosomal-mediated secretion of A β_{42} and A β_{40} , 3) establish the effects of Rab27b mutants on Rab27b distribution, and 4) establish the effects of Rab27b mutants on secretion of A β_{42} and A β_{40} . We predicted that: 1) loading of Neuro-2a (N2A) cells with exogenous A β_{40} and A β_{42} will result in storage of exogenous A β_{42} and A β_{40} in lysosomes, 2) initiation of calcium-dependent exocytosis with calcium ionophore ionomycin will result in secretion of lysosome-stored exogenous A β_{42} and A β_{40} , 3) there will be an increase in co-localization of Rab27b and lysosomes post-treatment with ionomycin in comparison to pre-treatment in Rab27b wild-type (WT) samples loaded with A β_{42} or A β_{40} , 4) there will be no significant differences in co-localization of Rab27b and lysosomes post-treatment in comparison to pre-treatment in Rab27b mutant (T23N, N133I, and Q78L) samples loaded with A β_{42} or A β_{40} , 5) there will be a decrease in co-localization of Rab27b and A β_{42} or A β_{40} post-treatment in comparison to pre-treatment in Rab27b WT samples, 6) there will be no significant differences in co-localization of Rab27b and A β_{42} or A β_{40} post-treatment in comparison to pre-treatment in Rab27b mutant samples, 7) Rab27b T23N and N133I samples will secrete significantly less A β_{42} and A β_{40} in comparison to Rab27b WT, Q78L and control samples, when stimulated with ionomycin, 8) Rab27b Q78L samples will secrete significantly more A β_{42} and A β_{40} in comparison to Rab27b T23N, N133I, WT and control samples, and 9) there will be no significant differences in secretion of A β_{42} in comparison to secretion of A β_{40} , in control and Rab27b samples.

4.1 A β Secretion is Mediated by Lysosomes

In line with our predictions, LAMP1-mChFP co-localized with exogenous A β_{42} and A β_{40} pre-treatment with ionomycin in control samples.

Co-localization of LAMP1-mChFP and A β_{42} or A β_{40} was significantly reduced post-treatment with ionomycin in comparison to pre-treatment in control samples. Rather than remaining stored within lysosomes, A β_{42} and A β_{40} were observed as extracellular accumulations proximal to the plasma membranes of N2A cells. These results demonstrate that exogenous A β_{42} and A β_{40} can be stored within and subsequently secreted by lysosomes.

4.1.1 Intracellular and Extracellular A β Observations

Proteases are enzymes that catalyze the breakdown of proteins via hydrolysis. Many *in vivo* and *in vitro* studies have observed that the breakdown of A β can be mediated by proteases such as neprilysin (NEP), insulin degrading enzyme (IDE), and cathepsin D. Cathepsin D in particular is a resident lysosomal aspartyl protease that has been shown to be elevated in extracellular amyloid plaques in the brains of both transgenic AD mice and humans with AD, suggesting that cathepsin D may play a role in AD prevention by catalyzing the breakdown of A β [4], [166]. However, previous studies have shown that A β aggregation can result in structural changes in A β that confer resistance to protease activity [142], [170]. Indeed, studies observing cathepsin D-mediated cleavage of A β utilized monomeric forms of this protein in their experiments, rather than aggregated forms [171]. In accordance with this finding, many studies have observed that an acidic pH promotes the aggregation of A β , with exogenous A β observed to accumulate specifically within lysosomal lumens [3]. These results suggest that A β can aggregate within the lysosome prior to its extracellular release and evade digestion by resident lysosomal acid hydrolases due to its aggregated structure. In addition to intracellular aggregation, A β aggregates have been observed to associate with lipid rafts on the extracellular surface of cells to induce further A β aggregation and neurotoxicity [145].

Our observations provide evidence that support many of these previous findings. Although exogenous A β was added to cells in monomeric form, we observed accumulations of A β

specifically within the lumens of lysosomes, prior to treatment with ionomycin. In being able to evade degradation by lysosomal proteases, this observation suggests that the accumulation of A β either occurred within the lysosome at a very fast rate, or that it was first initiated within late endosomes/MVBs and A β accumulations were then trafficked to lysosomes. It is interesting to note that the lysosomal accumulation of A β peptides and the ability of A β to evade degradation within lysosomes is comparable to lysosomal storage diseases (LSDs). In LSDs, material that has been trafficked to lysosomes cannot be degraded (for example, due to a mutation in the material's corresponding acid hydrolase) and thus accumulates within the compartment, resulting in a variety of symptoms [40].

After treatment with ionomycin, we observed A β accumulations to be associated with the extracellular surface of the plasma membranes of fixed N2A cells. It is possible that these A β accumulations occurred within lipid rafts of plasma membranes [145], [146], due to the hydrophobic properties of A β [141], [142].

4.2 Subcellular Distribution of Rab27b

Distribution of Rab27b WT relative to LAMP1-mChFP slightly varied from our initial predictions. Although LAMP1-mChFP and Rab27b-EBFP were predicted to increase in co-localization post-treatment with ionomycin in comparison to pre-treatment in WT samples loaded with A β_{42} or A β_{40} , we observed no significant differences in co-localization post-treatment in comparison to pre-treatment. The initial prediction was made in line with previous findings indicating that active Rab27b is recruited to the membranes of lysosomes through interactions involving Rab-GDIs and GDFs during calcium-dependent exocytosis [86], [87]. We therefore reasoned that distribution of Rab27b WT should be diffuse pre-treatment due to sequestration of Rab27b in the cytosol, and should be localized to the membranes of lysosomes upon initiation of exocytosis with ionomycin. This pattern of distribution has previously been observed with Rab27a expression [169]. Our unexpected result might be attributed to the rate that Rab27b WT underwent a catalytic cycle (GTP-bound to GDP-bound) and the length of the ionomycin treatment. It is possible that within Rab27b WT samples, active Rab27b was recruited to the membranes of lysosomes to enable vesicle docking after addition of ionomycin. However, over the span of the two-minute treatment, a large portion of active Rab27b might have undergone catalytic cycles

such that the majority would have become inactive and sequestered within the cytosol prior to fixation with PFA. If this were the case, Rab27b distribution in Rab27b WT samples would have been diffuse within the cytosol and would have resulted in a low amount of LAMP1-mChFP and Rab27b-EBFP co-localization, both pre- and post-treatment. This pattern of distribution and co-localization was indeed observed.

Distributions of Rab27b T23N, N133I, and Q78L relative to LAMP1-mChFP were consistent with initial predictions. LAMP1-mChFP and Rab27b-EBFP co-localization was expected to not change post-treatment relative to pre-treatment in Rab27b T23N, N133I, and Q78L mutants loaded with A β ₄₂ or A β ₄₀. This was predicted because ionomycin treatment should not alter the effects of Rab27b proteins that are always active (Q78L) or always inactive (T23N and N133I). As such, co-localization of LAMP1-mChFP and Rab27b-EBFP in Rab27b Q78L samples should have remained high (relative to all other Rab27b samples) both pre- and post-treatment, while co-localization in Rab27b T23N and N133I samples should have remained low. Subcellular distribution of Rab27b T23N and N133I in particular should have been diffuse throughout the cytosol both pre- and post-treatment. Accordingly, there were no significant differences in post-treatment co-localization of LAMP1-mChFP and Rab27b-EBFP in comparison to pre-treatment in Rab27b mutants. It is important to note that pre- and post-treatment co-localization of LAMP1-mChFP and Rab27b-EBFP in all Rab27b mutants was low, although Rab27b T23N and N133I did appear to distribute more diffusely in the cytosol, in comparison to Rab27b Q78L.

Distribution of Rab27b WT relative to A β varied from our initial predictions. Co-localization of Rab27b-EBFP and A β ₄₂ or A β ₄₀ was predicted to decrease post-treatment in comparison to pre-treatment in Rab27b WT samples. This was expected because Rab27b WT samples should have undergone normal lysosomal-mediated exocytosis upon treatment with ionomycin, such that there would have been a decrease in amount of A β within lysosomal lumens post-treatment in comparison to pre-treatment. This result was observed in Rab27b WT samples that were loaded with A β ₄₀. Rab27b WT samples that were loaded with A β ₄₂, however, did not display significant differences in amount of Rab27b-EBFP and A β ₄₂ co-localization post-treatment in comparison to pre-treatment.

Distributions of Rab27b T23N, N133I, and Q78L relative to A β likewise varied from our initial predictions. It was predicted that co-localization of Rab27b-EBFP and A β_{42} or A β_{40} would not be altered post-treatment in comparison to pre-treatment in Rab27b mutant samples. As described for distribution of Rab27b relative to LAMP1-mChFP, addition of ionomycin should not alter the effects of Rab27b proteins that are always active (Q78L) or always inactive (T23N and N133I). Co-localization of Rab27b-EBFP and A β_{42} or A β_{40} should therefore always remain low in Rab27b Q78L samples, as Rab27b Q78L samples should always be undergoing lysosomal-mediated exocytosis. Similarly, co-localization of Rab27b-EBFP and A β_{42} or A β_{40} should always remain low in Rab27b T23N and N133I samples, as dominant-negative Rab27b cannot facilitate lysosomal-mediated exocytosis. Results supported predictions for all Rab27b mutant samples, with the exception of Rab27b Q78L samples loaded with A β_{42} and Rab27b N133I samples loaded with A β_{40} . In these samples, co-localization of Rab27b-EBFP and A β significantly decreased post-treatment in comparison to pre-treatment.

4.3 Rab27b Mutants Alter Lysosomal-Mediated Secretion of Exogenous A β

When comparing within Rab27b samples, lysosomal-mediated secretion of A β varied from initial predictions. Within-group comparisons of LAMP1-mChFP and A β_{42} co-localization demonstrated significant decreases in Rab27b T23N, N133I, and Q78L post-treatment samples when compared to their respective pre-treatment samples. We did not observe a similar significant decrease in Rab27b T23N, N133I, and Q78L samples when comparing LAMP1-mChFP and A β_{40} co-localization. Instead, we observed significant decreases in LAMP1-mChFP and A β_{40} co-localization in Rab27b WT post-treatment samples when compared to Rab27b WT pre-treatment samples. A β_{40} findings were consistent with our initial predictions and are consistent with our current knowledge of Rab GTPases. As mentioned for subcellular distribution above, Rab27b WT is expected to act as a normal Rab GTPase. Specifically, active Rab27b WT should interact with Munc13-4 to dock the lysosome at the plasma membrane and enable calcium-dependent exocytosis of A β to occur upon treatment with ionomycin. This would result in decreased post-treatment co-localization of LAMP1-mChFP and A β in comparison to pre-treatment, as was observed.

Akin to subcellular distribution, Rab27b T23N, N133I, and Q78L post-treatment co-localization of LAMP1-mChFP and A β should not be altered in comparison to pre-treatment, as these Rab GTPases are consistently inactive (T23N and N133I) or active (Q78L) regardless of treatment with ionomycin.

It is important to note that despite our predictions, a general decrease in post-treatment co-localization of LAMP1-mChFP and A β in comparison to pre-treatment was observed in all Rab27b samples. One possible explanation for this observation in Rab27b T23N and N133I samples is functional compensation by other Rab GTPases upon inactivity of Rab27b. As described in Section 1.3.2, Rab27 isoforms have been modeled to act separately, cooperatively, redundantly, or sequentially (contingent on cell type and secretory pathway). The “redundant activity” model of Rab27 suggests that Rab27a and Rab27b act in parallel to elicit the same response(s), due to targeting of the same effector protein(s) [9]. If one of these isoforms was not able to function, the other isoform would compensate accordingly. In line with this theory, both Rab27a and Rab27b have been shown to interact with effector protein Munc13-4 [7], [92]. It is likely that functional compensation can occur in the pancreas and in pituitary tissues, where Rab27a and Rab27b are both expressed [169], [172]. However, only isoform Rab27b has been localized to the brain [172]. Previous studies have shown that small GTPase Rab3a both localizes to the brain and functions in a similar manner to Rab27b, suggesting that Rab3a may be able to compensate for inactivity of Rab27b (T23N and N133I) during exocytosis [93].

When comparing between Rab27b samples, lysosomal-mediated secretion of A β in Rab27b Q78L samples differed from initial predictions. Although we expected to observe significantly greater secretion of A β in Rab27b Q78L samples in comparison to Rab27b T23N, N133I, WT and control samples, we observed no significant differences in secretion of A β in Rab27b Q78L samples in relation to all other samples. Nevertheless, there was a trend toward significance that was clearly observed in Rab27b Q78L samples loaded with A β ₄₂, demonstrated by a decrease in post-treatment co-localization of LAMP1-mChFP and A β ₄₂ in these samples when compared to Rab27b N133I, T23N, WT and control samples. One explanation for this finding entails permanent binding of Rab27b Q78L to lysosomal membranes. Specifically, as Rab27b Q78L is always bound to GTP, Rab27b Q78L would

likely remain permanently attached to the lysosomal membrane to which it was initially recruited. After stimulation of calcium-dependent exocytosis, Rab27b Q78L would remain permanently attached to the plasma membrane. This is due to the inability of Rab-GDI to sequester active Rab GTPases in the cytosol. In other words, Rab27b Q78L would not be able to be recycled [87]. If this were the case, the number of lysosomes that undergo exocytosis in Rab27b Q78L samples and the amount of intraluminal A β released to the extracellular space would be limited by the amount of Rab27b Q78L that is initially expressed in the cell.

Conversely, lysosomal-mediated secretion of A β in Rab27b dominant-negative samples coincided with initial predictions. We observed significantly less secretion of A β_{42} in Rab27b T23N and N133I samples relative to control samples. This was demonstrated by a significant increase in post-treatment co-localization of LAMP1-mChFP and A β_{42} in Rab27b T23N and N133I samples when compared to control samples. Similarly, we observed significantly less secretion of A β_{40} in Rab27b N133I samples relative to control samples, demonstrated by a significant increase in post-treatment co-localization of LAMP1-mChFP and A β_{40} in Rab27b N133I samples when compared to control samples. These results suggest that lysosomal-mediated secretion of A β is dependent on Rab27b.

Despite its increased hydrophobicity and associated propensity to aggregate [141], [142], there is no evidence to suggest that A β_{40} would secrete in a different manner relative to variant A β_{42} . Accordingly, there were no significant differences in pre- or post-treatment co-localization of LAMP1-mChFP and A β in Rab27b T23N, N133I, WT, and Q78L samples when comparing between A β_{42} and A β_{40} groups. Therefore, there were no significant differences in lysosomal-mediated secretion of A β in Rab27b T23N, N133I, WT, and Q78L samples when comparing between A β_{42} and A β_{40} groups.

4.4 Relation to *In Vivo* Calcium-Dependent Exocytosis

The Neuro-2a (N2A) cells used in this study were neuroblast cells derived from *Mus musculus* neuroblastoma (ATCC). Neuroblasts are post-mitotic primitive nerve cells that are committed to developing into neurons upon differentiation, or maturation [173]. Both neurons and their primitive counterparts are excitable cells; therefore, they are capable of propagating electrical signals (action potentials) upon depolarization that surpasses a threshold value [174]. Neurons and neuroblasts possess an intracellular negative charge at rest. Depolarization can be defined as an increase in intracellular positive charge, such that the extracellular and intracellular charge difference is reduced. In neurons and neuroblasts, initial depolarization is dependent on an influx of sodium ions (Na^+) through voltage-gated sodium channels [175]. As mentioned above, sufficient depolarization can result in an action potential that is propagated through the neuron or neuroblast [174], which in turn enables the opening of voltage-gated calcium channels. This opening allows the influx of Ca^{2+} from the extracellular space to the cytosol [175], in addition to calcium-induced calcium release (CICR) from ryanodine receptors (RyR) and inositol 1,4,5-trisphosphate receptors (IP_3Rs) of the endoplasmic reticulum (ER) [70]–[72]. An increase in intracellular Ca^{2+} is necessary for Synaptotagmin-mediated fusion of vesicles to occur during calcium-dependent exocytosis [66], [73], as described in Section 1.2.1. Due to increases in intracellular Ca^{2+} concentration, treatment of cells with ionomycin results in a process that mimics calcium-dependent exocytosis *in vivo* while by-passing the requirement of an action potential. This is due to the mechanism of action of ionomycin. As a calcium ionophore, ionomycin can directly increase intracellular Ca^{2+} to induce transient vesicle fusion [76]. Because ionomycin is able to directly increase the intracellular Ca^{2+} concentration, an associated problem with excessive application of this ionophore is calcium overload [176]. Calcium overload has been shown in many studies to elicit cell death through the activation of pro-apoptotic factors, such as cytochrome *c* [177], [178]. To avoid calcium overload and subsequent cell death in this study, the minimum concentration of ionomycin required to elicit calcium-dependent exocytosis in N2A cells was added to each sample (1 μM). This amount was determined by titrating the concentration of ionomycin that was used to treat samples, prior to the start of experiments.

4.5 Conclusion

4.5.1 Significance

AD is a progressive neurodegenerative disease that decreases quality of life tremendously. Afflicted individuals experience symptoms of dementia and personality changes that negatively affect both themselves and their loved ones [102]. As no curative treatments are currently available for AD, therapeutic approaches rely on medication that purely alleviate symptoms [113]. Presently, there are over 750 000 Canadians living with AD [103]. With increasing age being a primary risk factor for progression of AD [104], the aging population of baby boomers are predicted to yield more than 130 million new cases of AD worldwide by the year 2050 [179]. Conducting relevant research can both enhance our understanding of how this disease progresses and facilitate the development of treatments that target underlying disease mechanisms, overall reducing the occurrence of future AD cases.

The basis of this study was the amyloid cascade hypothesis of AD, which postulates that the production of A β prompts AD development [121]. This hypothesis is supported by numerous studies showing that the overexpression of Amyloid Precursor Protein (APP) can result in the development of AD. As the gene encoding APP is found on chromosome 21, this was an especially important finding for individuals with Down syndrome (Trisomy 21) that possess an extra copy of chromosome 21 and are therefore likely to develop AD at some point in their lives [161], [162]. The discovery of autosomal dominant mutations in *APP*, *PSEN1*, and *PSEN2* genes that are directly linked to early-onset forms of AD (Familial AD) strongly support the amyloid cascade hypothesis as well [158].

In accordance with the amyloid cascade hypothesis, we aimed to elucidate the manner in which A β was being secreted from cells. As previous research suggested that lysosomes and small GTPase Rab27b may be involved in secretion of A β [2], [3], [7], we conducted experiments that allowed us to manipulate Rab27b activity while directly and indirectly observing lysosomal-mediated secretion of A β . We observed that lysosomes can undergo calcium-dependent exocytosis and release A β to the extracellular space. Moreover, we observed that this process was dependent on small GTPase Rab27b. These results reveal a

pharmaceutical target (Rab27b) that may alter the amount of A β that is being secreted from cells when its activity is modified.

4.5.2 Limitations

The results of this study demonstrate that lysosomal-mediated exocytosis of A β may in part rely on the activity of Rab27b. However, no significant differences were observed in post-treatment co-localization of LAMP1-mChFP and A β_{42} or A β_{40} when comparing Rab27b WT samples to Rab27b mutant samples. It is important to note that the pattern of endogenous Rab27b expression and turnover is presently unknown and as such, total amount of endogenous Rab27b protein present in a cell at any one time is unknown. As endogenous Rab27b expression was not altered in this study, control samples expressed less Rab27b protein than Rab27b WT samples. Moreover, Rab27b WT protein expression was mediated by a constitutive cytomegalovirus promoter. This resulted in a pattern of Rab27b expression that did not mimic that of endogenous Rab27b expression in Rab27b WT samples, and instead gave rise to an overexpression system. When comparing control samples to Rab27b WT samples, there were no significant differences in LAMP1-mChFP and A β_{42} or A β_{40} co-localization post-treatment with ionomycin. However, there was a trend toward significance; specifically, amount of LAMP1-mChFP and A β_{42} or A β_{40} co-localization post-treatment with ionomycin was higher in Rab27b WT samples than control samples. These observations may be indicative of an issue in Rab27b overexpression systems. It is possible that even minor overexpression of Rab27b can modify the activity of effector protein Munc13-4. For example, overexpression of Rab27b (WT and Q78L) may result in over-recruitment of Munc13-4. This over-recruitment could lead to unstable ternary bundle formation due to sequestration of bundle proteins by disproportionate Rab27b-Munc13-4 complexes, which would ultimately reduce the amount of exocytosis that the cell can undergo.

When focusing on pre-treatment raw data, approximately 40% of exogenous A β co-localized with LAMP1-mChFP (on average, across samples). As only a minimal amount of A β was observed in the extracellular space by eye, this suggests that at least 50% of A β was both internalized and stored in subcellular locations other than the lysosome. It is possible that overnight incubation with exogenous A β did not allow all the incubated A β

to enter lysosomes. Consistent with APP processing and the endocytic pathway [18], [180], the remainder of A β could potentially be found in early endosomes and/or late endosomes/multivesicular bodies (MVBs). Likewise, not all A β that was loaded into cells was released upon initiation of calcium-dependent exocytosis. This might be due to an insufficient concentration of ionomycin that was used to treat the samples. This is unlikely, as various concentrations of ionomycin were tested on N2A cells prior to initiation of experiments, thus allowing us to elucidate the minimum concentration of ionomycin required to elicit an exocytotic response in N2A cells (as described in Section 4.4).

It is also possible that calcium-dependent exocytosis of A β did not solely occur via lysosomes. Indeed, secretory vesicles and late endosomes/MVBs are also capable of undergoing calcium-dependent exocytosis [21]. In addition, APP processing and production of A β has been shown in previous studies to ensue within the *trans*-Golgi network (TGN) [181]. In accordance with this observation, it is possible that A β can be packaged into secretory vesicles that subsequently follow the constitutive pathway of exocytosis. Furthermore, rather than functioning as an intermediate compartment for transfer of APP and/or A β from the early endosome to the lysosome, it is very possible that late endosomes/MVBs may mediate the secretion of A β directly [182], [183]. As late endosomes/MVBs contain numerous ILVs, fusion of a late endosome/MVB with the plasma membrane during exocytosis would result in the release of ILVs to the extracellular space. These extracellular vesicles are termed exosomes [183]. Despite its ability to recruit only a few (known) types of effector proteins, Rab27b has been shown to recruit effector Slac2-b during secretion of exosomes in HeLa cells [184].

The foremost limitation of this study, however, was the use of exogenous A β as opposed to observation of endogenous A β . It is possible that the exogenous A β that was utilized does not traffic or secrete in a similar manner as endogenous A β in AD. Although difficult to say whether this is unlikely, the A β that was used in this study was derived from humans and carefully prepared, handled, and stored to maintain its monomeric form prior to treatment of cells.

4.5.3 Future Directions

Future experiments related to this study may consider repeating the experiments described herein with a focus on other small GTPases or SNAREs that have also been shown to be important for lysosomal-mediated secretion. These proteins can include ternary bundle SNARE proteins VAMP-2, Syntaxin-11, and SNAP-23 [67], [91]. For example, cells could be transfected with LAMP1-mChFP and VAMP-2 WT or mutant constructs, loaded with exogenous A β , and imaged under confocal microscopy before and after treatment with ionomycin. This would allow one to observe whether secretion of A β is dependent on VAMP-2. Future experiments might also consider repeating this study with a focus on other subcellular compartments that could be mediating secretion of A β . These compartments can include late endosomes/MVBs and associated exosomes [182]. Experiments can also be repeated in neurons derived from the brain of an AD mouse model, or human neurons derived from epilepsy patients (via temporal lobe resections). Cells of these types may secrete A β in a manner more similar to neurons in the brains of individuals with AD, in comparison to the N2A cells that were used in this study. Use of AD mouse models may also provide with the additional advantage of being able to observe trafficking and secretion of endogenous A β .

It might also be useful for future experiments to silence endogenous Rab27b expression using small interfering ribonucleic acid (siRNA), for example. Such a study would allow for direct comparison of A β secretion between Rab27b control and knockdown samples. Use of Rab27b WT samples (cells transfected with a Rab27b WT construct) in these experiments would further elucidate whether overexpression of Rab27b can indeed reduce lysosomal-mediated secretion, potentially through sequestration of proteins as described in Section 4.5.2. It would also be interesting to compare the effects of gene silencing and alteration of gene expression on upstream versus downstream calcium-dependent exocytosis factors. For example, we might observe different results in secretion of A β if we were to shift our focus from Rab27b to exocyst subunit EXOC6.

References

- [1] M. P. Murphy and H. Levine, “Alzheimer’s disease and the amyloid- β peptide,” *Journal of Alzheimer’s Disease*, vol. 19, no. 1. pp. 311–323, 2010.
- [2] D. Burdick, J. Kosmoski, M. F. Knauer, and C. G. Glabe, “Preferential adsorption, internalization and resistance to degradation of the major isoform of the Alzheimer’s amyloid peptide, A β 1-42, in differentiated PC12 cells,” *Brain Res.*, vol. 746, no. 1–2, pp. 275–284, 1997.
- [3] Y. Su and P. T. Chang, “Acidic pH promotes the formation of toxic fibrils from β -amyloid peptide,” *Brain Res.*, vol. 893, no. 1–2, pp. 287–291, 2001.
- [4] A. M. Cataldo and R. A. Nixon, “Enzymatically active lysosomal proteases are associated with amyloid deposits in Alzheimer brain,” *Proc. Natl. Acad. Sci. U. S. A.*, vol. 87, pp. 3861–3865, 1990.
- [5] J. K. Jaiswal, N. W. Andrews, and S. M. Simon, “Membrane proximal lysosomes are the major vesicles responsible for calcium-dependent exocytosis in nonsecretory cells,” *J. Cell Biol.*, vol. 159, no. 4, pp. 625–635, 2002.
- [6] T. Tolmachova, M. Abrink, C. E. Futter, K. S. Authi, and M. C. Seabra, “Rab27b regulates number and secretion of platelet dense granules,” *Proc. Natl. Acad. Sci.*, vol. 104, no. 14, pp. 5872–5877, 2007.
- [7] E. D. Elstak *et al.*, “The munc13-4-rab27 complex is specifically required for tethering secretory lysosomes at the plasma membrane,” *Blood*, vol. 118, no. 6, pp. 1570–1578, 2011.
- [8] Y. T. Shen *et al.*, “Rab27b is Involved in Lysosomal Exocytosis and Proteolipid Protein Trafficking in Oligodendrocytes,” *Neurosci. Bull.*, vol. 32, no. 4, pp. 331–340, 2016.
- [9] M. Fukuda, “Rab27 Effectors, Pleiotropic Regulators in Secretory Pathways,” *Traffic*, vol. 14, no. 9, pp. 949–963, 2013.

- [10] G. M. Cooper, "Lysosomes," in *The Cell: A Molecular Approach*, 2nd ed., Sunderland: Sinauer Associates, 2000.
- [11] B. Alberts, A. Johnson, J. Lewis, M. Raff, K. Roberts, and P. Walter, "Transport from the Trans Golgi Network to Lysosomes," in *Molecular Biology of the Cell. 4th edition*, 4th ed., New York: Garland Science, 2002, p. Transport from the Trans Golgi Network to Lysosome.
- [12] S. Ohkuma, Y. Moriyama, and T. Takano, "Identification and characterization of a proton pump on lysosomes by fluorescein isothiocyanate-dextran fluorescence," *Proc. Natl. Acad. Sci. U. S. A.*, vol. 79, no. 9 I, pp. 2758–2762, 1982.
- [13] D. Kasper *et al.*, "Loss of the chloride channel CIC-7 leads to lysosomal storage disease and neurodegeneration," *EMBO J.*, vol. 24, no. 5, pp. 1079–1091, 2005.
- [14] A. R. Graves, P. K. Curran, C. L. Smith, and J. A. Mindell, "The Cl⁻/H⁺ antiporter CIC-7 is the primary chloride permeation pathway in lysosomes," *Nature*, vol. 453, no. 7196, pp. 788–792, 2008.
- [15] Y. Feng, D. He, Z. Yao, and D. J. Klionsky, "The machinery of macroautophagy," *Cell Research*. 2014.
- [16] H. Lodish, A. Berk, and S. Zipursky, "Molecular Mechanisms of Vesicular Traffic," in *Molecular Cell Biology*, 4th ed., New York: W.H. Freeman and Company, 2000.
- [17] G. J. Doherty and H. T. McMahon, "Mechanisms of Endocytosis," *Annu. Rev. Biochem.*, vol. 78, no. 1, pp. 857–902, Jun. 2009.
- [18] S. D. Conner and S. L. Schmid, "Regulated portals of entry into the cell," *Nature*, vol. 422, no. 6927, pp. 37–44, 2003.
- [19] R. S. Flannagan, V. Jaumouillé, and S. Grinstein, "The Cell Biology of Phagocytosis," *Annu. Rev. Pathol. Mech. Dis.*, vol. 7, no. 1, pp. 61–98, 2012.

- [20] J. P. Luzio, Y. Hackmann, N. M. G. Dieckmann, and G. M. Griffiths, “The Biogenesis of Lysosomes and Lysosome-Related Organelles,” *Cold Spring Harb. Perspect. Biol.*, pp. 1–17, 2014.
- [21] E. J. Blott and G. M. Griffiths, “Secretory lysosomes,” *Nat. Rev. Mol. Cell Biol.*, vol. 3, no. 2, pp. 122–131, 2002.
- [22] E. Dell’Angelica, C. Mullins, S. Caplan, and J. Bonifacino, “Lysosome-Related Organelles,” *FASEB J.*, vol. 14, pp. 1265–1278, 2000.
- [23] J. D. Wilson, S. A. Shelby, D. Holowka, and B. Baird, “Rab11 Regulates the Mast Cell Exocytic Response,” *Traffic*, vol. 17, no. 9, pp. 1027–1041, 2016.
- [24] D. Axelrod, “Total internal reflection fluorescence microscopy in cell biology,” *Traffic*, vol. 2, no. 11, pp. 764–774, 2001.
- [25] E. C. Jensen, “Types of Imaging, Part 2: An Overview of Fluorescence Microscopy,” *Anat. Rec.*, vol. 295, no. 10, pp. 1621–1627, 2012.
- [26] J. K. Jaiswal, S. Chakrabarti, N. W. Andrews, and S. M. Simon, “Synaptotagmin VII restricts fusion pore expansion during lysosomal exocytosis,” *PLoS Biol.*, vol. 2, no. 8, 2004.
- [27] G. Miesenböck, D. A. De Angelis, and J. E. Rothman, “Visualizing secretion and synaptic transmission with pH-sensitive green fluorescent proteins,” *Nature*, vol. 394, no. 6689, pp. 192–195, 1998.
- [28] W. Hunziker and H. J. Geuze, “Intracellular trafficking of lysosomal membrane proteins,” *BioEssays*, vol. 18, no. 5, pp. 379–389, 1996.
- [29] T. Braulke and J. S. Bonifacino, “Sorting of lysosomal proteins,” *Biochim. Biophys. Acta - Mol. Cell Res.*, vol. 1793, no. 4, pp. 605–614, 2009.
- [30] J. S. Bonifacino and L. M. Traub, “Signals for Sorting of Transmembrane Proteins to Endosomes and Lysosomes,” *Annu. Rev. Biochem.*, vol. 72, no. 1, pp. 395–447,

2003.

- [31] M. S. Robinson and J. S. Bonifacino, “Adaptor-related proteins,” *Current Opinion in Cell Biology*, vol. 13, no. 4. pp. 444–453, 2001.
- [32] M. Jovic, M. Sharma, J. Rahajeng, and S. Caplan, “The early endosome: A busy sorting station for proteins at the crossroads,” *Histology and Histopathology*, vol. 25, no. 1. pp. 99–112, 2010.
- [33] J. Huotari and A. Helenius, “Endosome maturation,” *EMBO J.*, vol. 30, no. 17, pp. 3481–3500, 2011.
- [34] J. H. Hurley and P. I. Hanson, “Membrane budding and scission by the ESCRT machinery: It’s all in the neck,” *Nature Reviews Molecular Cell Biology*, vol. 11, no. 8. pp. 556–566, 2010.
- [35] J. Gruenberg and H. Stenmark, “The biogenesis of multivesicular endosomes,” *Nature Reviews Molecular Cell Biology*, vol. 5, no. 4. pp. 317–323, 2004.
- [36] M. Sachse, “Bilayered Clathrin Coats on Endosomal Vacuoles Are Involved in Protein Sorting toward Lysosomes,” *Mol. Biol. Cell*, vol. 13, no. 4, pp. 1313–1328, 2002.
- [37] C. Bissig and J. Gruenberg, “Lipid sorting and multivesicular endosome biogenesis,” *Cold Spring Harbor Perspectives in Biology*, vol. 5, no. 10. 2013.
- [38] H. Lodish, A. Berk, S. Zipursky, and E. Al, “Glycosylation in the ER and Golgi Complex,” in *Molecular Cell Biology*, 4th ed., no. 4, New York: W.H. Freeman and Company, 2000, p. section 17.7.
- [39] P. Ghosh, N. M. Dahms, and S. Kornfeld, “Mannose 6-phosphate receptors: New twists in the tale,” *Nature Reviews Molecular Cell Biology*, vol. 4, no. 3. pp. 202–212, 2003.
- [40] W. R. Wilcox, “Lysosomal storage disorders: The need for better pediatric

recognition and comprehensive care,” in *Journal of Pediatrics*, 2004, vol. 144, no. 5 SUPPL.

- [41] R. O. Brady, J. N. Kanfer, R. M. Bradley, and D. Shapiro, “Demonstration of a deficiency of glucocerebrosidase in Gaucher’s disease,” *J. Clin. Invest.*, vol. 45, no. 7, pp. 1112–1115, 1966.
- [42] R. O. Brady, J. N. Kanfer, and D. Shapiro, “Metabolism of glucocerebrosides II. Evidence of an enzymatic deficiency in Gaucher’s disease,” *Biochem. Biophys. Res. Commun.*, vol. 18, no. 2, pp. 221–225, 1965.
- [43] N. W. Barton *et al.*, “Replacement therapy for inherited enzyme deficiency — macrophage-targeted glucocerebrosidase for Gaucher’s disease,” *N. Engl. J. Med.*, vol. 324, no. 21, pp. 1464–1470, 1991.
- [44] L. K. Hein, P. J. Meikle, J. J. Hopwood, and M. Fuller, “Secondary sphingolipid accumulation in a macrophage model of Gaucher disease,” *Mol. Genet. Metab.*, vol. 92, no. 4, pp. 336–345, 2007.
- [45] B. E. Rosenbloom and N. J. Weinreb, “Gaucher disease: A comprehensive review,” *Crit. Rev. Oncog.*, vol. 18, no. 3, pp. 163–175, 2013.
- [46] S. Tiede *et al.*, “Mucopolysaccharidosis II is caused by mutations in GNPTA encoding the α/β GlcNAc-1-phosphotransferase,” *Nat. Med.*, vol. 11, no. 10, pp. 1109–1112, 2005.
- [47] S. Hickman and E. F. Neufeld, “A hypothesis for I-cell disease: Defective hydrolases that do not enter lysosomes,” *Biochem. Biophys. Res. Commun.*, vol. 49, no. 4, pp. 992–999, 1972.
- [48] G. Ménasché *et al.*, “Griscelli syndrome restricted to hypopigmentation results from a melanophilin defect (GS3) or a MYO5A F-exon deletion (GS1),” *J. Clin. Invest.*, vol. 112, no. 3, pp. 450–456, 2003.
- [49] E. Pastural *et al.*, “Griscelli disease maps to chromosome 15q21 and is associated

- with mutations in the myosin-Va gene,” *Nat. Genet.*, vol. 16, no. 3, pp. 289–292, 1997.
- [50] G. Ménasché *et al.*, “Mutations in RAB27A cause Griscelli syndrome associated with haemophagocytic syndrome,” *Nat. Genet.*, vol. 25, no. 2, pp. 173–176, 2000.
- [51] C. Wasmeier, A. N. Hume, G. Bolasco, and M. C. Seabra, “Melanosomes at a glance,” *J. Cell Sci.*, vol. 121, no. 24, pp. 3995–3999, 2008.
- [52] K. Van Den Bossche, J. M. Naeyaert, and J. Lambert, “The quest for the mechanism of melanin transfer,” *Traffic*, vol. 7, no. 7, pp. 769–778, 2006.
- [53] T. S. Kuroda and M. Fukuda, “Rab27A-binding protein Slp2-a is required for peripheral melanosome distribution and elongated cell shape in melanocytes,” *Nat. Cell Biol.*, vol. 6, no. 12, pp. 1195–1203, 2004.
- [54] M. Ishida, N. Ohbayashi, and M. Fukuda, “Rab1A regulates anterograde melanosome transport by recruiting kinesin-1 to melanosomes through interaction with SKIP,” *Sci. Rep.*, vol. 5, 2015.
- [55] G. G. Farías, C. M. Guardia, R. De Pace, D. J. Britt, and J. S. Bonifacino, “BORC/kinesin-1 ensemble drives polarized transport of lysosomes into the axon,” *Proc. Natl. Acad. Sci. U. S. A.*, vol. 114, no. 14, pp. E2955–E2964, 2017.
- [56] M. Encarnação *et al.*, “A Rab3a-dependent complex essential for lysosome positioning and plasma membrane repair,” *J. Cell Biol.*, vol. 213, no. 6, pp. 631–640, 2016.
- [57] S. O. Rizzoli and W. J. Betz, “Synaptic vesicle pools,” *Nature Reviews Neuroscience*, vol. 6, no. 1, pp. 57–69, 2005.
- [58] D. R. TerBush, T. Maurice, D. Roth, and P. Novick, “The Exocyst is a multiprotein complex required for exocytosis in *Saccharomyces cerevisiae*,” *EMBO J.*, vol. 15, no. 23, pp. 6483–6494, 1996.

- [59] Y. Kee, J. S. Yoo, C. D. Hazuka, K. E. Peterson, S. C. Hsu, and R. H. Scheller, "Subunit structure of the mammalian exocyst complex," *Proc. Natl. Acad. Sci. U. S. A.*, vol. 94, no. 26, pp. 14438–14443, 1997.
- [60] W. Guo, D. Roth, C. Walch-Solimena, and P. Novick, "The exocyst is an effector for Sec4P, targeting secretory vesicles to sites of exocytosis," *EMBO J.*, vol. 18, no. 4, pp. 1071–1080, 1999.
- [61] S. Wu, S. Q. Mehta, F. Pichaud, H. J. Bellen, and F. A. Quioco, "Sec15 interacts with Rab11 via a novel domain and affects Rab11 localization in vivo," *Nat. Struct. Mol. Biol.*, vol. 12, no. 10, pp. 879–885, 2005.
- [62] S. Martens and H. T. McMahon, "Mechanisms of membrane fusion: Disparate players and common principles," *Nature Reviews Molecular Cell Biology*, vol. 9, no. 7, pp. 543–556, 2008.
- [63] R. B. Sutton, D. Fasshauer, R. Jahn, and A. T. Brunger, "Crystal structure of a SNARE complex involved in synaptic exocytosis at 2.4 Å resolution," *Nature*, vol. 395, no. 6700, pp. 347–353, 1998.
- [64] I. Dulubova *et al.*, "A conformational switch in syntaxin during exocytosis: Role of munc18," *EMBO J.*, vol. 18, no. 16, pp. 4372–4382, 1999.
- [65] U. zur Stadt *et al.*, "Familial Hemophagocytic Lymphohistiocytosis Type 5 (FHL-5) Is Caused by Mutations in Munc18-2 and Impaired Binding to Syntaxin 11," *Am. J. Hum. Genet.*, vol. 85, no. 4, pp. 482–492, 2009.
- [66] S. K. Rao, C. Huynh, V. Proux-Gillardeaux, T. Galli, and N. W. Andrews, "Identification of SNAREs Involved in Synaptotagmin VII-regulated Lysosomal Exocytosis," *J. Biol. Chem.*, vol. 279, no. 19, pp. 20471–20479, 2004.
- [67] Y. Lai *et al.*, "Molecular mechanisms of synaptic vesicle priming by Munc13 and Munc18," vol. 344, no. 6188, pp. 1173–1178, 2015.
- [68] J. Tang, A. Maximov, O. H. Shin, H. Dai, J. Rizo, and T. C. Südhof, "A

- Complexin/Synaptotagmin 1 Switch Controls Fast Synaptic Vesicle Exocytosis,” *Cell*, vol. 126, no. 6, pp. 1175–1187, 2006.
- [69] W. A. Catterall, “Structure and Regulation of Voltage-Gated Ca²⁺ Channels,” *Annu. Rev. Cell Dev. Biol.*, vol. 16, no. 1, pp. 521–555, 2000.
- [70] A. Verkhratsky and A. Shmigol, “Calcium-induced calcium release in neurones,” *Cell Calcium*, vol. 19, no. 1, pp. 1–14, 1996.
- [71] R. F. Irvine, K. D. Brown, and M. J. Berridge, “Specificity of inositol trisphosphate-induced calcium release from permeabilized Swiss-mouse 3T3 cells,” *Biochem. J.*, vol. 222, no. 1, pp. 269–272, 1984.
- [72] M. H. Nathanson, P. J. Padfield, A. J. O’Sullivan, A. D. Burgstahler, and J. D. Jamieson, “Mechanism of Ca²⁺ wave propagation in pancreatic acinar cells,” *J. Biol. Chem.*, vol. 267, no. 25, pp. 18118–18121, 1992.
- [73] A. R. Flannery, C. Czibener, and N. W. Andrews, “Palmitoylation-dependent association with CD63 targets the Ca²⁺ sensor synaptotagmin VII to lysosomes,” *J. Cell Biol.*, vol. 191, no. 3, pp. 599–613, 2010.
- [74] R. Fesce, F. Grohovaz, F. Valtorta, and J. Meldolesi, “Neurotransmitter release: fusion or ‘kiss-and-run’?,” *Trends Cell Biol.*, vol. 4, no. 1, pp. 1–4, 1994.
- [75] Z. Zhang *et al.*, “Regulated ATP release from astrocytes through lysosome exocytosis,” *Nat. Cell Biol.*, vol. 9, no. 8, pp. 945–953, 2007.
- [76] T. E. Hermann, “Characterization of Ionomycin as a Calcium Ionophore,” *J. Biol. Chem.*, vol. 253, no. 17, pp. 5892–5894, 1978.
- [77] V. M. Olkkonen and E. Ikonen, “When intracellular logistics fails - genetic defects in membrane trafficking,” *J. Cell Sci.*, vol. 119, no. 24, pp. 5031–5045, 2006.
- [78] A. D. Cox and C. J. Der, “Ras history: The saga continues,” *Small GTPases*, vol. 1, no. 1, pp. 2–27, 2010.

- [79] P. Chavrier, J. P. Gorvel, E. Stelzer, K. Simons, J. Gruenberg, and M. Zerial, "Hypervariable C-terminal domain of rab proteins acts as a targeting signal," *Nature*, vol. 353, no. 6346, pp. 769–772, 1991.
- [80] N. Segev, "Ypt and Rab GTPases: Insight into functions through novel interactions," *Current Opinion in Cell Biology*, vol. 13, no. 4, pp. 500–511, 2001.
- [81] J. Bos, H. Rehmann, and A. Wittinghofer, "GEFs and GAPs: Critical Elements in the Control of Small G Proteins," *Cell*, vol. 129, pp. 865–877, 2007.
- [82] M. Trahey and F. McCormick, "A cytoplasmic protein stimulates normal N-ras p21 GTPase, but does not affect oncogenic mutants," *Science (80-.)*, 1987.
- [83] H. Stenmark and V. M. Olkkonen, "Protein family review: The Rab GTPase family," *Genome Biol.*, vol. 2, no. 5, pp. 1–7, 2001.
- [84] J. S. Anant *et al.*, "Mechanism of Rab geranylgeranylation: Formation of the catalytic ternary complex," *Biochemistry*, vol. 37, no. 36, pp. 12559–12568, Sep. 1998.
- [85] M. A. Bustos, O. Lucchesi, M. C. Ruete, and C. N. Tomes, "Membrane-permeable Rab27A is a regulator of the acrosome reaction: Role of geranylgeranylation and guanine nucleotides," *Cell. Signal.*, vol. 44, pp. 72–81, 2018.
- [86] A. B. Dirac-Svejstrup, T. Sumizawa, and S. R. Pfeffer, "Identification of a GDI displacement factor that releases endosomal Rab GTPases from Rab-GDI," *EMBO J.*, vol. 16, no. 3, pp. 465–472, 1997.
- [87] O. Ullrich *et al.*, "Rab GDP dissociation inhibitor as a general regulator for the membrane association of rab proteins," *J. Biol. Chem.*, vol. 268, no. 24, pp. 18143–18150, 1993.
- [88] M. C. Seabra and C. Wasmeier, "Controlling the location and activation of Rab GTPases," *Current Opinion in Cell Biology*, vol. 16, no. 4, pp. 451–457, 2004.

- [89] R. N. Collins, “‘Getting it on’ - GDI displacement and small GTPase membrane recruitment,” *Molecular Cell*, vol. 12, no. 5, pp. 1064–1066, 2003.
- [90] O. Ullrich, H. Horiuchi, C. Bucci, and M. Zerial, “Membrane association of Rab5 mediated by GDP-dissociation inhibitor and accompanied by GDP/GTP exchange,” *Nature*, vol. 368, no. 6467, pp. 157–160, 1994.
- [91] A. C. Valdez, J. P. Cabaniols, M. J. Brown, and P. A. Roche, “Syntaxin 11 is associated with SNAP-23 on late endosomes and the trans-Golgi network,” *J. Cell Sci.*, vol. 112, no. 6, pp. 845–854, 1999.
- [92] M. Neeft *et al.*, “Munc13-4 is an effector of Rab27a and controls secretion of lysosomes in hematopoietic cells,” *Mol. Biol. Cell*, 2005.
- [93] N. J. Pavlos *et al.*, “Quantitative Analysis of Synaptic Vesicle Rabs Uncovers Distinct Yet Overlapping Roles for Rab3a and Rab27b in Ca²⁺-Triggered Exocytosis,” *J. Neurosci.*, vol. 30, no. 40, pp. 13441–13453, 2010.
- [94] S. Wang, C. Hu, F. Wu, and S. He, “Rab25 GTPase: Functional roles in cancer,” *Oncotarget*, 2017.
- [95] H. Chertkow, H. H. Feldman, C. Jacova, and F. Massoud, “Definitions of dementia and predementia states in Alzheimer’s disease and vascular cognitive impairment: Consensus from the Canadian conference on diagnosis of dementia,” in *Alzheimer’s Research and Therapy*, 2013.
- [96] R. D. Terry *et al.*, “Physical basis of cognitive alterations in alzheimer’s disease: Synapse loss is the major correlate of cognitive impairment,” *Ann. Neurol.*, vol. 30, no. 4, pp. 572–580, 1991.
- [97] C. A. Davies, D. M. A. Mann, P. Q. Sumpter, and P. O. Yates, “A quantitative morphometric analysis of the neuronal and synaptic content of the frontal and temporal cortex in patients with Alzheimer’s disease,” *J. Neurol. Sci.*, vol. 78, no. 2, pp. 151–164, 1987.

- [98] J. Z. Tsien, P. T. Huerta, and S. Tonegawa, "The essential role of hippocampal CA1 NMDA receptor-dependent synaptic plasticity in spatial memory," *Cell*, vol. 87, no. 7, pp. 1327–1338, 1996.
- [99] L. Detolledo-Morrell, Y. Geinisman, and F. Morrell, "Age-dependent alterations in hippocampal synaptic plasticity: Relation to memory disorders," *Neurobiology of Aging*, vol. 9, no. C. pp. 581–590, 1988.
- [100] C. Harper, "The neuropathology of alcohol-related brain damage," *Alcohol and Alcoholism*, vol. 44, no. 2. pp. 136–140, 2009.
- [101] H. K. Wang *et al.*, "Population based study on patients with traumatic brain injury suggests increased risk of dementia," *J. Neurol. Neurosurg. Psychiatry*, vol. 83, no. 11, pp. 1080–1085, 2012.
- [102] J. A. Levy and G. J. Chelune, "Cognitive-behavioral profiles of neurodegenerative dementias: Beyond alzheimer's disease," *Journal of Geriatric Psychiatry and Neurology*, vol. 20, no. 4. pp. 227–238, 2007.
- [103] M. Prince, A. Wimo, M. Guerchet, A. Gemma-Claire, Y.-T. Wu, and M. Prina, "World Alzheimer Report 2015: The Global Impact of Dementia - An analysis of prevalence, incidence, cost and trends," *Alzheimer's Dis. Int.*, 2015.
- [104] J. Lindsay *et al.*, "Risk factors for Alzheimer's disease: A prospective analysis from the Canadian Study of Health and Aging," *Am. J. Epidemiol.*, vol. 156, no. 5, pp. 445–453, 2002.
- [105] N. Zilka and M. Novak, "The tangled story of Alois Alzheimer.," *Bratisl. Lek. Listy*, vol. 107, no. 9–10, pp. 343–345, 2006.
- [106] R. A. Stelzmann, H. Norman Schnitzlein, and F. Reed Murtagh, "An english translation of alzheimer's 1907 paper, 'über eine eigenartige erkankung der hirnrinde,'" *Clin. Anat.*, vol. 8, no. 6, pp. 429–431, 1995.
- [107] G. McKhann, D. Drachman, M. Folstein, R. Katzman, D. Price, and E. M. Stadlan,

- “Clinical diagnosis of Alzheimer’s disease: report of Health and Human Services Task Force on Alzheimer’s disease,” *Neurology*, vol. 34, no. 7, pp. 939–944, 1984.
- [108] G. M. McKhann *et al.*, “The diagnosis of dementia due to Alzheimer’s disease: Recommendations from the National Institute on Aging-Alzheimer’s Association workgroups on diagnostic guidelines for Alzheimer’s disease,” *Alzheimer’s Dement.*, vol. 7, no. 3, pp. 263–269, 2011.
- [109] M. Ball *et al.*, “Consensus recommendations for the postmortem diagnosis of Alzheimer’s disease,” *Neurobiol. Aging*, vol. 18, no. 4 SUPPL., 1997.
- [110] S. E. Arnold, B. T. Hyman, J. Flory, A. R. Damasio, and G. W. Van Hoesen, “The topographical and neuroanatomical distribution of neurofibrillary tangles and neuritic plaques in the cerebral cortex of patients with alzheimer’s disease,” *Cereb. Cortex*, vol. 1, no. 1, pp. 103–116, 1991.
- [111] D. R. Thal, U. Rüb, M. Orantes, and H. Braak, “Phases of A β -deposition in the human brain and its relevance for the development of AD,” *Neurology*, vol. 58, no. 12, pp. 1791–1800, 2002.
- [112] H. Braak and E. Braak, “Neuropathological staging of Alzheimer-related changes,” *Acta Neuropathologica*, vol. 82, no. 4, pp. 239–259, 1991.
- [113] G. W. Small *et al.*, “Diagnosis and treatment of Alzheimer disease and related disorders: Consensus statement of the American Association for Geriatric Psychiatry, the Alzheimer’s Association, and the American Geriatrics Society,” in *Journal of the American Medical Association*, 1997.
- [114] N. H. Trinh, J. Hoblyn, S. Mohanty, and K. Yaffe, “Efficacy of cholinesterase inhibitors in the treatment of neuropsychiatric symptoms and functional impairment in Alzheimer disease: A meta-analysis,” *Journal of the American Medical Association*. 2003.
- [115] K. N. Franco and B. Messinger-Rapport, “Pharmacological treatment of neuropsychiatric symptoms of dementia: A review of the evidence,” *J. Am. Med.*

Dir. Assoc., 2006.

- [116] M. E. Hasselmo, “The role of acetylcholine in learning and memory,” *Current Opinion in Neurobiology*. 2006.
- [117] P. J. Whitehouse, D. L. Price, A. W. Clark, J. T. Coyle, and M. R. DeLong, “Alzheimer disease: Evidence for selective loss of cholinergic neurons in the nucleus basalis,” *Ann. Neurol.*, 1981.
- [118] E. K. Perry, P. H. Gibson, G. Blessed, R. H. Perry, and B. E. Tomlinson, “Neurotransmitter enzyme abnormalities in senile dementia. Choline acetyltransferase and glutamic acid decarboxylase activities in necropsy brain tissue,” *J. Neurol. Sci.*, 1977.
- [119] J. Birks, “Cholinesterase inhibitors for Alzheimer’s disease,” *Cochrane Database Syst. Rev.*, no. 1, 2006.
- [120] M. Goedert, M. G. Spillantini, and R. A. Crowther, “Tau Proteins and Neurofibrillary Degeneration,” *Brain Pathol.*, vol. 1, no. 4, pp. 279–286, 1991.
- [121] J. Hardy and G. Higgins, “Alzheimer’s disease: the amyloid cascade hypothesis,” *Science (80-.)*, vol. 256, no. 5054, pp. 184–185, 1992.
- [122] S. Lammich *et al.*, “Constitutive and regulated α -secretase cleavage of Alzheimer’s amyloid precursor protein by a disintegrin metalloprotease,” *Proc. Natl. Acad. Sci. U. S. A.*, vol. 96, no. 7, pp. 3922–3927, 1999.
- [123] F. S. Esch *et al.*, “Cleavage of amyloid β peptide during constitutive processing of its precursor,” *Science (80-.)*, vol. 248, no. 4959, pp. 1122–1124, 1990.
- [124] K. Furukawa *et al.*, “Increased Activity-Regulating and Neuroprotective Efficacy of α -Secretase-Derived Secreted Amyloid Precursor Protein Conferred by a C-Terminal Heparin-Binding Domain,” *J. Neurochem.*, vol. 67, no. 5, pp. 1882–1896, 2002.

- [125] M. P. Mattson, B. Cheng, A. R. Culwell, F. S. Esch, I. Lieberburg, and R. E. Rydel, "Evidence for excitoprotective and intraneuronal calcium-regulating roles for secreted forms of the β -amyloid precursor protein," *Neuron*, vol. 10, no. 2, pp. 243–254, 1993.
- [126] W. Tang *et al.*, "Arf6 controls beta-amyloid production by regulating macropinocytosis of the Amyloid Precursor Protein to lysosomes," *Mol. Brain*, vol. 8, no. 1, 2015.
- [127] J. R. Cirrito *et al.*, "Endocytosis Is Required for Synaptic Activity-Dependent Release of Amyloid- β In Vivo," *Neuron*, vol. 58, no. 1, pp. 42–51, Apr. 2008.
- [128] A. Lorenzen *et al.*, "Rapid and Direct Transport of Cell Surface APP to the Lysosome defines a novel selective pathway," *Mol. Brain*, vol. 3, no. 1, pp. 1–13, 2010.
- [129] R. Vassar *et al.*, " β -Secretase cleavage of Alzheimer's amyloid precursor protein by the transmembrane aspartic protease BACE," *Science (80-.)*, vol. 286, no. 5440, pp. 735–741, 1999.
- [130] S. Jin *et al.*, "Evidence for dimeric BACE-mediated APP processing," *Biochem. Biophys. Res. Commun.*, vol. 393, no. 1, pp. 21–27, 2010.
- [131] F. Grüninger-Leitch, D. Schlatter, E. Küng, P. Nelböck, and H. Döbeli, "Substrate and inhibitor profile of BACE (β -secretase) and comparison with other mammalian aspartic proteases," *J. Biol. Chem.*, vol. 277, no. 7, pp. 4687–4693, 2002.
- [132] B. De Strooper, "Aph-1, Pen-2, and Nicastrin with Presenilin generate an active γ -Secretase complex," *Neuron*, vol. 38, no. 1, pp. 9–12, 2003.
- [133] M. S. Wolfe, W. Xia, B. L. Ostaszewski, T. S. Diehl, W. T. Kimberly, and D. J. Selkoe, "Two transmembrane aspartates in presenilin-1 required for presenilin endoproteolysis and γ -secretase activity," *Nature*, vol. 398, no. 6727, pp. 513–517, 1999.

- [134] S. H. Pasternak *et al.*, “Presenilin-1, nicastrin, amyloid precursor protein, and γ -secretase activity are co-localized in the lysosomal membrane,” *J. Biol. Chem.*, vol. 278, no. 29, pp. 26687–26694, 2003.
- [135] Y. M. Li *et al.*, “Presenilin 1 is linked with γ -secretase activity in the detergent solubilized state,” *Proc. Natl. Acad. Sci. U. S. A.*, vol. 97, no. 11, pp. 6138–6143, 2000.
- [136] C. McLendon *et al.*, “Cell-free assays for gamma-secretase activity,” *FASEB J.*, 2000.
- [137] E. H. Koo and S. L. Squazzo, “Evidence That Production and Release of Amyloid-Beta Protein Involves the Endocytic Pathway,” *J. Biol. Chem.*, vol. 269, no. 26, pp. 17386–17389, 1994.
- [138] F. Chen *et al.*, “Carboxyl-terminal fragments of alzheimer β -amyloid precursor protein accumulate in restricted and unpredicted intracellular compartments in presenilin 1-deficient cells,” *J. Biol. Chem.*, vol. 275, no. 47, pp. 36794–36802, 2000.
- [139] J. Knops, S. Suomensari, M. Lee, L. McConlogue, P. Seubert, and S. Sinha, “Cell-type and amyloid precursor protein-type specific inhibition of A β release by bafilomycin A1, a selective inhibitor of vacuolar ATPases,” *J. Biol. Chem.*, vol. 270, no. 6, pp. 2419–2422, 1995.
- [140] D. Dries and G. Yu, “Assembly, Maturation, and Trafficking of the Gamma-Secretase Complex in Alzheimers Disease,” *Curr. Alzheimer Res.*, vol. 5, no. 2, pp. 132–146, 2008.
- [141] J. T. Jarrett, E. P. Berger, and P. T. Lansbury, “The Carboxy Terminus of the β Amyloid Protein Is Critical for the Seeding of Amyloid Formation: Implications for the Pathogenesis of Alzheimer’s Disease,” *Biochemistry*, vol. 32, no. 18, pp. 4693–4697, 1993.
- [142] M. F. Knauer, B. Soreghan, D. Burdick, J. Kosmoski, and C. G. Glabe,

- “Intracellular accumulation and resistance to degradation of the Alzheimer amyloid A4/beta protein.” *Proc. Natl. Acad. Sci. U. S. A.*, vol. 89, no. 16, pp. 7437–7441, 1992.
- [143] R. Resende, E. Ferreiro, C. Pereira, and C. Resende de Oliveira, “Neurotoxic effect of oligomeric and fibrillar species of amyloid-beta peptide 1-42: Involvement of endoplasmic reticulum calcium release in oligomer-induced cell death,” *Neuroscience*, vol. 155, no. 3, pp. 725–737, 2008.
- [144] Y. Verdier, M. Zarándi, and B. Penke, “Amyloid β -peptide interactions with neuronal and glial cell plasma membrane: Binding sites and implications for Alzheimer’s disease,” *J. Pept. Sci.*, vol. 10, no. 5, pp. 229–248, 2004.
- [145] K. S. Vetrivel and G. Thinakaran, “Membrane rafts in Alzheimer’s disease beta-amyloid production,” *Biochimica et Biophysica Acta - Molecular and Cell Biology of Lipids*, vol. 1801, no. 8, pp. 860–867, 2010.
- [146] T. Kawarabayashi, “Dimeric Amyloid-Beta Protein Rapidly Accumulates in Lipid Rafts followed by Apolipoprotein E and Phosphorylated Tau Accumulation in the Tg2576 Mouse Model of Alzheimer’s Disease,” *J. Neurosci.*, vol. 24, no. 15, pp. 3801–3809, 2004.
- [147] H. A. Lashuel, D. Hartley, B. M. Petre, T. Walz, and P. T. Lansbury, “Amyloid pores from pathogenic mutations,” *Nature*, vol. 418, no. 6895, pp. 291–291, Jul. 2002.
- [148] R. M. Nisbet, J. C. Polanco, L. M. Ittner, and J. Götz, “Tau aggregation and its interplay with amyloid- β ,” *Acta Neuropathol.*, vol. 129, no. 2, pp. 207–220, 2015.
- [149] M. D. Weingarten, A. H. Lockwood, S. Y. Hwo, and M. W. Kirschner, “A protein factor essential for microtubule assembly,” *Proc. Natl. Acad. Sci. U. S. A.*, 1975.
- [150] G. Lindwall and R. D. Cole, “The purification of tau protein and the occurrence of two phosphorylation states of tau in brain,” *J. Biol. Chem.*, 1984.

- [151] M. L. Billingsley and R. L. Kincaid, "Regulated phosphorylation and dephosphorylation of tau protein: Effects on microtubule interaction, intracellular trafficking and neurodegeneration," *Biochemical Journal*, vol. 323, no. 3, pp. 577–591, 1997.
- [152] J. Z. Wang, I. Grundke-Iqbal, and K. Iqbal, "Kinases and phosphatases and tau sites involved in Alzheimer neurofibrillary degeneration," *Eur. J. Neurosci.*, vol. 25, no. 1, pp. 59–68, 2007.
- [153] I. Grundke-Iqbal, K. Iqbal, and Y. C. Tung, "Abnormal phosphorylation of the microtubule-associated protein τ (tau) in Alzheimer cytoskeletal pathology," *Proc. Natl. Acad. Sci. U. S. A.*, vol. 83, no. 13, pp. 44913–44917, 1986.
- [154] C. Ballatore, V. M. Y. Lee, and J. Q. Trojanowski, "Tau-mediated neurodegeneration in Alzheimer's disease and related disorders," *Nat. Rev. Neurosci.*, vol. 8, no. 9, pp. 663–672, Sep. 2007.
- [155] S. Xie *et al.*, "O-GlcNAcylation of protein kinase A catalytic subunits enhances its activity: A mechanism linked to learning and memory deficits in Alzheimer's disease," *Aging Cell*, vol. 15, no. 3, pp. 455–464, 2016.
- [156] C. C. Swanwick, M. E. Shapiro, Z. Yi, K. Chang, and R. J. Wenthold, "NMDA receptors interact with flotillin-1 and -2, lipid raft-associated proteins," *FEBS Lett.*, 2009.
- [157] G. Mairet-Coello, J. Curchet, S. Pieraut, V. Curchet, A. Maximov, and F. Polleux, "The CAMKK2-AMPK Kinase Pathway Mediates the Synaptotoxic Effects of A β Oligomers through Tau Phosphorylation," *Neuron*, 2013.
- [158] D. Scheuner *et al.*, "Secreted amyloid β -protein similar to that in the senile plaques of Alzheimer's disease is increased in vivo by the presenilin 1 and 2 and APP mutations linked to familial Alzheimer's disease," *Nat. Med.*, vol. 2, no. 8, pp. 864–870, 1996.
- [159] D. Campion *et al.*, "Early-onset autosomal dominant Alzheimer disease:

- Prevalence, genetic heterogeneity, and mutation spectrum,” *Am. J. Hum. Genet.*, 1999.
- [160] R. J. Harvey, M. Skelton-Robinson, and M. N. Rossor, “The prevalence and causes of dementia in people under the age of 65 years,” *J. Neurol. Neurosurg. Psychiatry*, 2003.
- [161] D. M. A. Mann *et al.*, “An Analysis of the Morphology of Senile Plaques in Down Syndrome Patients of Different Ages Using Immunocytochemical and Lectin Histochemical Techniques,” *Neuropathol. Appl. Neurobiol.*, vol. 15, no. 4, pp. 317–329, 1989.
- [162] B. Rumble *et al.*, “Amyloid A4 Protein and Its Precursor in Down’s Syndrome and Alzheimer’s Disease,” *N. Engl. J. Med.*, vol. 320, no. 22, pp. 1446–1452, 1989.
- [163] A. Thathiah and B. De Strooper, “The role of G protein-coupled receptors in the pathology of Alzheimer’s disease,” *Nature Reviews Neuroscience*. 2011.
- [164] A. Reddy, E. V. Caler, and N. W. Andrews, “Plasma membrane repair is mediated by Ca²⁺-regulated exocytosis of lysosomes,” *Cell*, vol. 106, no. 2, pp. 157–169, 2001.
- [165] L. Zheng, A. Cedazo-Minguez, M. Hallbeck, F. Jerhammar, J. Marcusson, and A. Terman, “Intracellular distribution of amyloid beta peptide and its relationship to the lysosomal system,” *Transl. Neurodegener.*, vol. 1, pp. 1–7, 2012.
- [166] J. A. Snir *et al.*, “An Aspartyl Cathepsin Targeted PET Agent: Application in an Alzheimer’s Disease Mouse Model,” *J. Alzheimer’s Dis.*, vol. 61, no. 3, pp. 1241–1252, 2018.
- [167] Y. T. Bryceson *et al.*, “Defective cytotoxic lymphocyte degranulation in syntaxin-11-deficient familial hemophagocytic lymphohistiocytosis 4 (FHL4) patients,” *Blood*, vol. 110, no. 6, pp. 1906–1915, 2007.
- [168] J. F. Dice, “Biogenesis, Structure and Function of Lysosomes,” in *Encyclopedia of*

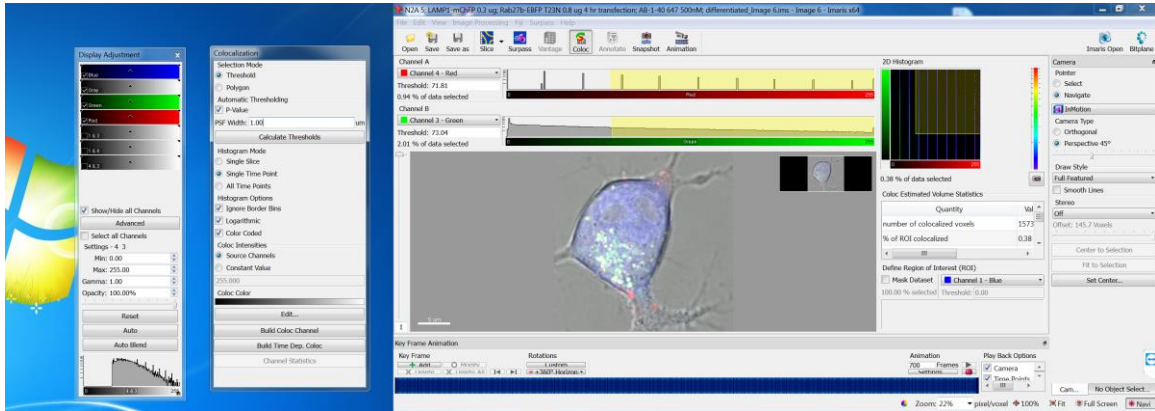
Molecular Cell Biology and Molecular Medicine, 2006.

- [169] Z. Yi *et al.*, “The Rab27a/Granuphilin Complex Regulates the Exocytosis of Insulin-Containing Dense-Core Granules,” *Mol. Cell. Biol.*, vol. 22, no. 6, pp. 1858–1867, 2002.
- [170] C. Nordstedt, J. Näslund, L. O. Tjernberg, A. R. Karlström, J. Thyberg, and L. Terenius, “The Alzheimer A β peptide develops protease resistance in association with its polymerization into fibrils,” *J. Biol. Chem.*, vol. 269, no. 49, pp. 30773–30776, 1994.
- [171] H. Hamazaki, “Cathepsin D is involved in the clearance of Alzheimer’s β -amyloid protein,” *FEBS Lett.*, vol. 396, no. 2–3, pp. 139–142, 1996.
- [172] S. Zhao, S. Torii, H. Yokota-hashimoto, T. Takeuchi, and T. Izumi, “Involvement of Rab27b in the Regulated Secretion of Pituitary Hormones,” *Endocrinology*, vol. 143, no. 5, pp. 1817–1824, 2002.
- [173] G. Augusti-Tocco and G. Sato, “Establishment of functional clonal lines of neurons from mouse neuroblastoma,” *Proc. Natl. Acad. Sci. U. S. A.*, vol. 64, no. 1, pp. 311–315, 1969.
- [174] P. Nelson, W. Ruffner, and M. Nirenberg, “NEURONAL TUMOR CELLS WITH EXCITABLE MEMBRANES GROWN *in vitro*,” *Proc. Natl. Acad. Sci.*, vol. 64, no. 3, pp. 1004–1010, Nov. 1969.
- [175] B. P. Bean, “The action potential in mammalian central neurons,” *Nature Reviews Neuroscience*, vol. 8, no. 6, pp. 451–465, 2007.
- [176] M. B. Collatz, R. Rüdell, and H. Brinkmeier, “Intracellular calcium chelator BAPTA protects cells against toxic calcium overload but also alters physiological calcium responses,” *Cell Calcium*, vol. 21, no. 6, pp. 453–459, 1997.
- [177] D. Boehning, R. L. Patterson, L. Sedaghat, N. O. Glebova, T. Kurosaki, and S. H. Snyder, “Cytochrome c binds to inositol (1,4,5) trisphosphate receptors, amplifying

- calcium-dependent apoptosis,” *Nat. Cell Biol.*, vol. 5, no. 12, pp. 1051–1061, 2003.
- [178] N. Brustovetsky, T. Brustovetsky, R. Jemmerson, and J. M. Dubinsky, “Calcium-induced Cytochrome c release from CNS mitochondria is associated with the permeability transition and rupture of the outer membrane,” *J. Neurochem.*, vol. 80, no. 2, pp. 207–218, 2002.
- [179] E. Dolgin, “How to defeat dementia,” *Nature*, vol. 539, no. 7628, pp. 156–158, 2016.
- [180] G. Thinakaran and E. H. Koo, “Amyloid precursor protein trafficking, processing, and function,” *Journal of Biological Chemistry*, vol. 283, no. 44, pp. 29615–29619, 2008.
- [181] H. Xu *et al.*, “Generation of Alzheimer β -amyloid protein in the trans-Golgi network in the apparent absence of vesicle formation,” *Proc. Natl. Acad. Sci. U. S. A.*, vol. 94, no. 8, pp. 3748–3752, 1997.
- [182] R. Perez-Gonzalez, S. A. Gauthier, A. Kumar, and E. Levy, “The exosome secretory pathway transports amyloid precursor protein carboxyl-terminal fragments from the cell into the brain extracellular space,” *J. Biol. Chem.*, vol. 287, no. 51, pp. 43108–43115, 2012.
- [183] L. Rajendran *et al.*, “Alzheimer’s disease β -amyloid peptides are released in association with exosomes,” *Proc. Natl. Acad. Sci. U. S. A.*, vol. 103, no. 30, pp. 11172–11177, 2006.
- [184] M. Ostrowski *et al.*, “Rab27a and Rab27b control different steps of the exosome secretion pathway,” *Nat. Cell Biol.*, vol. 12, no. 1, pp. 19–30, 2010.

Appendices

Appendix 1 – Imaris Software 7 Co-Localization Module



Curriculum Vitae

Name: Shany Lahan

Post-secondary Education and Degrees: University of Toronto
Toronto, Ontario, Canada
2013-2017 Honours B.Sc.

Related Work Experience

Graduate Teaching Assistant
Western University
Anatomy and Cell Biology 3319
2018-2019

Graduate Teaching Assistant
Western University
Anatomy and Cell Biology 4452
2018

Research Assistant
University of Toronto
Moscovitch Laboratory
2016-2017